Pathogenic mechanisms of kidney defects in the mutants for PCP effector gene Fuzzy

Rhythm Sharma

Faculty of Medicine

Division of Experimental Medicine

McGill University

Montreal, Quebec, Canada

April 2021

A thesis submitted to McGill University in partial fulfilment of the requirements of the degree of Master of Science

Table of Contents

Abstract (English)

Congenital anomalies of the kidney and urinary tract (CAKUT) are among the most common human birth defects diagnosed in 1 per 500-600 newborns and the leading cause of end-stage renal disease in children. CAKUT include renal hypoplasia, complete renal agenesis, cystic kidney disease and others. These conditions are caused by the mutations in various genes, including the genes that control formation and function of the primary cilia on renal tubular cells. We discovered hypoplastic kidneys with cystic glomeruli and tubules in the mice mutant for the Planar Cell Polarity (PCP) effector gene, *Fuzzy*. *Fuzzy* was originally discovered in *Drosophila* where it regulates actin polymerization required for assembly of a single, distally pointing, actin-based hair on each fly wing cell; loss of *Fuzzy* in flies leads to excessive actin polymerization and generation of multiple hairs with randomized polarity. However, in vertebrates, Fuzzy was shown to control ciliogenesis by organizing trafficking of certain molecules needed for the assembly of the primary cilium. The molecular and cellular mechanisms whereby Fuzzy regulates ciliogenesis and causes hypodysplastic kidney phenotype in vertebrates that are not well understood.

To understand the extent of the kidney defects in the *Fuzzy*$^{-/-}$ mouse, we conducted a quantitative morphological analysis of the mutant kidneys at embryonic day E16.5. We found that both the proximal part of nephron (glomerulus and proximal tubules) and distal part (collecting duct tubules) are significantly dilatated due to defects in the directional cell movement, a morphogenetic process during tubule formation regulated by the PCP pathway.

Recent evidence points at the critical role of actin at the base of the cilium: too much actin appears to negatively affect cilia formation, likely, due to interference with vesicle trafficking of cargo proteins to the basal body. We hypothesized that Fuzzy's involvement in ciliogenesis may be similar to its role in *Drosophila* as an actin regulator. We capitalized on our recent observations

on potential links between Fuzzy and p190A proteins in control of ciliogenesis. p190A is a GTPase activating protein that acts as an inhibitor of RhoA GTPase and regulates actin polymerization at the base of the cilium required for proper cilia elongation. Mutations of the *p190A* gene cause shorter cilia, renal hypoplasia and glomerulocystic kidney, phenotypically identical to the E16.5 *Fuzzy*$^{-/-}$ kidneys. In this thesis, we demonstrate that Fuzzy biochemically interacts with p190A and that p190A is lost at the base of cilium in *Fuzzy*$^{-/-}$ cells, indicating that Fuzzy controls p190A recruitment to the basal body. To ascertain whether there is a genetic interaction between *Fuzzy* and *p190A* genes, we generated double heterozygous (HETS) mice by crossing *Fuzzy*$^{+/-}$ and *p190A*$^{+/-}$ mice. The majority of double HETS survived, yet we detected a low, yet significant, loss of double HETs in the adult colony. We next generated mice with various dosages of *Fuzzy* and *p190A* genes by mating double HET *Fuzzy*$^{+/-}$*;p190A*$^{+/-}$ mice, which were examined at E14.5 due to frequent *Fuzzy*$^{-/-}$ death at this stage**.** We discovered that some double HET embryos have neural tube defects (NTD) explaining double HETS attrition in adult colony. We found that loss of 3 alleles (e.g., two *Fuzzy* and one *p190A* or one *Fuzzy* and two *p190A*) significantly exacerbated penetrance of the phenotypes seen in the single homozygotes, such as cranial NTD, polydactyly or anophthalmia. New phenotype, spina bifida, that was never seen in either single homozygote, was also noticed. Double homozygous mice exhibited 100% penetrance of NTD, polydactyly, and anophthalmia. With respect to the kidney defects, we found a significant exacerbation of renal hypoplasia and a new phenotype (renal agenesis) as the gene dosages decreased. Together, our data revealed a molecular, genetic, and mechanistic links between the PCP effector Fuzzy and p190A RhoGAP. We propose that Fuzzy and p190A participate in the same pathway to control RhoA GTPase activity at the base of the cilium, and that hypoplastic cystic phenotype in the Fuzzy$^{-/-}$ mouse may be caused by the inappropriate RhoA activation at the cilium.

Résumé

Les anomalies congénitales du rein et des voies urinaires (ACRTU) font partie des malformations congénitales humaines les plus courantes diagnostiquées chez 1 nouveau-né sur 500 à 600. Ces anomalies sont aussi la principale cause d'insuffisance rénale terminale chez les enfants. ACRTU comprend l'hypoplasie rénale, l'agénésie rénale complète, la maladie rénale kystique ainsi qu'une myriade d'autres. Ces conditions sont causées par des mutations dans divers gènes, y compris les gènes qui contrôlent la formation et la fonction des cils primaires sur les cellules tubulaires rénales. Notre recherche porte sur l'examination des reins hypoplasiques avec des glomérules et des tubules kystiques chez des souris mutantes pour le gène effecteur de polarité planaire cellulaire (PPC), *Fuzzy*.

À l'origine, *Fuzzy* a été découvert chez l'espèce *Drosophila melanogaster*, où il réglemente la polymérisation de l'actine. L'actine est requise pour l'assemblage d'un seul poil à base d'actine, pointant dans le sens distal sur chaque cellule de l'aile de la mouche. Ainsi, la perte de *Fuzzy* chez les mouches *Drosophiles* conduit à une polymérisation excessive de l'actine et à la génération de plusieurs poils avec une polarité aléatoire. Cependant, chez les vertébrés, il a été démontré que Fuzzy contrôle la ciliogenèse en organisant le trafic de certaines molécules nécessaires à l'assemblage du cil primaire. Les mécanismes moléculaires et cellulaires par lesquels Fuzzy réglemente la ciliogenèse et provoque un phénotype rénal hypodysplastique chez les vertébrés lors du'une mutation ne sont pas élucidés.

Pour comprendre le niveau ou la sévérité des malformations des reins chez la souris *Fuzzy*$^{-/-}$, nous avons effectué une analyse morphologique quantitative des reins mutants au jour embryonnaire E16.5. Nous avons constaté que la partie proximale du néphron (composé du glomécorule et des tubules proximaux) et la partie distale (composé des tubules collecteurs) sont considérablement

dilatées. Cette constation s'explique par une anomalie dans le mouvement directionnel des cellules, un processus morphogénétique critique au cours de la formation des tubules règlementé par la PPC.

Des preuves récentes soulignent le rôle critique de l'actine à la base du cil : un excès d'actine semble affecter négativement la formation des cils, probablement en raison de l'interférence avec le trafic vésiculaire des protéines cargo vers le corps basal du cil. Nous avons émis l'hypothèse que l'implication de Fuzzy dans la ciliogenèse pourrait être similaire à son rôle chez la *Drosophil*e en tant que régulateur de l'actine. Nous avons capitalisé sur nos observations récentes sur les liens potentiels entre les protéines Fuzzy et p190A dans le contrôle de la ciliogenèse. La p190A est une protéine activant la GTPase qui agit comme un inhibiteur de la RhoA GTPase et régule la polymérisation de l'actine à la base du cil nécessaire à l'allongement approprié des cils. Les mutations du gène *p190A* provoquent la formation de cils plus courts, une hypoplasie rénale et un rein glomérulocystique, phénotypiquement identique aux reins des souris *Fuzzy*$^{-/-}$ E16.5.

Dans cette thèse, nous démontrons que Fuzzy interagit biochimiquement avec p190A et que l'activité p190A est perdu à la base du cil dans les cellules *Fuzzy*$^{-/-}$, indiquant que Fuzzy contrôle le recrutement de p190A vers le corps basal. Pour vérifier s'il existe une interaction génétique entre les gènes *Fuzzy* et *p190A*, nous avons généré des souris doubles hétérozygotes (HETS) en croisant les souris *Fuzzy*$^{+/-}$ et *p190A*$^{+/-}$. La majorité des doubles HETS ont survécu, mais nous avons pourtant détecté une perte faible mais significative de doubles HETS dans la colonie adulte. Nous avons ensuite généré des souris avec diverses doses de gènes *Fuzzy* et *p190A* en accouplant des souris doubles HETS *Fuzzy* $^{+/-}$, *p190A*$^{+/-}$, qui ont été examinées à E14.5 en raison de la mort fréquente des *souris Fuzzy*$^{-/-}$ à ce stade. Nous avons découvert que certains embryons doubles HETS ont une anomalie du tube neural (ATN), expliquant la mortalité plus élevée des double

HETS dans la colonie adulte. Nous avons constaté que la perte de 3 allèles (par exemple, deux *Fuzzy* et un *p190A* ou un *Fuzzy* et deux *p190A*) exacerbait significativement la pénétrance des phénotypes observés chez les homozygotes uniques, tels que les ATN crâniennes, la polydactylie et l'anophtalmie. Un nouveau phénotype, spina bifida, qui n'a pas été retrouvé dans l'une ou l'autre des mutations homozygotes a été remarqué. Les souris doublement homozygotes présentaient une pénétrance de 100% de l'ATN, la polydactylie et l'anophtalmie. En ce qui concerne les anomalies rénales, nous avons trouvé une exacerbation significative de l'hypoplasie rénale et un nouveau phénotype (agénésie rénale) à mesure que les doses de gènes diminuaient. Ensemble, nos données ont démontré des liens moléculaires, génétiques et mécanistiques entre l'effecteur PCP Fuzzy et p190A RhoGAP. Nous proposons que Fuzzy et p190A participent au même processus génétique pour contrôler l'activité RhoA GTPase à la base du cil, et que le phénotype kystique hypoplasique chez la souris *Fuzzy*$^{-/-}$ peut être causé par l'activation inappropriée de RhoA dans le cil.

Acknowledgement

First and foremost, I would like to thank and express my sincere gratitude to my supervisor Dr. Elena Torban, for giving me this opportunity. From Dr. Torban I learned many valuable skills like project management, how to approach/critique a paper and how to be more concise. I am grateful for her continuous guidance, patience, enthusiasm, and support throughout this project. I would also like to thank members of my thesis committee, Dr. Paul Goodyer, Dr. Daniel Dufort and my academic advisor, Dr. Sushmita Pamidi for their helpful advice and critical input that helped to guide my progress in master program. I would like to extend my thanks to our collaborators and professors of the nephrology division, Dr. Maxime Bouchard, Dr. Andrey Cybulsky, Dr. Tomoka Takano, Dr. Serge Lemay for their help and equipment.

I would like to thank my friends and colleagues, Aiken Chung, Ida Derish, Nadezda Kachurina, Sima Babaveya and Tamara Sogomonian. I would like to especially thank Sima for helping me learn all the experiments and troubleshooting, that showed me a path in the lab, and for performing countless tasks that helped the lab run smoothly. I wholeheartedly appreciate and acknowledge the support and terrific help provided to me by all the members of nephrology department of McGill University. I am also thankful for the financial support provided by department of Experimental Medicine and MUHC - studentship scholarship.

Finally, I thank my grandmother Padma whom I dedicate this thesis. Thanks to my parents Nimisha and Naresh, and my kid sister Sammy for their love, encouragement, and unconditional support. I also thank Uncle Neeraj and Aunt Jyoti for all the help and moral support. I thank my friends Tanu, Iris, Anna, Mady, Adi, Pri, Mitsi, Nik and A.A for being there for me through this incredible journey. Last but not least I thank Manoj for his encouragement, support and for always making me laugh when science didn’t.

Author contributions

Sima Babaveya performed basal body Co-localization experiment and Co-IP assay to investigate the biochemical link between Fuzzy and p190A gene. Sima also performed ELISA to calculate the protein concentration in the urine of 6 months old double heterozygous mice. Nadezda Kachurina contributed to the staining and imaging of E14.5 kidney sections of *Fuzzy*$^{+/-}$*;p190A*$^{+/-}$ crosses. All other experimental work and analysis was carried out by Rhythm Sharma.

List of Abbreviations

ADP	Adenosine diphosphate
ADPKD	Autosomal dominant polycystic kidney disease
AMP	Adenosine monophosphate
ARPKD	Autosomal recessive polycystic kidney disease
ATP	Adenosine triphosphate
BBS	Bardet Biedl syndrome
BM	Branching morphogenesis
BMP	Bone morphogenetic protein
BSA	Bovine serum albumin
CAKUT	Congenital anomalies of the kidneys and urinary tract
CE	Convergent extension
Cited1	Cbp/P300 interacting trans activator with Glu/Asp rich carboxy-terminal domain1
CM	Cap mesenchyme
CPLANE	Ciliogenesis and planar polarity effector
CSB	Comma-shaped body
CXCL12	Stromal cell-derived factor 1/ C-X-C motif chemokine 12
CXCR4	C-X-C chemokine receptor type 4
DAPI	4’,6- diamidino-2-phenylindole
DBA	Dolichos biflorus agglutinin
Dgo	Diego
DMEM	Dulbecco's Modified Eagle's medium
DNA	Deoxyribonucleic acid
Dpc	days post coitum
Ds	Dachsous

DT	Distal tubule
ECM	Extracellular matrix
EGF	Epidermal growth factor
EGFR	Epidermal growth factor receptor
ELISA	Enzyme linked immunosorbent assay
ENU	*N*-ethyl-*N*-nitrosourea
ES	Embryonic stem
ESRD	End stage renal disease
Etv	ETS translocation variant
FBS	Fetal bovine serum
FC	Fibrocystin
Fgf	Fibroblast growth factor
FgfrL1	Fibroblast growth factor receptor like 1
Fj	Golgi ectokinase Four-jointed
Foxc2	Forkhead/winged helix transcription factors 2
FP	Foot processes
FRS2	Fibroblast growth factor receptor substrate 2
Fy	Fuzzy
Fz	Fritz
Fz	Frizzled
GAP	GTPase-activating proteins
GBD	GTPase-binding domain
GBM	Glomerular basement membrane
Gdnf	Glial cell line derived neurotrophic factor
GDP	Guanosine diphosphate

GEF	Guanine nucleotide exchange factor
GFL	Glial cell line derived neurotrophic factor family
GTP	Guanosine triphosphate
HETS	Heterozygous
HGF	Hepatocyte growth factor
HRP	horseradish peroxidase
IFT	Intraflagellar transport
IM	Intermediate mesoderm
In	Inturned
Jnk	c-Jun N terminal kinases
JS	Joubert syndrome
Lef/Tcf	Lymphoid-enhancing factor/T-cell factor
LH	Loop of Henle
Lhx1	The LIM (Lin11, Isl-1&Mec-3) homeodomain containing transcription factor 1
Lp	Looptail
LPM	Lateral plate mesoderm
LTA	Lotus tetragonolobus agglutinin
MAPK	Mitogen-Activated protein kinase
MET	Mesenchyme-to-epithelial transition
MIM	Monomer-binding protein
MKS	Meckel-Gruber syndrome
MLC	Myosin regulatory light chain
MM	Metanephric mesenchyme
mTOR	mechanistic target of rapamycin
Mwh	Multiple wing hair

MYPT1	myosin phosphatase-targeting subunit 1
NC	Nephric cord
ND	Nephric duct
NDS	Normal donkey serum
NGS	Normal goat serum
NPHP	Nephronophthisis
Nphs	Nephrosis
NTD	Neural tube defect
OCD	Orientation cell division
Osr1	Protein odd-skipped-related 1
Pax	Paired-box family transcription factor
PBS	Phosphate -buffered saline
PC1	Polycystin 1
PCP	Planar cell polarity
PCR	Polymerase chain reaction
PDGF B	Platelet-derived growth factor B
PFA	Paraformaldehyde
Pk	Prickle
PKC	Protein kinase C
PKD	Polycystic kidney disease
PLC	Phospholipase C
PM	Paraxial mesoderm
Pou3f3	POU-domain transcription factor
PPE	Planar polarity effector
PT	Proximal tubule

Ptch	Patched
RBP-J	recombination signal-binding protein Jk
RC	Renal corpuscle
RET	Receptor tyrosine kinase
ROCK	Rho-associated Coiled-coil Containing Kinases
RT	Renal tubule
RV	Renal vesicle
Sall1	Sal-like 1
SD	Slit diaphragm
Shh	Sonic hedgehog
Six1	Sineoculis homeobox homolog 1
Smo	Smoothened
SSB	S-shaped body
UB	Ureteric Bud
Vang	Van Gogh
VEGF	Vascular endothelial growth factor
WD	Wolffian duct
WT1	Wilm’s tumor protein 1

List of figures

List of Table

Chapter 1: Introduction

1.1 Kidney development

The mammalian urinary system is a vital system with cellular diversity and functional complexity to support organism's life. The urinary system consists of bilateral kidneys, each connected by a single ureter to a common bladder (**Figure 1.1**). The kidney functions to control the water and acid-base homeostasis, sodium and potassium ion balance to maintain pH and blood pressure and to allow the reabsorption of essential molecules and solutes required for the further maintenance of life (Costantini 2006). These functions are regulated by the glomerular filtration of blood, passage of water and solutes through the tubules of a nephron to selectively reabsorb ions, amino acids, sugars, etc., and to concentrate urine, which then exhausts into the collecting ducts and renal pelvis. From the renal pelvis, urine is excreted through the ureter to the bladder where it can be stored and then discharged out (Costantini 2006). A nephron is the functional unit of the kidney, with an average number of nephrons approximately 1 million per kidney ranging from 300,000 to 1.9 million depending on the individuals. As such, nephron number and functions are important contributors to determine the propensity for hypertension and chronic kidney disease (Pohl, Stuart et al. 2000).

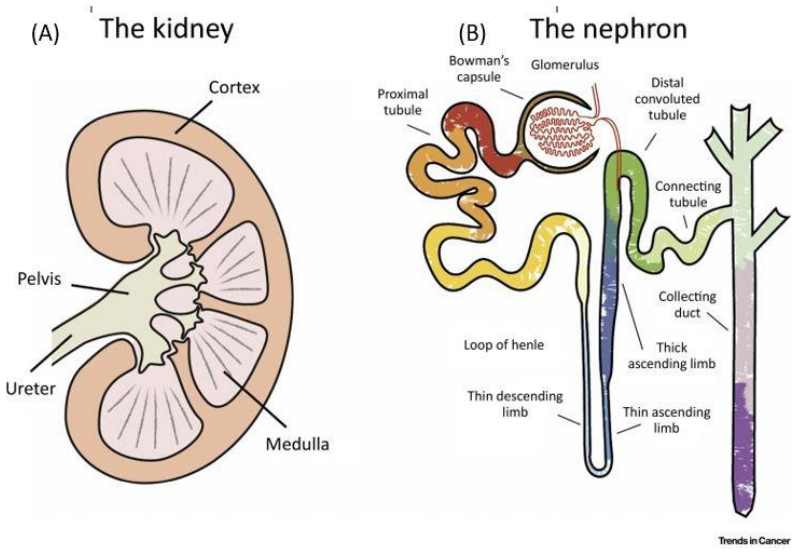

Figure 1.1. The adult mammalian urinary system

(A) The urinary system is comprised of the paired kidneys that regulate the solute and ion balance. The waste products are disposed into urine, which is collected in the pelvis of each kidney and then drained further to the bladder. (B) The functional unit of the kidney – nephron. Filtered solutes and water pass through the nephron segments to the collecting duct: the glomerulus, confined within Bowman's capsule, is positioned at he most proximal aspect of the nephron; the glomerulus is linked to proximal tubule, that is followed by the Loop of Henle (it includes descending thin limb and ascending thick limb), distal convoluted tubule and, finally, by the connecting tubule that links nephron with the collecting duct. Each nephron segment and the collecting duct tubule are characterized by selective permeability to water and express specific transporters, channels and receptors enabling retention and/or secretion of distinct sets of ions, acids, amino-acids, sugars, etc. *Reprinted with permission from (Lindgren, Sjolund et al. 2018).*

1.1.1 Initiation of kidney development

The classic work in kidney morphogenesis indicates that kidney development is regulated by reciprocal and sequential inductive mechanisms. The mammalian kidney development is initiated at embryonic (E) day 9.0 in mice and 5th week of gestation in humans. Three different kidneys sequentially develop: the pronephros, mesonephros, and metanephros. Only the metanephric kidney is maintained in adulthood in mammals, whereas the mesonephric duct, required for the formation of all three kidneys, later develops into the genital system in males (vas deferens and epididymis) or degenerates in females (Pohl, Stuart et al. 2000). The kidney is derived from the intermediate mesoderm (IM), that lies between the paraxial mesoderm and lateral plate mesoderm along the anteroposterior axis on both sides of the spinal cord. Cells of the dorsal IM epithelialize to form the dorsal pronephric duct, also known as Wolffian duct, while the ventral IM cells become nephric cord (NC) (**Figure 1.2**). NC is populated by future renal progenitor cells. Interaction between the nephric duct and nephric cord triggers the formation of the first transient kidney, the pronephros. In some fish and amphibians, the pronephros represents the permanent kidney that is functional in adult organisms (Dressler 1995). However, in mammals, the nephric duct (ND) continues to elongate caudally through cell migration and cell proliferation and induces the formation of a second kidney, the mesonephros. Unlike pronephros, which is non-functional and quickly degenerates in mammals, mesonephric tubules are well-developed with proximal glomerulus-like structures and convoluted tubules that empty directly into the nephric duct. The mesonephros serves as the main excretory organ in aquatic vertebrates such as fish and amphibians. Even though the pronephros and mesonephros represent transient organs in reptiles, birds and mammals, their formation is critical for normal development of the final, metanephric, kidney (Dressler 1995, Basson, Watson-Johnson et al. 2006, Little, Georgas et al. 2010).

Once the ND has reached the hindlimb level of the mammalian embryo, it becomes positioned in the vicinity of the adjacent metanephric mesenchyme (MM) within the NC and is involved in MM specification (**Figure 1.2**). The MM is a group of cells that consists of predetermined renal progenitor cells that will give rise to all segments of the nephron and other specific cell lineages, such as stromal cells and vascular pericytes (Little, Georgas et al. 2010). Several transcriptional factors, such as Lhx1 and Osr1, are important early players in the sequential signalling cascade that decides the fate of the NC cells that eventually become MM (Mugford, Yu et al. 2009, Little, Georgas et al. 2010).

Once the MM has formed, these cells send inductive signals that initiate the development of nephric duct outgrowth, which is known as the Ureteric Bud (UB). If the timing of ND elongation is delayed, this may affect the establishment and maintenance of MM and, as a result, the UB outgrowth may fail to form. Abnormal UB formation may lead to renal agenesis, unilateral or duplex kidneys and, in less severe cases, to an improper insertion of the ureter to the bladder, leading to vesicoureteral reflux. These abnormalities of early renal development cause human diseases known as "Congenital anomalies of the kidney and urinary tract" (CAKUT), which are among the most common congenital defects in humans, arising in 1 in 500-600 live births (Mugford, Yu et al. 2009, Little, Georgas et al. 2010).

At E9.0, the ND extends caudally along a stereotypical path to the cloaca. High-resolution imaging of mouse nephric duct illustrated that the cells at the tip of the elongating duct are highly dynamic and form multiple cytoskeleton-based protrusions, such as filopodia, that may sense the environment and direct cell migration (Chia, Grote et al. 2011, Soofi, Levitan et al. 2012, Atsuta, Tadokoro et al. 2013). Furthermore, it was observed in chick system that RhoA-mediated tail retraction of the migrating cells particularly contributes to the generation of the traction forces via

actin-based stress fibre formation, as RhoA inhibition may result in the disruption in the elongation of the nephric duct (Meyer, Schwesinger et al. 2006). However, other small GTPases may also be required to control cell protrusions, as overstimulation or inhibition of Rho signalling did not affect the cell behaviour of the ND tip cells (Atsuta, Tadokoro et al. 2013). The experiments in various animal models suggest a vital role of extracellular matrix proteins, such as fibronectin and laminin, in the migration of the nephric duct (Jacob, Christ et al. 1991, Morris, Drawbridge et al. 2003). However, the directional cues controlling the nephric duct elongation and descent are still unclear.

One of the most important signalling molecules that regulate outgrowth of the ureteric bud from the nephric duct is the glial cell line-derived neurotrophic factor (GDNF), which signals through its receptor RET (receptor tyrosine kinase) and co-receptor GFAR1 (Costantini and Kopan 2010) (**Figure 1.3**). The significance of GDNF-RET signalling in UB budding during mammalian kidney development was demonstrated in the mutation screen of CAKUT patients: heterozygous *RET* mutations were found in 5–30% of CAKUT patients that exhibited unilateral renal agenesis or smaller kidneys (Davis et al., 2014). The absence of UB outgrowth was observed in the mice with knockout of *Gdnf* and *Ret* (Schuchardt, D'Agati et al. 1994, Moore, Klein et al. 1996, Pichel, Shen et al. 1996, Sanchez, Silos-Santiago et al. 1996). *Gdnf* is expressed in the metanephric mesenchyme, while *Ret* and *Gfra1* are expressed in the nephric duct epithelium. *Gdnf* expression in the MM is highly regulated. Many transcription factors/transcriptional regulators are expressed in the MM such as the *Hox11* cluster (Wellik, Hawkes et al. 2002), *Pax2* (Brophy, Ostrom et al. 2001), *Eya1* (Sajithlal, Zou et al. 2005), *Sall1* (Kiefer, Robbins et al. 2010), *Six1* (Kobayashi, Valerius et al. 2008), *Six2* (Brodbeck, Besenbeck et al. 2004), and *Six4* (Kobayashi, Kawakami et al. 2007). These molecules were shown to regulate *Gdnf* expression. *Pax2 and Pax8* are some of the earliest known transcription factors that are expressed in the nephric duct and MM (Bouchard,

Souabni et al. 2002); *Pax2* is considered to be the master transcription factor that initiates the expression of nephron epithelial genes (Dressler 2011). Deletion of *Pax2* leads to a complete loss of kidneys due to failure of UB initiation; loss of *Pax2* also affects the expression of *Gdnf* in the MM (Dressler 2011). Signalling between the UB epithelium and extracellular matrix also impacts *Gdnf* expression within the MM, as the mouse mutants for the extracellular matrix genes nephronectin (*Npnt*) and integrin genes *Itga8* and *Itgb1* (the products of these genes form α8β1) display severe renal defects along with a disrupted *Gdnf* expression in the MM at the time of UB outgrowth (Linton, Martin et al. 2007). Furthermore, mice lacking *Gdf11*, encoding a transforming growth factor β *(*TGFβ*)*-family ligand, exhibit kidney agenesis, which was shown to be the result of the loss of *Gdnf* expression in the metanephric mesenchyme (Jiang, Seo et al. 2003). The Lhx1, a LIM-homeodomain containing transcription factor, acts downstream of Pax2; it is necessary for the nephric duct epithelial maintenance but is not required for the nephric duct formation. Conditional knockout of *Lhx1* in mice leads to an extreme reduction in the expression of Wnt9b (one of the 19 known Wnt ligands) and E-cadherin (the major structural component of adherens junctions), suggesting that differentiation of the nephric duct epithelium may be blocked (Drews, Senkel et al. 2011). In *Lhx1*$^{-/-}$ mouse mutants, a stunted ureteric bud is formed (Drews, Senkel et al. 2011).

Several negative regulators of *Gdnf* expression and signalling play a critical role during the commencement of kidney development. Such negative regulatory loops are necessary for inhibiting ectopic UB budding, thereby ensuring the emergence of only a single UB outgrowth from the nephric duct in response to the signals from the MM. Embryo deficient for *Gata3* gene, that encodes transcription factor Gata3, in the nephric duct displays the ectopic UB budding, as Gata3 participates in specifying the location of UB outgrowth (Grote, Boualia et al. 2008).

Together with retinoic acid signalling, Gata3 is required for *Ret* expression in the nephric duct (Chia, Grote et al. 2011). Mouse embryos lacking *Ret* gene and retinoic acid synthesis enzyme *Raldh2* fail to form a proper insertion of nephric duct to cloaca (Grote, Boualia et al. 2008, Chi, Michos et al. 2009). Slit2-Robo2 and Foxc2 transcription factors are expressed in the metanephric mesenchyme; their genetic excision permits an expansion of Gdnf signalling domain, which affects ureteric bud outgrowth from the nephric duct and leads to a duplication of the ureteric bud, hydroureter, or renal hypo-dysplasia. (Kume, Deng et al. 2000, Grieshammer, Cebrian et al. 2005). In contrast, Spry1, a negative regulator of Gdnf-Ret signalling, modulates the response of UB epithelial cells to Gdnf levels and, thus, prevents supernumerary UB outgrowths along the length of the nephric duct (Chi, Zhang et al. 2004, Basson, Akbulut et al. 2005). Bone morphogenesis protein 4 (BMP4*)* and its antagonist gremlin 1 (GREM1) also ensure that only one UB arises from the nephric duct, although the mechanism remains elusive (Michos, Cebrian et al. 2010). Fibroblast growth factor (FGF) signalling pathway also plays a role in proper positioning and outgrowth of the UB from the nephric duct (Michos, Cebrian et al. 2010, Bates 2011). Fgf10, a FGF signalling ligand, is expressed in the MM. A fraction of E11.5-E12.5 *Fgf10*$^{-/-}$ mutant mice exhibits renal agenesis due to UB absence (Michos, Cebrian et al. 2010). Interestingly, excision of the FGF receptor gene 2 (*Fgfr2)* from the MM resulted in the opposite effect with a majority of mutants displaying multiple UB outgrowths (Hains, Sims-Lucas et al. 2008). Surprisingly, the expression of Gdnf and the known negative regulators of Gdnf signalling were not affected in these mutants, so the exact mechanism of action is not well understood (Jeanpierre, Mace et al. 2011). Taken together, these findings demonstrate that the finely tuned balance between various signalling pathways during early steps of kidney development is required to ensure the proper level/domain of Gdnf and RET expression so that one and only one ureteric bud outgrowth forms from the

nephric duct. It also highlights the importance of the initial UB outgrowth event for proper metanephric kidney development, and the central role of GDNF-RET signalling in its regulation (Jeanpierre, Mace et al. 2011). The properly formed UB induces nephrogenesis in the adjacent predetermined MM via sequential reciprocal tissue interactions between MM and UB branches.

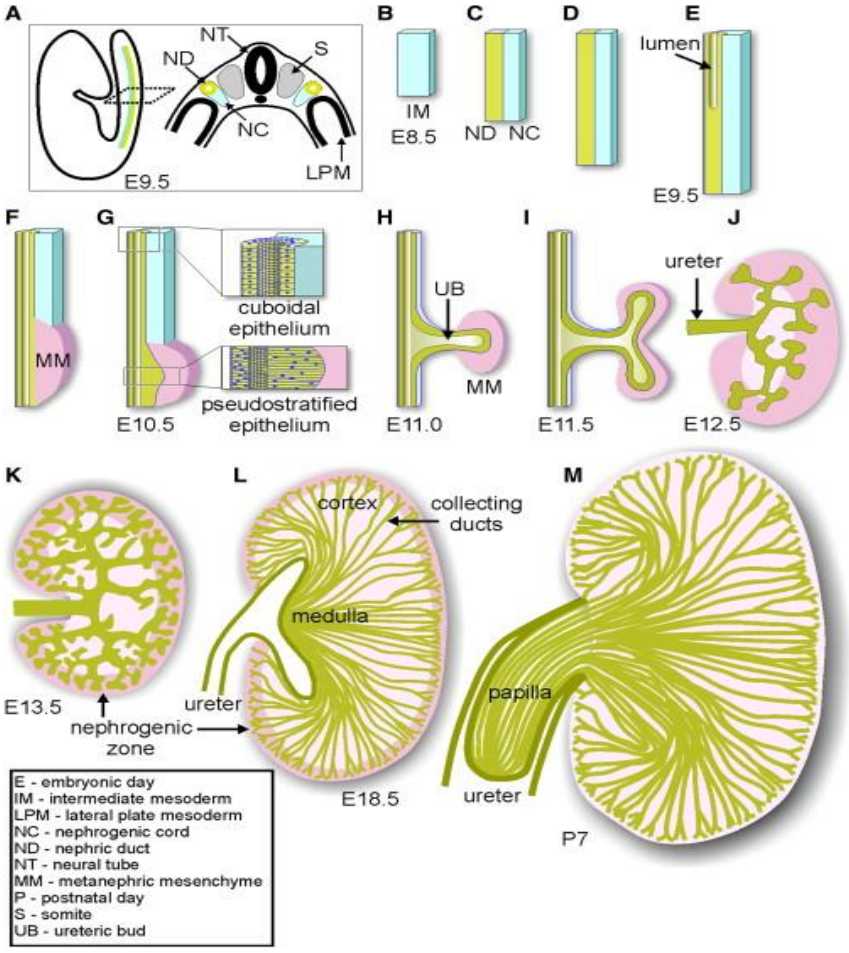

Figure 1.2 Nephrogenesis and renal collecting duct system

(A). E9.5 mouse embryos: in green - ND (nephric duct), blue - NC (nephric cord); NT - neural tube, S - somites, LPM -lateral plate mesoderm. (B) IM - intermediate mesoderm in ~E8.5 mouse embryo. (C) Development of nephric duct and nephric cord. (D) Elongation of nephric duct. (E-F) Nephric duct epithelialization and induction of metanephric mesenchyme, MM. (G) Development

of pseudostratified epithelium in caudal ND where UB will soon form, while rostral side of ND is populated by cuboidal epithelium. (H) At E11, initiation of UB outgrowth and interactions with MM. (I) At E11.5-12.0, the first UB branching event is regulated by the signalling from the MM cells. (J) At E12.5, 4-5th generation of UB branching; in dark pink are the nephrogenic cells localized in the cortical layer, these cells are recruited by the UB and give rise to all nephron segments; in light pink – stromal cells. (K) Latter stage of UB branching showing progressive UB branching. (L) At E18.5, the division between cortical collecting duct (CD) and medulla is established; the medulla is formed by coalescence of the UB trunks. (M) Post-natal CD elongation leads to the formation of papilla. *Reprinted with permission from (Costantini and Kopan 2010).*

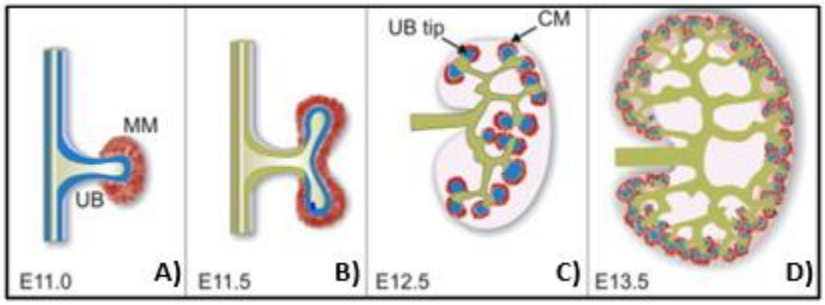

Figure 1.3. Gdnf and Ret signalling regulates UB outgrowth and branching

Blue: *Ret* expression; Red: *Gdnf* expression; Green: branching UB. (A) At E11.0, *Ret* is expressed in the nephric duct and the forming UB; the *Gdnf* is expressed in the MM. (B) The initial outgrowth of UB from the ND and invasion of UB into MM. Note that *Ret* expression becomes confined only to the branching UB. (C) 4-5th generation of UB branching. *Ret* is now expressed only at the tips of the UB; *Gdnf* expression becomes localized to the nephrogenic cells surrounding each UB tip (cap mesenchyme, CM). (D) *Ret-Gdnf* expression continues to localize to the UB tip/CM cells for as long as nephrogenesis continues (in mice ~ up to 7-10 days postnatally). *Modified and reprinted from (Riccio, Cebrian et al. 2016).*

1.1.2 Ureteric bud branching morphogenesis

At ~E11.0-12.5, the UB invades the MM as it elongates and undergoes branching morphogenesis in response to the factors secreted by the MM cells (Blake and Rosenblum 2014). The first event of UB bifurcation leads to a T-shaped bud with the UB tip and UB stalk (**Figures 1.2 and 1.3**). The cells of the UB tip are bi-potential progenitors; some of the cells proliferate promptly and form the ampulla that acts as a repository for the upcoming generation of branches; meanwhile, the daughter cells remain behind and contribute to the UB stalk. During this event, two genetically distinct UB cell domains are formed with the gene expression patterns of the cells from the UB tip being differently compared to the cells of the UB trunk. The Ret-expressing cells migrate to the UB tip and contribute to repetitive UB branching morphogenesis. The other domain is populated by the Ret-deficient cells, which are present in the UB trunk. The trunk cells of the initial UB are localized outside of the MM and will eventually participate in the development of the ureter. The UB tip cells remain fast-proliferating, undifferentiated cells, and express specific genes such as *Ret, Gfra1* or *Wnt11* (Majumdar, Vainio et al. 2003). It appears that trunk cells start expressing *Wnt7b* and other characteristic markers of the mature collecting duct. At ~E12-E13, branching UB starts to form an arborized collecting duct tree in a very stereotypical geometry. At E15.5, UB tree has formed more than 300-500 branches, and, by this stage, the rate of branching has somewhat slowed down and become more random. UB branching morphogenesis does not follow a predefined program unlike observed in the pulmonary branching morphogenesis (Blake and Rosenblum 2014). Instead, 10th-11th generations of branches are generated with 3 different branching morphologies: tip-specific bifid branching, tip-specific trifid branching and stalk-specified lateral branching. Bifid branching is the most common branching mode and occurs ~75% of the time, followed by trifid branching at ~18% and lateral branching at only ~6% of the time in

a mouse kidney explant model (Blake and Rosenblum 2014). Later, the trunks of the UB give rise to the collecting duct system (Blake and Rosenblum 2014). The key molecular mechanisms that govern this stereotypical branching pattern are not completely elucidated, however, appropriate spatiotemporal patterning requires growth factor signals from the surrounding mesenchyme and stroma. Positive regulators of branching include the secreted molecules GDNF, FGFs, HGF, EGF, Wnts which signal to their cognate receptors expressed in the UB tip epithelium to activate different downstream signalling pathways (Kispert, Vainio et al. 1996, Majumdar, Vainio et al. 2003, Shakya, Watanabe et al. 2005). Similar to the initial UB formation, positive receptor activation is achieved by a concomitant negative regulation of BMP4 and semaphorins (Miyazaki, Oshima et al. 2003, Tufro, Teichman et al. 2008). This process triggers the BMP4 antagonist Cer1, to regulate the negative feedback and to allow fine-tuning of the UB branching pattern (Basson, Watson-Johnson et al. 2006). The appropriate amount of Ret leads to the activation of PLCγ, PI3K and Erk-MAPK signalling pathways (Kurtzeborn, Kwon et al. 2019). Interestingly, any disruption in these pathways also affects the UB branching morphogenesis. Moreover, three major cellular pathways are known to be involved in the UB tree branching: ureteric cell proliferation (Michael and Davies 2004), planar cell polarity-dependent cell organization (Lienkamp, Liu et al. 2012) and a novel mitosis-dependent cellular process (Packard, Georgas et al. 2013). The formation of the tubular diameters and development of collecting duct are controlled by intrinsic mechanisms such as oriented cell division, changes of cell shape and convergent extension. Oriented cell division (OCD) refers to the orientation of mitotic spindles in the dividing cells parallel to the tubular axis. The convergent extension (CE) describes the directional cell movement and cell intercalation during tubular elongation. OCD and CE are regulated by the planar cell polarity pathway, at least in some tissues (Karner, Chirumamilla et al. 2009). OCD is regulated by Wnt ligand Wnt7b. Mice

with a homozygous loss of *Wnt7b* fail to develop proper medulla and pelvis leading to the abnormally short and wide collecting ducts. In the *Wnt9b* mutants, the orientation of elongated tubular cells and their intercalation in embryonic renal tubules are abnormal, indicating a deficient CE during tubular elongation (Karner, Chirumamilla et al. 2009, Yu, Carroll et al. 2009).

1.1.2.1 Role of actin cytoskeleton dynamics during kidney development

Although significant information about the UB branching morphogenesis has been acquired, the cellular behaviours involved in UB formation remain unclear. Regulation of UB branching morphogenesis firmly suggests that actin cytoskeletal rearrangements are involved in the motion of ampulla cells to allow bifid branch formation (Pohl, Stuart et al. 2000, Meyer, Schwesinger et al. 2006). Pharmacological disruption of F-actin polymerization or Rho-ROCK mediated actomyosin contractile fibre formation results in a distorted shape of the UB tip and fewer branches (Meyer, Schwesinger et al. 2006). Genetic ablation of actin depolymerization factors *Cofilin1 (Cfl1)* and *Destrin (Dstn)* in double knockout mice results in the disruption of cell shape, cell organization, cell migration, and significant delay in UB branching morphogenesis, but leads to a stabilisation of F-actin polymerization (Kuure, Cebrian et al. 2010), suggesting that timely and spatially-regulated actin dynamic is instrumental for the UB branching events. The mutants with UBs lacking *Ret* expression, however, exhibit normal F-actin, indicating that the cytoskeleton arrangement is rather independent of Ret signalling, or that alternative tyrosine kinase receptors might sufficiently contribute to and/or compensate functionally for Ret deficiency to allow appropriate cytoskeleton arrangement during UB branching morphogenesis. Overall, understanding the role of actin polymerization in the UB branching requires future studies.

1.1.3 Nephron induction, segmentation, and patterning

It has been demonstrated that interactions between the ureteric bud and metanephric mesenchyme are critical for normal kidney development. The MM gives rise to the nephron epithelia via mesenchyme-to-epithelial transition (MET), and is a precursor to all segments of nephron including glomerulus, proximal tubule, the loop of Henle, and distal convoluted tubules (Little, Georgas et al. 2010) (**Figure 1.4**). The MM is composed of two progenitor populations: 1) the cells immediately adjacent to the UB tip, known as "cap mesenchyme", populated by the nephron progenitors that express a combination of Six2 and Cited1 transcription factors, as well as GDNF; 2) the cells localized further away from the UB tip. These cells will form the stromal/interstitial progenitor lineage that is marked by Foxd1 transcription factor (Yu, Carroll et al. 2002, Airik and Kispert 2007) (**Figure 1.4**). The nephron progenitor population is sandwiched between the UB epithelia and the peripheral stromal progenitors, responds to the signals from both to control the balance between its self-renewal and differentiation (Carroll, Park et al. 2005, Kobayashi, Valerius et al. 2008). The progenitor pool is first expanded while maintaining multipotency, and then becomes gradually depleted with successive rounds of UB branching and nephron induction by the growing number of forming UB tips supporting continuous nephrogenesis at the outer layer of the cortex (nephrogenic zone) (Basson, Akbulut et al. 2005). The CM can be subdivided into two domains: a) the committed mesenchyme situated above the UB tip and b) induced mesenchyme located in the armpit of the UB tip. The induced mesenchyme further evolves through the MET to form nephrons (Mugford, Yu et al. 2009, Costantini and Kopan 2010). To control the continued nephrogenesis during kidney development, committed CM endures sufficient self-renewal to generate nephrons and to increase in number. Six2 is not only a good marker of CM but is an essential protein for CM self-renewal, simultaneously suppressing

differentiation. *Six2* deficient kidneys rapidly deplete their progenitor cells leading to the formation of smaller, hypoplastic kidneys (Self, Lagutin et al. 2006). Additionally, the survival and maintenance of the progenitor pool require secretion of specific factors from the UB, such as FGFs, BMPs and Wnts (Krause, Rak-Raszewska et al. 2015). Transcription factor Wilm's Tumor gene 1 (WT1) is expressed in the undifferentiated MM at the low level as well as in the podocyte progenitors at a higher level. However, the role of the *Wt1* gene in the maintenance of the progenitor cells is critical since the entire MM dies of apoptosis in the absence of *Wt1*, which leads to renal agenesis (Sim, Smith et al. 2002).

The differentiated progenitor cells undergo MET to initially form pre-tubular aggregates and then to become polarized along the apical-basal axis, forming renal vesicle (RV) with a lumen at the apical surface (inside) (**Figure 1.4**). The signals from the UB tip, in particular canonical Wnt ligand Wnt9b, which activates Wnt4 expression, elicit several responses within the nephron progenitor population (Carroll, Park et al. 2005, Karner, Das et al. 2011). Wnt4 is detected in the peritubular aggregates and required for the early nephron differentiation. Loss of *Wnt4* gene leads to the failure of nephron differentiation, which is halted after the formation of pre-tubular aggregates (Halt and Vainio 2014). Thus, canonical Wnt signalling is required to maintain the progenitor population, but it also simultaneously commits a proportion of the progenitor cells to differentiate, thus serving as a molecular rheostat to balance progenitor number with nephron induction (Karner, Das et al. 2011). BMP7 is required for CM survival (Tomita, Asada et al. 2013). However, canonical Smad signalling induced by BMP7 suppresses self-renewal while BMP7-mediated signalling via Jnk kinase is required for CM self -renewal. In addition, molecules from Foxd1+ stromal cells, including the atypical cadherin Fat4, cooperate with Wnt9b to antagonize nephron progenitor renewal and promote appropriate differentiation (Mao, Francis-West et al.

2015). Loss of *Fat4* in stroma or loss of Fat4 ligand *Dachsous* in nephron progenitors leads to a dramatic expansion of progenitor cells that are abnormally wired and therefore cannot participate in normal nephrogenesis (Mao, Francis-West et al. 2015).

1.1.3.1 Nephron fate specification

The first evidence of regional fate specification within a future nephron becomes evident during renal vesicle (RV) formation and is seen along a proximal-distal axis. The RV starts to disentangle to form the comma-shaped body (CSB) and then S-shaped body (SSB) (**Figure 1.4**). Further differentiation and patterning of SSB lead to a mature nephron. At the most distal end, early SSB fuses with UB tip to form a continuous lumen between the nephron segments derived by MET and a branch of collecting duct. The proximal-distal axis is thought to form in response to a classic Wnt9b morphogen gradient in which those cells nearest to the ureteric tip upregulate Wnt4 and Wnt4 target gene *Lhx1;* the latter is necessary for the formation of the end of nephron that will fuse with the UB (Halt and Vainio 2014). On the contrary, those cells furthest from the Wnt9b source express *Lhx1* at lower levels and instead adopt a proximal fate (Halt and Vainio 2014). Complete loss of *Lhx1* in the RV results in a proximal-most Bowman's capsule fate; in such scenario, the proximal fate would seem to be the default (Drews, Senkel et al. 2011). Thereafter, the transcriptional program established by Lhx1, which includes the expression of the Notch ligand Dll1 and the transcription factor Brn1, is essential to distinguish distal vs proximal components (Kobayashi, Kwan et al. 2005, Potter, Hartman et al. 2007, Liu, Chen et al. 2013). The diverged expression of these signalling molecules along the proximal-distal axis is maintained as the RV grows and sequentially converts into a comma- and S-shaped bodies. Several distinct combinations of signalling pathways and transcription factors subdivide the S-shaped body into

an upper, mid and lower limbs. The upper limb gives rise to distal convoluted tubule, specified by the *Lhx1* and *Hnf1b* target gene, *Brn1,* in combination with *Lrg5*, a G-protein coupled receptor that upregulates canonical Wnt signalling (Nakai, Sugitani et al. 2003). The distal region is also responsible for establishing a luminal connection with the differentiating UB tip, which seems to occur through a local increase in proliferation. The medial region of the S-shaped body is further subdivided into proximal and intermediate regions that form anlagen for the Loop of Henle and proximal tubules, respectively. Many transcriptional programs established by Lhx1 and Hnf1b help in the regionalization of these structures, leading to the upregulation of Brn1, Irx1/2 and Osr2 transcriptional factors and establishing the intermediate region (Nakai, Sugitani et al. 2003, Heliot, Desgrange et al. 2013). On the contrarily, in the proximal region, Lhx1 and Hnf1b activity led to the upregulation of Notch ligands Dll1, Jag1 and Lnfg that activate Notch2-dependent signalling required for a proximal tubule fate (Heliot, Desgrange et al. 2013). Notch signalling, together with transcriptional factor WT1, is necessary to establish the podocyte lineage in the most proximal part of the S-shaped body (Palmer, Kotsianti et al. 2001, O'Brien and McMahon 2014).

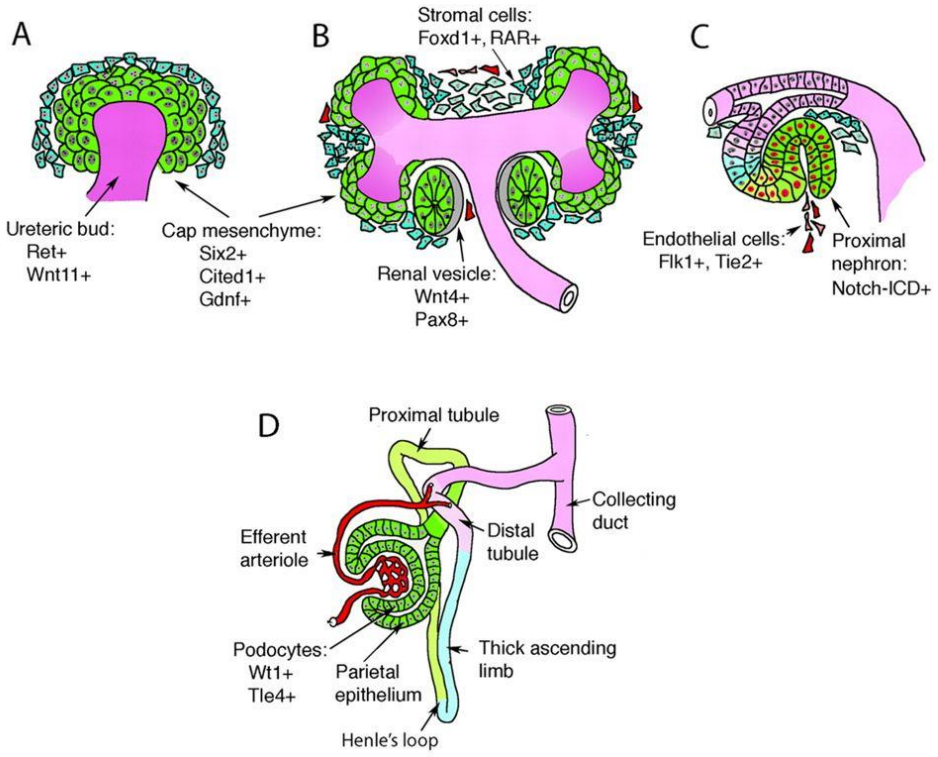

Figure 1.4. Formation of nephron and specification of nephron segments

Green: metanephric mesenchyme; purple: ureteric bud; light blue: stromal cells. (A) In response to the signal secreted by the UB tip cells, MM cells condense around the UB tip at ~E11.5 to become "cap mesenchyme" (CM); CM cells express Six2, Gdnf and Cited1. (B) CM cells undergo mesenchyme-to-epithelial transition to form renal vesicle with a visible lumen; renal vesicle expresses Wnt4 and Pax8; the MM cells above CM express Foxd1 and retinoic acid receptors; these cells participate in the formation of stromal cells. (C) Renal vesicle further changes shape and elongates to form comma- and S-shaped body (shown); the latter is subdivided into distal, mid and proximal segments expressing various markers. Activation of Notch signalling in the proximal S-shaped body is critical for specification of proximal tubule and glomerulus. Endothelial cells positive for expression of Flk1 and Tie2 migrate to the cleft of the S-shaped body to initiate development of the glomerular capillary tuft. (D) Mature nephron structure: vascular glomerular

tuft is enveloped by the glomerular podocytes expressing WT1 and TLE4 and is enclosed within Bowman's capsule lined by the parietal epithelial cells. Bowman's capsule is fused with the proximal tubules allowing transfer of the glomerular filtrate directly to the tubular nephron segments. The proximal tubule connects to the Loop of Henle, and distal convoluted tubule, which is fused with the collecting duct. *Reprinted and modified with the permission of (Dressler 2009)*

1.1.4. Glomerular morphogenesis

Glomerular development is a complex process that is dependent on the differentiation programs within the epithelia of the S-shaped body and signalling between the epithelia and the cells of the future glomerular capillary. The proximal end of the S-shaped body forms epithelial components of the glomerulus, which are further stratified into visceral epithelial cells (a.k.a. podocytes) and parietal epithelial cells that line Bowman's capsule (**Figure 1.5**). The main feature of developing podocytes is the formation of unique actin-based cellular protrusions, podocyte foot processes (FPs). FPs from neighbouring podocytes interdigitate in a strict one-by-one manner. The mature podocytes become suspended in the urinary space. The FPs are connected via the slit diaphragms (SDs), unique cell-cell junctions that represent a modification of both adherens and tight junctions. Hence, some molecules from both types of epithelial cell junctions are found in the SDs. The SDs play several roles: a) act as podocyte cell-cell junctions; b) function as size-specific sieves that filtrate the blood; c) as signalling complexes connecting podocytes along underlying capillary (Schell, Wanner et al. 2014). Notch signalling plays an important role in podocyte development and upregulates the expression of WT1, Pod1 and Mafb transcription factors. Together, these transcription factors decide the fate of podocyte lineage by controlling an expression of crucial components of the slit diaphragm, which include nephrin, podocin and

synaptopodin (Schell, Wanner et al. 2014). Importantly, at the S-shaped body stage, the cleft-like structure is formed adjacent to the podocyte precursors where the endothelial progenitors appear, contributing to the formation of a single capillary loop. The simple capillary loop subsequently matures into 7-9 capillary loops leading to a mature glomerular capillary tuft.

During glomerular development, in addition to podocytes, two other cell lineages are found in the mature glomerular space, namely the endothelial and mesangial cells. Endothelial cells are separated from podocytes and mesangial cells by the glomerular basement membrane (GBM), a thick layer of the extracellular matrix that is produced by both endothelium and podocytes. Regulated by WT1 and Notch signalling, podocytes secrete VEGF (vascular endothelial growth factor), which supports endothelial migration, proliferation, and survival. VEGF also serves as a chemoattractant for the endothelial Flk1+ precursor cells (Herzlinger and Hurtado 2014). *Semaphorin 3a* expressed in podocytes repels endothelia; overexpression of Sema 3a leads to apoptosis of endothelia resulting in fewer endothelial cells in the glomerulus (Schell, Wanner et al. 2014). Collectively, these data suggest that podocytes control both endothelial components and GBM during glomerular formation.

Many genes are essential for glomerular development. They encode molecules that mediate the maturation of the glomerulus from a single capillary-loop stage into a mature, looped capillary tuft. Platelet-derived growth factor B (PDGF B), secreted by endothelia, and PDGF-receptor β, expressed by mesangial cells, regulate the capillary maturation (Ostendorf, Boor et al. 2014) (Herzlinger and Hurtado 2014). Similarly, disruption of RBP-J, the main Notch signalling transcriptional transducer, results in an absence of mesangial cells and aneurysm-like glomerular capillaries (Herzlinger and Hurtado 2014). Moreover, CXCL12 (Stromal cell-derived factor 1/ C-X-C motif chemokine 12), a high-affinity ligand for CXCR4, is expressed in mesangial cells,

podocytes and in endothelial cells and regulates migration of the latter (Takabatake, Sugiyama et al. 2009, Herzlinger and Hurtado 2014). Mutations in *Vangl2*, a planar polarity gene, result in delayed glomerular development and abnormal actin regulation within podocytes (Yates, Papakrivopoulou et al. 2010, Babayeva, Zilber et al. 2011, Rocque, Babayeva et al. 2015). Targeted loss or spontaneous mutations of the genes that encode SD proteins lead to dramatic changes of podocyte shape, widening or loss of FPs (a process known as FP effacement) and a partial or complete disruption of SDs culminating in the leaking of plasma proteins into Bowman's capsule and then to the urine – condition known as proteinuria (Herzlinger and Hurtado 2014). Effaced podocytes are easily lost into urinary space and are replaced by a scarring tissue that reduces glomerular filtration function and may eventually lead to a significant or complete loss of filtration and end-stage kidney disease (Wickman, Afshinnia et al. 2013, Herzlinger and Hurtado 2014).

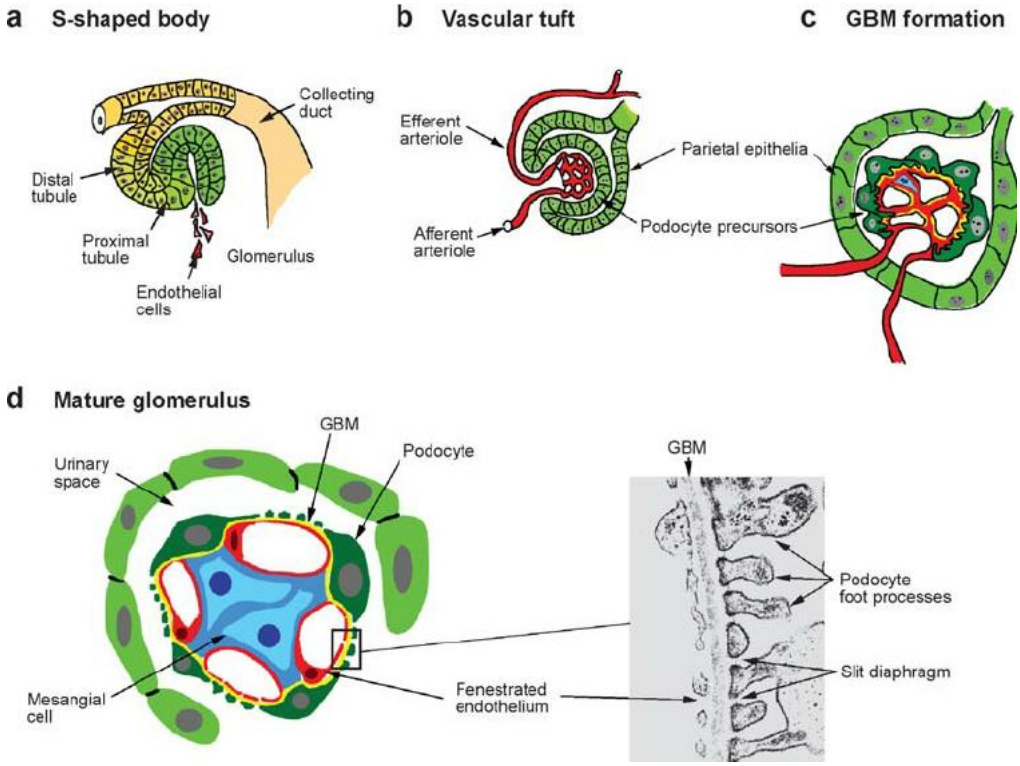

Figure 1.5. Glomerular Morphogenesis

(A) Vascular tuft formation is initiated when endothelial cells are attracted into the cleft of the S-shaped body. (B) Mature glomerulus is characterized by the presence of a multi-looped glomerular capillary; the efferent arteriole (entry point into glomerular tuft) and afferent arteriole (exit end from the glomerular tuft). (C) A magnified drawing of glomerular structure with podocytes enveloping underlying glomerular capillaries; glomerular basement membrane (yellow) is formed between the endothelial cells and podocytes. (D) Cross-section of mature glomerulus, depicting the endothelia capillary cells (red), GBM (yellow), mesangial cells (blue), podocytes (dark green), and parietal epithelial cells (light green). High magnification electron micrograph shows the glomerular cross-section: fenestrated endothelium, GBM and interdigitated FPs on the urinary side. The gaps between adjacent FPs indicate the presence of intact slit diaphragms.

Reprinted and modified with permission from (Dressler 2006).

1.2 Planar cell polarity pathway

The polarization of the cells along the plane of the tissue perpendicular to the apical-basal polarity axis is termed Planar Cell Polarity (PCP). It is the property of multicellular tissues that is required for coordinated cell behaviours along the tissue axis (Gubb and Garcia-Bellido, 1982). The PCP pathway controls multiple cellular behaviours including directional cell movements and oriented cell divisions, that are critical for the morphogenesis of various tissues and organs (Lawrence et al., 1972; Vinson et al., 1989).

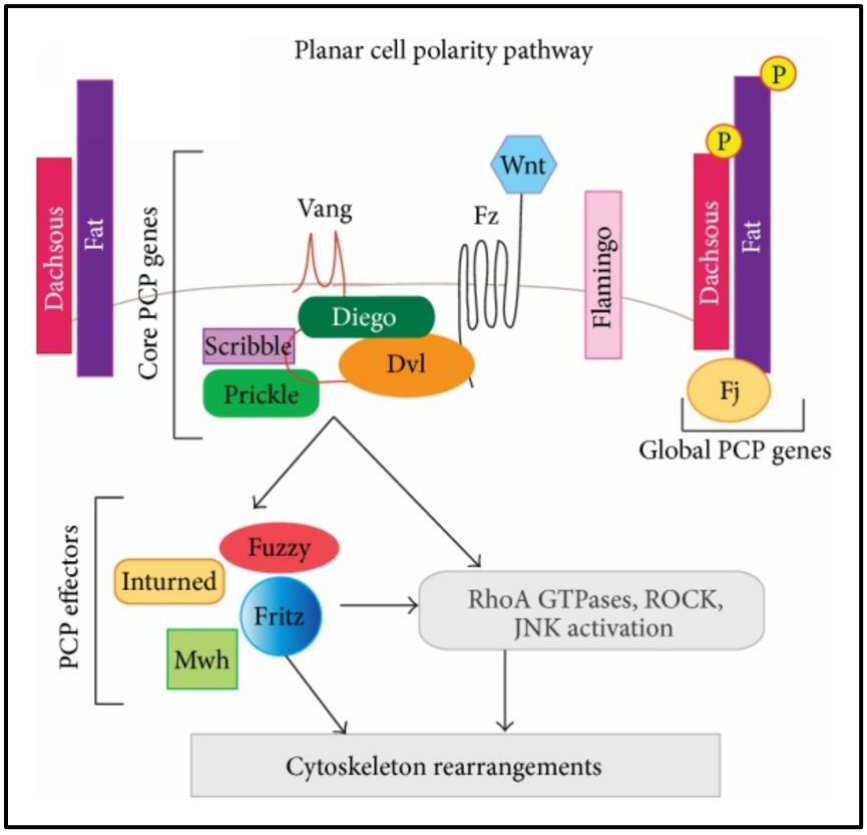

Figure 1.6 Planar cell polarity pathway

PCP signalling is activated upon binding of certain Wnt ligands to the Frizzled receptors. The activation results in asymmetric distribution of core PCP proteins Van Gogh (Vang) and Prickle (Pk) to the proximal domain and Dishevelled (Dvl) and Fz to the distal cellular domain. Cadherin Flamingo is found at both cell sides where it serves to stabilize transmembrane proteins Vang and

Fz at the cell surface by interacting with both of them. Inside the cell, cytoplasmic proteins Pk, Dvl, and Diego amplify Vangl and Fz distribution to the opposite cell sides. Atypical cadherins Fat (Ft) and Dachsous (Ds) form heterotypic complexes found at both sides of cells. Golgi kinase Four Jointed (Fj) regulates the strength of the Ds-Ft complex by phosphorylating Ft and Ds. PCP effectors Inturned, Fuzzy, Fritz and Multiple wing hair (Mwh) act to contain actin polymerization at the proximal side of the cell. Additional downstream effectors such as Rho GTPases, ROCKs and Jun kinase, participate in PCP signalling in some but not all tissues to regulate actin rearrangement that leads to changes in cell shape, cell motility, orientation of cell divisions and other processes. *Reprinted from (Torban 2015)*

1.2.1 PCP in Drosophila

PCP was initially discovered in *Drosophila melanogaster* almost 40 years ago where it is seen as the uniform arrangement of small actin hairs on each wing cell; all hairs point uniformly towards the distal wing margin. PCP is also observed as the asymmetric, uniform arrangement of photoreceptor cells within each ommatidium in the compound fly eye. (Adler 2002). A mature *Drosophila* wing is the best-characterized model system for studying PCP. Each wing cell produces a single actin-rich protrusion known as a 'trichome'. Each trichome is polarized along the proximal-distal axis and is positioned at the posterior wing cell margin. During larva development in flies, the wing develops from a single-layered epithelium known as wing imaginal disc. Wing hair formation begins when actin and microtubule-rich aggregates localise at the distal apical surface of each wing imaginal disc cell. The actin and microtubule polymerization in each aggregate leads to the formation of microvilli and, later, of the pre-hair, which grows at the distal end of each cell (Garcia-Bellido and Merriam 1971). The subcellular point of pre-hair initiation is polarized within a plane and mutations in the genes that regulate PCP lead to changes in the number and localization of pre-hair per cell. In specific PCP mutants, single or multiple trichomes may arise at the centre or periphery of the cell, and the trichomes are not uniformly aligned along the wing axis (Adler 2002, Aigouy, Farhadifar et al. 2010).

Several PCP genes have been identified in *Drosophila* by genetic and phenotypic screenings (Garcia-Bellido and Merriam 1971). These screenings were instrumental in revealing a conserved mechanism for generating PCP in cells and tissues, i.e Frizzled-dependent PCP pathway (Adler 2012). Based on their unique characteristics, the PCP components are assembled into three groups: the core, the global and the effectors. These groups are aligned in the two major systems contributing to PCP signalling: the "global" Fat/Dachsous system (a.k.a. Ft/Ds signalling)

and the "core" PCP system (a.k.a Frizzled/Fmi (Fz/Fmi) system). The link between the two remains elusive. The core PCP protein components comprise of 6 proteins: the seven-pass transmembrane receptor Frizzled *(*Fz*)*, the atypical cadherin Flamingo/Starry night *(*Fmi/Stan*)*, the tetra-transmembrane-spanning protein Van Gogh/Strabismus (Vang/Stbm*)*, the cytoplasmic modular PDZ domain-containing protein Dishevelled (Dsh/Dvl), the cytoplasmic protein Prickle (Pk), and cytoplasmic protein with ankyrin repeats Diego (Dgo) (Adler, 2002) (**Figure 1.6**). Since the PCP protein network includes Frizzled and Dishevelled (these proteins have been previously associated with Wnt/β-catenin pathway), the core PCP proteins are considered to be the components of the "non-canonical Wnt/PCP" pathway. When a Wnt ligand binds to the Frizzled/Lrp receptor complex during canonical Wnt/β-catenin signalling, this activates the protein Dvl and leads to disassembly of the β-catenin destruction complex. When a stabilized β-catenin then enters the nucleus, it regulates the transcription of specific downstream targets through LEF/TCF transcription factors. The canonical Wnt signalling controls cell proliferation and differentiation in various tissues in flies and many other organisms (Clevers 2006). However, non-canonical Wnt signalling does not rely on β-catenin, but instead activates RhoA-dependent actin polymerization and, in general, leads to cytoskeleton rearrangement (Peng, Han et al. 2012, Carvajal-Gonzalez and Mlodzik 2014) (**Figure 1.6**).

The planar polarity in an individual cell is established via asymmetric distribution of the core PCP proteins: Fz, Dsh and Dgo accumulate on the distal side of the cells, while Vang and Pk assemble on the proximal side of the cells (**Figure 1.7**). Atypical cadherin Flamingo is an essential component which is found on both distal and proximal sides of each cell. Extracellular domains of Fmi molecules from the neighbouring cells form homodimers across the cell-cell junctions linking together adjacent cells. Fmi binds to and helps stabilize both Fz and Vang proteins at the

plasma membrane. Once the Fz and Vang are recruited to the opposite sides of the cell's plasma membrane, their extracellular domains form heterodimers in the extracellular space between the adjacent cells; this event further stabilizes their asymmetric distribution to the opposite facets of the cell. However, this arrangement is insufficient for formation of robust PCP patterns within the plane (Lu, Schafer et al. 2015). Inside each cell, the cytoplasmic PCP components Dvl, Dgo and Pk direct a feedback system that prohibits interactions between proximal and distal PCP complexes: for example, binding of Pk to Dvl tethered to Fz promotes Pk degradation at the distal side of the cell, whereas binding of Dgo to Pk linked to Vang leads to degradation of Dgo in the proximal cell domain (Devenport 2014, Butler and Wallingford 2017). Thus, stabilized "positive" interactions between the extracellular domains of Fmi, Vang and Fz coupled with antagonistic, "negative", interactions between cytoplasmic core PCP components result in the amplified, robust asymmetric distribution of the PCP proteins. In *Drosophila*, loss of any of the core PCP genes leads to typical PCP defects, such as wings with the abnormal polarity of hair emanating from the centre of the pupal wing cells instead of the distal side of the cell (Peng, Han et al. 2012). Importantly, asymmetric localization of all six core PCP components requires the presence and function of each component, revealing an interdependence among them (Adler, Zhu et al. 2004, Devenport 2014, Butler and Wallingford 2017).

The global PCP proteins deliver directional cues to the core PCP proteins. PCP global group comprises of atypical cadherins Fat (Ft) and Dachsous (Ds) and a Golgi kinase Four Jointed (Fj) (**Figure 1.7**). *Ds* and *Fj* mRNAs are expressed in an opposite gradient. Ft and Ds proteins form heterotypic complexes across cell membranes, and their affinity is controlled by phosphorylation by Fj. When the extracellular domain of Ft is phosphorylated, it leads to the increase in Ft affinity for Ds, while Ds phosphorylation decreases its affinity for Ft, indicating that

Fj polarizes the strength of a Ft/Ds interactions at both proximal and distal side of each cell. Loss of *Ft* or *Ds* gene causes PCP defects in multiple organs. However, Ft and Ds not only control proximal-distal patterning via PCP pathway but also regulate cell growth via Hippo signalling pathway complicating analysis of the mutant phenotypes (Strutt 2008, Peng, Han et al. 2012, Lawrence and Casal 2013)

The planar polarity effector (PPE) genes act downstream of the core PCP genes and are tissue specific --unlike core or global PCP genes that are required for PCP establishment in all cells (Wong and Adler, 1993). PPE genes include *Fuzzy (fy), Inturned (in), Fritz (fritz)* and *multiple wing hairs (Mwh)* (Park, Liu et al. 1996, Collier, Chan et al. 2000, Strutt 2008, Strutt and Strutt 2008, Yan, Huen et al. 2008) (**Figure 1.8**). Mwh is the most downstream member of the PCP pathway and accumulates at the proximal side of a wing cell. Functionally it depends on both core and other effectors proteins. Lu and colleagues observed the interaction between Mwh and In proteins (Lu, Yan et al. 2010). In participates in the recruitment of Mwh to the proximal side of the cells. On the other hand, Strutt and colleagues suggested that Mwh becomes phosphorylated in the PPE-dependent manner, and this step is vital to ensure that a single, distally pointing hair is formed. Mwh contains a Rho family GTPase-binding domain (GBD) and has a sequence similar to the formin homology 3 (FH3) domain. Formin domains nucleate actin and participate in the polymerization of actin filaments, yet FH3 domains are also involved in the autoinhibition of formins. Mutations of the core PCP genes lead to a single actin hair with abnormal polarity, while mutations of *Mwh* lead to several hairs per cell at the periphery of the cell. In and Fritz proteins localize to the apical proximal side of wing cells, similar to Vang and Pk, and their asymmetric localization relies on direct interactions with Vang (Wang, Yan et al. 2014). Interestingly, in the *Drosophila* pupal wing, In and Fy act in a complex with the Fritz WD40-repeat protein and all

three PPE proteins localize to the proximal side of the cell, where they control the phosphorylation and localization of the Mwh. Mwh then inhibits actin polymerization at the proximal cell side and, hence, directs the production of actin-rich trichomes to the distal cell edge. It is also observed that fly RhoA mutants show a strong wing hair defect. However, it is possible that the role of RhoA in PCP signalling is more complex and may reflect its general function in actin biology (Strutt 2008, Sedzinski, Hannezo et al. 2017). In a recent discovery, it was revealed that Fy and In proteins form a molecular complex that functions as a guanine nucleotide exchange factor (GEF) for small GTPase Rab23 (Gerondopoulos, Strutt et al. 2019). In earlier studies, Rab23 was established as a regulator of PCP in *Drosophila* wing (Pataki, Matusek et al. 2010). Strutt's group demonstrated that Rab23 functions downstream of In-Fy complex to regulate the planarly-polarized trichome localization in *Drosophila* wing cells. It was also revealed that GEFs for Rab7 GTPase (Mon1-Ccz1 and Hps1- Hps4) and vertebrate Inturned (Intu) and Fuzzy (Fuz) proteins have Longin domains (Gerondopoulos, Strutt et al. 2019): Longin domain-containing proteins often function in vesicle trafficking (De Franceschi, Wild et al. 2014).

Dynamic cytoskeleton rearrangement is critically involved in establishment and maintenance of planar cell polarity (Butler and Wallingford 2017). The actin cytoskeleton has been recognized as a major component of the cellular scaffold that is necessary for the regulation of cell shape, size, and motility. For the formation of hair, an appropriate amount of actin and microtubule cytoskeleton is required. Microtubules are hollow tubes formed from α and **β**-tubulin monomers and are the component of a cell's network of cytoskeletal filaments which govern cell shape and motility. The asymmetric arrangement of Frizzled in fly wing cells is controlled by directional microtubule arrays, indicating that polarized microtubules are an integral component of the initial

step in establishing planar cell polarity. However, the mechanism of function of this group of genes remains unclear (Butler and Wallingford 2017).

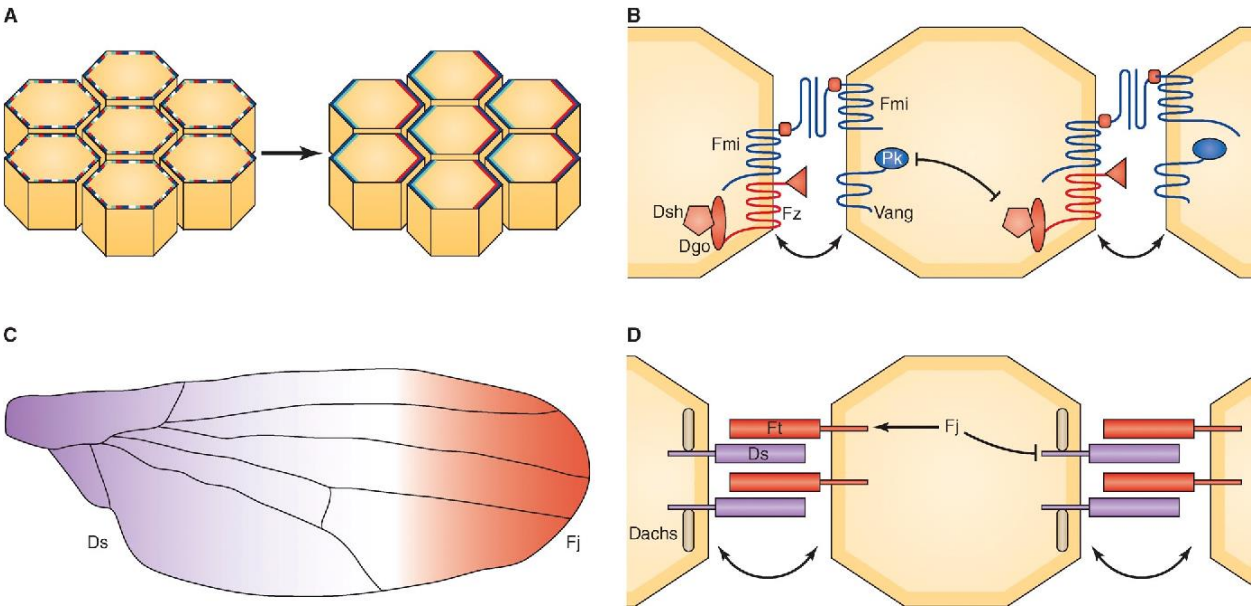

Figure 1.7. Asymmetric distribution of core PCP proteins in *Drosophila* wing cells

(A) Initially, core PCP components Fz, Dsh, Vang and Pk are localized randomly at all aspects of plasma membrane (left cartoon). Upon activation of PCP signalling, Vang and Pk become localized to the proximal/anterior side of the cell, while Fz and Dsh are found at the distal side of plasma membrane (right cartoon). (B) Positive interactions between Fmi with Vang and Fz stabilize all proteins at the plasma membrane. The intercellular interactions between Fmi, Vang and Fz expressed by the adjacent cells strengthen asymmetric distribution of these proteins to the opposite cell sides. Inside the cell, antagonistic actions between cytoplasmic proteins tethered to the proximal and distal cell facets amplify initially mild asymmetric distribution of the core PCP proteins. (C) *Ds* and *Fj* mRNAs are expressed at the opposite gradients along the wing blade. (D) Formation of the heterodimers between the Ds and Ft expressed at the surfaces of adjacent cells accomplishes two functions: a) it establishes a gradient of binding strengths within each wing cells

and b) it establishes a gradient of binding activity along the entire length of the wing blade. This provides a vector of directionality for core PCP proteins along the entire tissue.

Reprinted with the permission of (Devenport 2014).

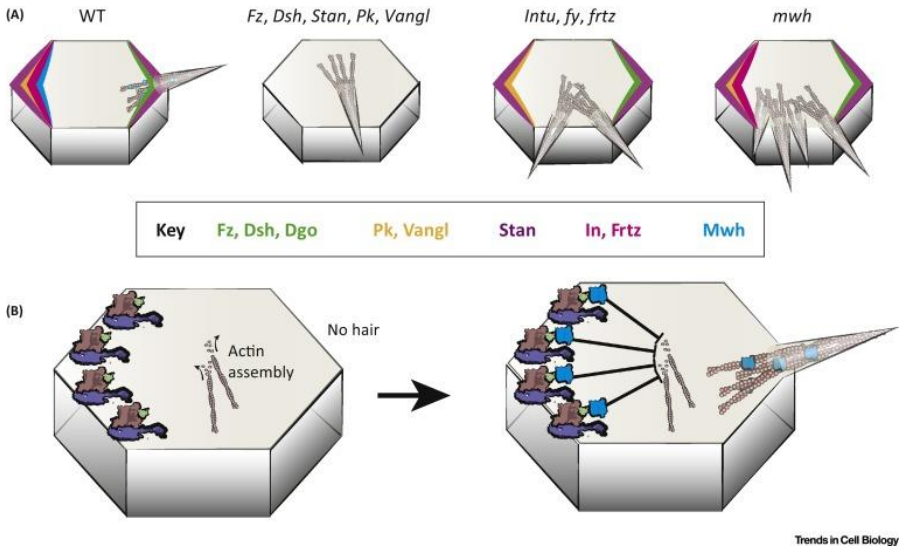

Figure 1.8. Role of planar cell polarity components in actin polymerization

(A) A wing cell of wildtype fly has a sole, distally appointed, actin-rich hair (trichome) whose position and orientation are regulated by the asymmetrically localized core PCP and PPE proteins. Mutation in core PCP genes alters the polarity of wing hair, but not the number of hairs. Core PCP gene mutations also affect precise localization of PPE proteins. Mutations in the PPE genes lead to disruption in the hair number and polarity, but core PCP protein localization is unaffected, confirming that core PCP proteins act upstream from PPE. Mutations in *Mwh* alter the polarity and induces multiple wing hair formation. (B) PPE proteins regulate localisation and function of Mwh, which acts to restrict the actin polymerization to the distal side of the wing cell.

Reprinted with permission from (Adler and Wallingford 2017).

1.2.2 PCP molecules and PCP signalling in vertebrates

The studies of PCP in vertebrates have uncovered surprising differences between the functions of fly and vertebrate PCP proteins. Planar polarization of the cells in the tissue is essential for diverse developmental processes in vertebrates, such as convergent extension that underlies neural tube closure or tubulogenesis, the uniform stereociliary bundle orientation of sensory cells in mammalian cochlea, direction of cilia tilting or cilia formation, and others processes (Strutt 2008).

Vertebrate PCP genes are homologous to the *Drosophila* PCP genes; however, they are more numerous and often have overlapping or specific expression patterns. Moreover, the functions of paralogous genes are often redundant, which makes the study of PCP signalling much more challenging. Ten *Frizzled* genes (*Fz1-10*) (Huang and Klein 2004), four *Prickle* genes (*Pk1-4*) (Wallingford, Goto et al. 2002), three *Dishevelled* genes (*Dvl1-3*) (Wang, Hamblet et al. 2006), two *Van Gogh-like* genes (*Vangl1-2*) (Torban, Kor et al. 2004), three *Flamingo* homologs (*Celsr1-3*) (Usui, Shima et al. 1999), two *Dachsous* genes (*Dash* 1-2) (Rodriguez 2004) and four *Fat* homologs (*Fat1-4*) (Matis and Axelrod 2013) are known to be present in mammalian cells. Several other genes are necessary for PCP but not solely dedicated to it. These include apicobasal proteins *Par3* (Landin Malt, Dailey et al. 2019) and *Patj* (Djiane, Yogev et al. 2005) that are involved in the PCP proteins localization to the apical edge of the cell or both lateral sides of the cell. Inversin and Diversin (both are Diego's paralogs) known to control the balance between canonical and noncanonical Wnt signalling and genetically interact with *Vangl2* (Simons, Gloy et al. 2005). c-Jun N-terminal kinase (JNK) (Yamanaka, Moriguchi et al. 2002) and the small RhoA GTPases Rho1 and Rac1 (Strutt, Weber et al. 1997) (Fanto, Weber et al. 2000) control cytoskeletal dynamics. Additional genes have been identified that function in vertebrate PCP signalling, but

do not seem to be involved in the regulation of PCP in *Drosophila* (Wang and Nathans 2007). Mutants for the apicobasal genes *Scribble1* (Murdoch, Henderson et al. 2003) and atypical protein kinase *Ptk7* (Lu, Borchers et al. 2004) exhibit typical PCP phenotypes and display genetic interactions with *Vangl2*, however, neither of them elicit any PCP phenotype in the flies.

In vertebrates, certain Wnt factors act as ligands for a subset of the Frizzled receptors involved in noncanonical Wnt/PCP signalling. Wnt ligands such as Wnt11 (Heisenberg, Tada et al. 2000), Wnt5a (Qian, Jones et al. 2007), and, likely, Wnt9b (Karner, Chirumamilla et al. 2009) bind to Frizzled receptors and initiate PCP signalling in vertebrates. However, specific Wnt/Fz pairs that control PCP signalling have not been established. Moreover, specific WNT co-receptors Ror1/2 (Green, Nusse et al. 2014) and Ryk1 (Green, Nusse et al. 2014) are required to engage Wnt/Fz pairs in PCP signalling. Dvl is a multidomain protein that functions as a common mediator of both canonical and noncanonical Wnt signalling (Smalley, Signoret et al. 2005); a specific mutation in *Xenopus Dsh* gene (*Xdd1*) compromises activation of PCP but not Wnt/**β**-catenin pathway (Fan, Gruning et al. 1998). In *Drosophila*, Fat signals through Hippo pathway, in addition to PCP signalling (Matakatsu and Blair 2012). Whether all four known vertebrate Fat paralogs signal through both PCP and Hippo pathways is still is unclear. Apicobasal polarity and PCP are interconnected: for example, core PCP proteins are localized at the apical junctions in a Par3-dependent manner; loss of Par3 results in a loss of Vangl2 at the junctional complexes leading to deficient PCP signalling and disruption in neural tube formation in *Xenopus* (Chuykin, Ossipova et al. 2018). Similar to the processes in *Drosophila*, the PCP pathway regulates cytoskeletal rearrangements which rely on the functions of actin regulators such as Jun kinase/Rac/Rho (Mezzacappa, Komiya et al. 2012), formin domain Daam1 (Corkins, Krneta-Stankic et al. 2019) and, likely, others.

Vertebrate PCP signalling was first discovered during gastrulation in *Xenopus laevis*, a morphogenetic process that relies on convergent extension (CE) (Wallingford, Rowning et al. 2000, Park, Haigo et al. 2006). Vertebrate gastrulation entails massive directional cell movements that establish and shape the three germ layers. The mesenchymal cells of gastrulating embryo acquire directional cell projections that allow them to move mediolaterally. As cells start moving, they exert traction against each other. This results in narrowing of the tissue in mediolateral direction accompanied by a simultaneous elongation of the tissue in the perpendicular anterior-posterior direction. During gastrulation, the individual cell behaviours are strictly regulated in time and space by many signalling pathways (Sepich, Usmani et al. 2011). These pathways direct cells proliferation, shape, fate and migration critical for generation of tissues and organs. The defects in CE result in embryos with shortened anterior-posterior body axis and wider dorsal structures such as the notochord or somites. The CE is controlled by PCP signaling, however, not all functional aspects of PCP molecules in the mesenchymal cells are well understood.

Another evolutionary-conserved fundamental process of embryonic development regulated by PCP signalling is neurulation (aka neural tube formation). CE is critical during neurulation to achieve neural tube (NT) closure. The neural plate is an early developmental structure that serves as a precursor of the neural tube; the latter gives rise to the central nervous system including cranial brain and spinal cord. The notochord structure underlying neural plate secrets noggin and chordin, which suppress BMP signalling, to begin the formation of a flat neural plate. As neurulation proceeds, the cells of the neural plate acquire directional protrusions enabling cells to undergo CE as they move directionally in the medio-lateral direction. The edges of the narrowing neural plate elevate to form neural folds that bend, move toward each other until they make contact and fuse, thus transforming the flat neural plate into a neural tube. Sonic hedgehog

signaling is required to allow bending (Harland 2000). However, the neuroepithelium cells of the neural plate fail to undergo proper mediolateral intercalation when the PCP pathway is defective, resulting in a shortened and widened neural plate. As a result, the neural folds fail to meet at the midline and cannot fuse leading to neural tube defects (NTDs). The condition in which the neural tube remains open from the hindbrain to the most caudal extremity of the embryo is known as *craniorachischisis* and is the most severe of all NTDs. Mutations of mouse *Vangl2* gene were identified as a cause of *craniorachischisis* (Kibar, Vogan et al. 2001). Mutations in Looptail (Lp, *Vangl2* gene mutant), *Crash (Crsh*) (*Celsr1* gene mutants), *Spin cycle (Scy),* or *Scribble1* invariably result in *craniorachischisis* and inner ear deficit, the prototypical PCP phenotypes (Kibar, Vogan et al. 2001, Murdoch, Henderson et al. 2003, Duncan, Stoller et al. 2017). Double homozygous mutants such as *Dvl1/2, Dvl2/3,* and *Fz3/6* also result in *craniorachischisis*, while mutants for any of these genes separately do not exhibit this phenotype, suggesting that this is due to redundancy between these paralogous genes. In addition, mutations in *Scrb 1* and *Ptk7* genes cause the same type of NTD (Hayes, Naito et al. 2013). Hence, based on the presence of *craniorachischisis*, both *Scrb1* and *Ptk7* are considered PCP genes, although in *Drosophila* their mutations do not cause PCP defects. Several other Wnt signalling -related genes (such as *Ror2*) (Gao, Song et al. 2011) have been implicated in neural tube closure by a genetic interaction with *Vangl2* (Murdoch, Damrau et al. 2014).

Similarly, to the functions of PCP signalling in flies, the PCP protein network controls not only the external structure orientation (e.g., epidermal hair in mammals) but also internal structures such as the stereocilia on the hair cells in the organ of Corti (Wang, Mark et al. 2005, Wu and Mlodzik 2009). Organ of Corti has one row of inner and three-rows of outer sensory hair cells that produce uniformly oriented stereociliary bundles, which represent the most vivid

example of PCP in vertebrates. The organ of Corti amplifies auditory signals and transmits them to specialized optic nerves (Wang, Mark et al. 2005). Each hair cell produces a microtubular cilium-like structure, kinocilium, at the center of the cell's apical surface; each kinocilium is surrounded by a V-shaped actin-based stereocilia bundle uniformly aligned at the lateral side. Homozygous mouse mutants for *Vangl2,* double homozygotes for *Fzd3/6* or *Dvl1,2,3* genes display stereocilia misorientation due to a loss of normal localization of kinocilium, which acts as an organizing center for stereocilia bundles (Etheridge, Ray et al. 2008). Importantly, the length of the organ of Corti is shorter in these mutants as well. Thus, the PCP pathway participates in the regulation for both extension of the organ of Corti and establishment of PCP of stereocilia (Etheridge, Ray et al. 2008)

In vertebrates, some PCP genes also control cilia functions. The establishment of the laterality (right-left asymmetry) relies on a leftward fluid flow in the embryonic node. Each cell of the node generates a single motile cilium and the cilia of all node cells point posteriorly to move the embryonic fluid in one direction, an event critical for breaking right-left asymmetry (Komatsu and Mishina 2013). Double homozygous mice for *Vangl1* and *Vangl2* exhibit severe laterality defects due to randomization of cilia beating (Song, Hu et al. 2010). The studies in *Xenopus leaves* revealed that PCP signalling modulates the orientation of motile cilia in multiciliated epidermal cells (Mitchell, Stubbs et al. 2009). The role of the PCP constituents in ciliogenesis is more controversial. Abnormal ciliogenesis was reported by knocking down *Dvl1-3* in *Xenopus* using morpholino oligonucleotides: the length and the number of cilia in the multiciliate epidermal cells were reduced (Park, Mitchell et al. 2008). However, the length of the primary cilia was not affected in the core PCP mutants in zebrafish or mice (Park, Haigo et al. 2006, Gray, Abitua et al. 2009). The most direct link between PCP and ciliogenesis has been observed in the experiment on

Xenopus embryos where homologs of the *Drosophila* PPE genes *fuzzy* and *inturned* were unexpectedly found to be required for ciliogenesis (Park, Haigo et al. 2006) (discussed in Chapter PCP effectors CPLANE proteins). More studies will be necessary to fully resolve the mechanism of action of various PCP components in cilia formation and functions. Overall, the accumulated evidence highlights the interconnections between planar cell polarity, cell morphology, and embryonic development.

1.2.3 Function of PCP effectors in vertebrates

The tissue-specific planar cell polarity effector (PPE) genes act downstream of the core PCP genes. The genes in this module are *Inturned* (*In*), *Fuzzy* (*Fuz*), *WDPCP* (homolog of *Fritz*) and *Mwh*, however, there is no evidence that a vertebrate homolog for *Mwh* exists (Lu, Schafer et al. 2015). Unlike the core PCP genes, which have been extensively studied in various animal models, PPE genes remain less understood. Localization of three PPE proteins In, Fy, and Fritz is governed by the core PCP proteins via direct biochemical interactions between the proteins of two modules (Wang, Yan et al. 2014). As a result, asymmetrically distributed core PCP proteins confer asymmetric distribution to the PPE effector proteins. Collectively, In, Fy and Fritz regulate the localization of Mwh that antagonizes the actin polymerization to maintain the adequate amount of actin for the initiation of wing hair in fly wing cells (Lu, Schafer et al. 2015). Thus, the actin polymerization at the side of the cell where PPE effectors localize is suppressed.

Inturned was originally discovered by Bridge in 1926 and *Fuzzy* by Ives in 1939 in fruit flies (Attrill, Falls et al. 2016). In both cases, the original mutants were identified due to their randomized sensory bristle polarity phenotype – although at that time identities of these genes were obviously unknown. *Fritz* was independently identified by Collier and colleagues in screens

for new mutations that altered PCP of fly wing hair (Collier, Lee et al. 2005). Loss in function mutations in *in, fy* and *fritz* produce two or three hairs per cell and their direction is randomized, indicating that the actin regulation is disrupted in the PPE mutants (Mayr, Deutsch et al. 1997), The vertebrate homologs of *Inturned* and *Fuzzy* were first discovered in *Xenopus laevis* by homology to the *Drosophila* genes (Park, Haigo et al. 2006). *Intu* and *Fuz* were found to be expressed at high levels in ciliated cell types, such as the neural floor plate cells and multiciliated skin cells. Curiously, morpholino knockdown of *Intu* and *Fuzzy* never evoked a strong PCP-related phenotype (usually noticed as a shortened body axis and dorsal curvature due to failed CE), but rather these phenotypes were consistent with defective ciliogenesis (Park, Haigo et al. 2006). Indeed, both neural tube cilia and motile cilia in multiciliated skin cells were substantially shorter and sparser. Moreover, studies of gene expression in the *Fuzzy* and *Intu* frog morphants also showed that disruption of ciliogenesis in these embryos leads to severe defects in the expression of Hedgehog target genes. Hence, these finding implicated PPE genes in control of Shh signalling since intact primary cilium is essential for Shh signal transduction (Park, Haigo et al. 2006, Wallingford 2006). *Wdpcp* was also discovered in *Xenopus* by homology to the *Drosophila* gene *fritz*. Similar to other PPE genes, *Wdpcp* was identified in the ciliated cells and was shown to be essential for ciliogenesis (Cui, Chatterjee et al. 2013).

Richard Finnell's group first described *Fuzzy* mutant mouse in which some defects were consistent with the loss of PCP signalling (Gray, Abitua et al. 2009). For example, the homozygous *Fuzzy*$^{-/-}$ mice have a kinked or curly tail, a phenotype that is frequently seen with heterozygous mutations in core PCP genes *Dvl* (Ohata, Nakatani et al. 2014) or *Vangl2* (Kibar, Vogan et al. 2001). The homozygous *Fuzzy* mutant mice exhibit cardiac defects including ventral septal defects, similar to those found in the mouse models lacking core PCP genes. However, both *Fuzzy*

Xenopus morphant embryos and *Fuzzy* mutant mice display comparatively mild PCP defects. Even double homozygous *Intu/Fuzzy* mouse mutants failed to display *craniorachischisis*, indicating that mutations in these genes do not alter CE required for neural plate formation (Heydeck and Liu 2011). Furthermore, no genetic interactions were observed between *Fuzzy* and *Vangl2*, suggesting that there is no significant link between the core PCP genes and PPE genes (Adler and Wallingford 2017). Subsequent work revealed that the function of PPE proteins may be cilia-related, as mice lacking either *Intu* or *Fuzzy* genes exhibited anterior neural tube defect known as *exencephaly*, as well as craniofacial defects, polydactyly, shortened and fewer cilia in the cells of various tissues and disruption of Shh signalling (Heydeck and Liu 2011), the phenotypes often associated with abnormal ciliogenesis and collectively known as "ciliopathies". *Wdpcp* mutant mice display phenotype reminiscent of human Meckel-Gruber ciliopathy syndrome (Adler and Wallingford 2017). Of note, cardiac outflow and cochlea stereo ciliary defects usually associated with PCP perturbation were also noted.

In a more recent study, Wallingford's lab used a systematic approach to characterize an essential but elusive PPE protein module (Intu, Fuzzy and Wdpcp), which was termed CPLANE (Ciliogenesis and Planar polarity effector proteins) (Toriyama, Lee et al. 2016). It was revealed by combining proteomics in mammalian cell culture, *in vivo* cell biology in *Xenopus* and genetic analysis in both mice and humans that CPLANE proteins have a vital role in ciliogenesis. It was observed that CPLANE proteins influence systematic ciliogenic machinery such as Intraflagellar transport (IFT), a conserved mechanism that transports cargo within the cilium (Toriyama, Lee et al. 2016). The IFT system is composed of two sub-complexes, IFT-A and IFT-B. IFT A controls retrograde and IFT-B controls anterograde traffic. Loss of Fuz function in cells disrupts the normal bidirectional transport of IFT proteins. When CPLANE genes were knockdown, IFT-B proteins,

Ift20 and Ift80, accumulated in the motile cilium, while the IFT-A protein Ift43 was completely lost from the cilium (Taschner, Bhogaraju et al. 2012, Scheidel and Blacque 2018). Interestingly, the IFT-A subcomplex is comprised of the three "core" and three "peripheral" IFT-A sub-units (Behal, Miller et al. 2012). A thorough analysis revealed that disruption of CPLANE function results specifically in the loss of IFT-A peripheral proteins from the axoneme, while the IFT-A core proteins entered the axoneme and trafficked bi-directionally (Toriyama, Lee et al. 2016). It was also noted that CPLANE proteins reside at the base of the cilia, where they assemble hierarchically. In addition to the three PPE proteins, Jbts17 (mutated in Joubert syndrome 17) and poorly understood small GTPase Rsg1 were found as parts of the CPLANE complex (Toriyama, Lee et al. 2016). Proteomics studies also revealed an association between CPLANE proteins and the NPHP proteins. Nephronophthisis (NPHP)-spectrum disorders are autosomal-recessive syndromes characterized by the presence of cystic kidneys and other abnormalities (cerebellar defects or ocular defects) in some patients; NPHP is one of the major genetic disorders causing end-stage renal disease in pediatric population. Physical and functional interactions between Nphp4 and Intu were also identified (Yasunaga, Hoff et al. 2015).

Mutations of human CPLANE genes have now been identified in several severe congenital birth defects. First, mutations in *FUZZY* have been identified in the patients with neural tube defects (Seo, Zilber et al. 2011), the finding that is consistent with the neural tube closure phenotypes reported in *Fuz* morphants in *Xenopus* (Park, Haigo et al. 2006) or homozygous *Fuzzy* mutants in mice (Zeng, Hoover et al. 2010) (Heydeck, Zeng et al. 2009). Mutations in CPLANE genes were also identified in various ciliopathies (Gray, Abitua et al. 2009, Toriyama, Lee et al. 2016). Experimentation in frog embryos and cell culture revealed a variety of potential pathogenic mechanisms involving these mutant proteins, including altered protein stability, loss of proper

localization at the basal body and failure to recruit specific constituents of the IFT machinery to the cilium (Toriyama, Lee et al. 2016)

Finally, it was also reported that Fuzzy plays a role in infectious disease. A genome-wide siRNA screen identified many novel host proteins in human cells that promote alphavirus infection, and PCP protein Fuzzy acts as one of the host proteins. Fuzzy participates in promoting endocytosis of both alphavirus and endocytic cargo, transferrin as well as it is essential for infection by several alphaviruses. Loss of Fuzzy restricts the entry of the alpha virus into the cells, revealing that it might be an important target for drugs to prevent the infection (Ooi, Stiles et al. 2013). Overall, research on the role of CPLANE proteins and their interactors is important to understand cell biology of ciliogenesis and pathogenesis of various human congenital anomalies and infectious disease.

1.2.4 PCP in kidney development

Several discoveries in the past decade have suggested a prominent role of PCP genes in regulating embryonic development of the kidney. PCP signalling has been proven essential for UB branching morphogenesis, tubulogenesis, directional cell migration (CE), oriented cell divisions and actin cytoskeleton networking.

During renal tubulogenesis in embryonic kidneys, Karner and colleagues in 2009 observed a randomized mitotic spindle orientation in the embryonic kidney epithelial tubule cells (Karner, Chirumamilla et al. 2009). Despite random OCD, the tubule diameter progressively became narrower from E13.5 to E19.5 while tubule elongated, after which, the diameter appeared to have reached its final size and OCD became oriented along tubular axis. The tissue elongation in one direction with a concomitant narrowing in the perpendicular direction is known as

convergent extension and, in some settings (e.g., gastrulation or neural tube closure), CE is under control of the PCP pathway. Indeed, loss of *Wnt9b* in the cells of the UB trunks led to an increased tubular diameter accompanied by the increased number of cells in the tubule cross-sections (Karner, Chirumamilla et al. 2009). Thus, the authors proposed that during embryonic tubulogenesis, tubule diameter is regulated by CE that is controlled by the PCP components.

Several cell behaviours have been studied in different developmental processes; the two processes that have been shown to participate in CE during tubular elongation are the mediolateral intercalation and multicellular rosette formation. In the case of intercalation, tubule cells are engaged in mediolateral movements that are perpendicular to the tubule extension axis. This decreases the number of cells in cross-section, reducing tubular diameter and elongating the tubule structure (Karner, Chirumamilla et al. 2009). In *Xenopus* pronephric duct, epithelial cells form multicellular rosettes. The rosettes are formed when 5-8 tubule epithelial cells assume wedged shapes and form a rosette structure with the longest apical rosette axis perpendicular to the plane of the tubule (Zallen and Blankenship 2008, Lienkamp, Liu et al. 2012). Further, the shape of the cells changes in a coordinated polarized manner, and the rosette resolves with its new, longest axis aligning along tubular plane. Thus, rosette remodeling elongates the tubule length while shrinking tubule diameter. Overexpression of the PCP-deficient variant of the core PCP gene *Dvl* (*Xdd1*) disrupts the PCP signalling resulting in abnormal rosette resolution and dilatation of the frog pronephros (Lienkamp, Liu et al. 2012).

Vertebrate genes *Dachsous 1* and *2* and *Fat1-4* are homologs of *Drosophila Fat/Ds* gene module. Their loss elicits multiple kidney phenotypes. Of the four *Fat* homologues, *Fat4* is the closest to the PCP *fat* gene (Saburi, Hester et al. 2008). Knockout of *Fat4* leads to dysplastic kidneys with small cysts and dilated tubules. Interestingly, incorporation of one mutant *Vangl2*

allele appeared to intensify cystic kidney phenotype, making authors to propose that PCP signaling was involved in the resultant phenotype (Saburi, Hester et al. 2008). More recent studies by the same group demonstrated that *Fat1* cooperates with *Fat*4 in kidney development and precipitates kidney dysplastic phenotype of the *Fat4*$^{-/-}$ mouse when one *Fat1* allele is mutated (Saburi, Hester et al. 2008). Importantly, *Fat4* is expressed in the stroma surrounding UB tips, and thus, the tubular phenotype seen in the *Fat4*$^{-/-}$ kidneys arises indirectly through a signaling between stromal and tubular compartments. Loss of *Fat4* gene also drastically enhances nephron progenitor pool in the cap mesenchyme (Mao, Francis-West et al. 2015). In this setting, Fat4 acts as a receptor for its ligands Dcsh1 and Dcsh2, both of which are expressed in the nephron progenitors. Knockout of *Dcsh1* and *2* mimics *Fat4* mutant phenotype and leads to the expansion of cap mesenchyme. However, the functionality of the *Fat4* or *Dcsh1/2* mutant nephron progenitors appears to be abnormal and, as a result, these cells are not properly recruited into MET and the mutant kidneys are hypodisplastic (Mao, Mulvaney et al. 2011). *Frizzled 4* and *8* are specifically expressed in the UB trunk; their excision from the UB lineage results in a mild defect seen as dilated tubules (Smallwood, Williams et al. 2007). The phenotype is similar to the one seen in the *Wnt11* mutant kidneys in which loss of *Wnt11* leads to the decreased levels of Ret receptor in UB and Gdnf in the metanephric mesenchyme.(Mao, Mulvaney et al. 2011). PCP core genes are also expressed during the branching morphogenesis, however, very little is understood about the functionality of this process. *Vangl2* gene knock-out (Looptail mouse) leads to a reduced UB branching seen as early as E13.5, that is particularly abnormal in the lower kidney pole along the anterior-posterior axis: the kidneys are smaller and dysplastic with occasional small cysts and enhanced tubular diameter (Yates, Papakrivopoulou et al. 2010). More recently, Derish *et al* (Derish, Lee et al. 2020) observed that loss of *Vangl2* in mice leads to a significant tubular dilation at the embryonic stage

of kidney development. However, postnatally, the tubular size of the collecting duct tubules appeared to have been rescued independently of PCP signalling, and there was no dilatation of tubule at postnatal day 7 onward up to 9 months (Derish, Lee et al. 2020). Similarly, knockout of both *Vangl1* and *Vangl2* did not produce cystic kidney phenotype (Kunimoto, Bayly et al. 2017). Collectively, these data suggest that loss of core PCP signaling does not cause cystogenesis, a popular assertion that was refuted based on these resent data. During the glomerulogenesis, *Vangl2* knock-out in podocytes resulted in the reduced number of actin-based cell projections, cell motility and stress fibres, as well as in the delay in glomerular maturation suggesting the role for the PCP pathway in glomerular development and actin regulation in these cells (Babayeva, Zilber et al. 2011)

1.3 Actin in Ciliogenesis

1.3.1 The Primary Cilium

Cilia are evolutionary conserved antenna-like sensory organelles that protrude from the apical cell surface in the majority of mammalian cells to regulate various signalling pathways during embryogenesis and postnatally. Cilia can be subdivided into two categories, namely motile cilia and non-motile cilia; the latter are also known as primary cilia (Eley, Yates et al. 2005). Motile cilia are present in several tissues, such as respiratory tract, and can beat in coordinated waves. On the other hand, primary cilia are found on the majority of cell types, blood cells are the prominent exception (Ke and Yang 2014). The core of the cilium is the microtubular axoneme. The axoneme of motile cilia is built from 9 sets of parallel doublet microtubules and a central microtubule pair ("9+2" axoneme) that powers cilial beating; the primary cilia do not contain the central microtubule pair ("9+0" axoneme) and are immotile (Ke and Yang 2014). The ciliary axoneme is anchored at the basal body, a modified mother centriole, which is made of 9 sets of microtubule triplets. The region where the axonemal doublets extend from the basal body is called transition zone. The transition zone acts as a diffusion barrier providing a selective gate for the proteins entering the cilium from the cytoplasm and exiting from the distal part of the cilium (Kim and Dynlacht 2013, Nachury 2018). The ciliary membrane covering the axoneme is continuous with the cell membrane but enriched for specific receptors, ion channels and other proteins, enabling primary cilium to function as a sensor of chemical and mechanical cues outside the cell and to transduce this information inside the cell (Kim and Dynlacht 2013). The primary cilium is formed after the cell exits cell cycle in the G0 phase of the cell cycle. The centrosome, that acts as a microtubule organizing center in mitosis, becomes liberated and one of the two centrioles, the mother centriole, differentiates into the basal body and migrates to the cell surface, docks beneath

the apical plasma membrane and nucleates outgrowth of the axoneme/cilium (Delling, DeCaen et al. 2013) The continuous import and transport of ciliary proteins to the tip of the cilium and back to the base of the cilium helps in the assembly, elongation and maintenance of the cilium. These processes are governed by an evolutionary-dedicated molecular process named intraflagellar transport (IFT) (Omori, Zhao et al. 2008) (**Figure 1.9**). The IFT is a bidirectional movement of protein complexes along the axoneme. Movement of the IFT cargos are catalyzed by the IFT motors kinesin-2 (anterograde transport) and dynein-2 (retrograde transport) and requires specialized IFT proteins that consist of the complex B (enables cargo movement from the base to the tip of the cilium) and complex A (moves proteins from the tip to the base of the cilium). Loss of IFT-B complex proteins leads to short or abrogated cilia. Loss of IFT-A proteins causes defective retrograde transport but also affects anterograde transport (Quarmby 2014). A number of additional IFT proteins, called IFT complex accessory proteins, have been identified to take part in ciliogenesis (Quarmby 2014). The small Guanosine Triphosphate hydrolase (GTPase) Rab8, which participates in cargo transport from Golgi apparatus to plasma membrane, promotes the vesicle trafficking to the base of the cilium, that is critical since there is no protein synthesis within the cilium and all proteins must be delivered to the base of the cilium (Omori, Zhao et al. 2008). Several BBSome proteins mutated in the human Bardet-Biedl syndrome (BBS) were found to bind Rabin8 (a guanine nucleotide exchange factor (GEF) of Rab8) and to control cargo delivery to the basal body (Nachury, Loktev et al. 2007, Yoshimura, Egerer et al. 2007, Blacque, Scheidel et al. 2018).

The primary cilium serves as an optical, osmotic, chemical, and mechanical sensory center that transduces signals from extracellular environment to intracellular signaling cascades (Blacque, Scheidel et al. 2018). Several signaling pathways (e.g., Shh signaling, Wnt signaling

and Platelet-derived growth factor pathway signaling) have been shown to rely on intact cilia. The Hippo intracellular signaling cascade is also coordinated at the primary cilium (Wheatley 1995, Breunig, Sarkisian et al. 2008, Spassky and Aguilar 2008, Ohazama, Haycraft et al. 2009, Schneider, Cammer et al. 2010, Lancaster, Schroth et al. 2011). Defects of primary cilia and/or mutations in the cilia-related genes cause dysregulation of embryonic development that leads to various genetic disorders, including polycystic kidney disease (PKD), randomization of left-right asymmetry (Eley, Yates et al. 2005), sensorineural deafness (Eley, Yates et al. 2005), nephronophthisis (NPHP) (Sang, Miller et al. 2011), Joubert syndrome (JBTS) (Davis and Katsanis 2012), Meckel–Gruber syndrome (MKS) (Sang, Miller et al. 2011) and others. These and other heterogeneous diseases have been referred to as "ciliopathies". Ciliopathies exhibit a broad spectrum of clinical phenotypes and sometimes share phenotypic overlap making it challenging to identify underlying causative genes (Eley, Yates et al. 2005, Sang, Miller et al. 2011).

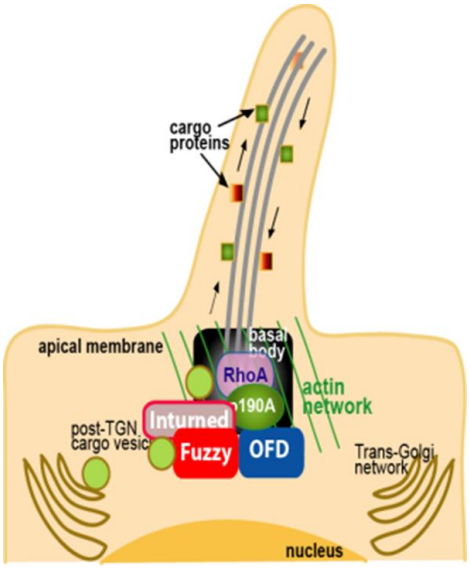

Figure 1.9. Structure of Primary Cilium and role of CPLANE proteins in ciliogenesis

The primary cilium is comprised of a microtubular core, axoneme, and covered by the ciliary membrane. The axoneme is templated at the basal body, that is a modified mother centriole.

Elongation of the microtubule-based axoneme as well as ciliary localization of selected receptors, transporters and channels rely on the intraflagellar transport machinery. The CPLANE proteins are localized to the basal body and function to recruit specific proteins to the base of the cilium. Among the proteins localized to the cilium in the CPLANE-dependent manner is the p190A, a major regulator of the RhoA activity in mammalian cells.

1.3.2 Kidney diseases caused by abnormal ciliogenesis

A possible role of primary cilia in the pathogenesis of autosomal-dominant polycystic kidney disease (ADPKD) was first established in 1999, when the *Caenorhabditis elegans* (worm) genes, *lov1* and *pkd2*, homologues of the human ADPKD genes, *PKD1* and *PKD2*, respectively, were found to encode proteins that localized to neuronal cilia (Barr and Sternberg 1999). Another protein, fibrocystin (FC), the product of the autosomal-recessive polycystic kidney disease (ARPKD) gene *PKHD1*, was also observed to be localized to the cilium (Zhang, Wu et al. 2010). Additional evidence for common pathogenic mechanisms in ARPKD and ADPKD was provided by the finding that PC1 and PC2 proteins (encoded by *PKD1* and *PKD2* gene, respectively) are colocalized to the cilia with the proteins from two known PKD mouse models, the orpk and cpk mice (Dell 2015). Proteins associated with other cystic kidney diseases have also been localized to the cilia or basal bodies, further expanding the family of "ciliopathies" with kidney component. These include proteins associated with Nephronophthisis, Bardet-Biedl Syndrome, Meckel-Gruber Syndrome and Joubert Syndrome (Hildebrandt and Zhou 2007, Hildebrandt, Benzing et al. 2011, Waters and Beales 2011, Reiter and Leroux 2017).

The localization of multiple PKD-associated proteins to the cilia and basal bodies was an important step towards defining the pathogenesis of cystic kidney disease. However, the

mechanisms by which cilia participate in normal physiology and PKD pathogenesis were largely undefined (Yoder 2007). Numerous subsequent studies have focused on connecting cystic kidney disease genes, cilia and cystogenic processes. Multiple cilia-associated signaling processes have been implicated in cystogenesis. These include pathways controlling cyclic AMP, mTOR as well as canonical Wnt signaling, G-protein coupled receptor signaling, epidermal growth factor receptor family, planar cell polarity, calcium and cell cycle signaling (Hildebrandt and Zhou 2007, Hildebrandt, Benzing et al. 2011, Waters and Beales 2011, Reiter and Leroux 2017). Despite these advances, there remain many unanswered questions about how mutant kidney proteins affect cilia and downstream signaling pathways to produce cysts.

Several animal models have implicated abnormal cilia structure in PKD pathogenesis. The orpk mouse phenotype (cystic kidney, polydactyly, and hydrocephalus) is caused by a mutation in the gene that encodes polaris (alternatively called IFT88), a key IFT protein (Yoder 2007). Renal tubular cells from the orpk mice have short cilia; targeted disruption of *IFT88* gene results in absent flagella in the single cell model organism *Chlamydomonas reinhartii* (Lin, Hiesberger et al. 2003). Mice that lack kidney-specific expression of *Kif3A*, one of the essential IFT-associated kinesin motors (Lin, Hiesberger et al. 2003), are born with normal kidneys but develop progressive renal cystic disease in early postnatal period (Patel, Chowdhury et al. 2009). Renal tubular epithelial cells from this model lack cilia and have characteristics of the typical cystic epithelia, including increased cell proliferation, apoptosis and abnormal EGFR localization and signaling (Dell 2015). These findings suggest that abnormal or absent cilia can lead to polycystic kidneys, but cilia are not required for the earliest steps of kidney development. In contrast, *Pkd1* null mice form largely normally appearing cilia, suggesting that polycystin1 may not be required for cilia assembly (Nauli, Alenghat et al. 2003). However, accumulated evidence

suggests that abnormal cilia function underlies pathogenesis of PKD (Dell 2015). The postulated mechanism is that cilia function as mechanosensors, transmitting external mechanical (flow) and chemical signals inside the cell. Defective cilial structure or function would be expected to cause abnormal response to flow, thereby altering downstream signaling and promoting activation of procystogenic pathways. Because of the putative role of PKD2 protein as a calcium channel (Praetorius and Spring 2001), many key observations have centered around the role of cilia and polycystins in flow-induced changes in intracellular calcium, an important component of second messenger signaling pathways. Normal kidney cells with intact cilia exhibit increased intracellular Ca2+ in response to flow-induced cilia bending; chemical removal of cilia blocks this response (Praetorius and Spring 2003). In contrast, cells from the *Pkd1* deficient mice have normal cilia but show defective responses to the flow-mediated Ca2+ influx (Nauli, Alenghat et al. 2003). Flow-induced Ca2+ signaling was shown to be dependent on PC2-mediated Ca2+ influx, and genetic removal of cilia abolishes this response. Taken together, these studies show that normal flow-induced intracellular Ca2+ signaling requires not only intact cilia and polycystins but also a correct PC2 localization to maintain tight control of Ca2+ entry into the cell.

Studies in other ciliopathies also supported a role of cilia in the pathogenesis of not only cystic kidney disease but also extrarenal manifestations, particularly those involving the skeleton, liver and eyes (Ferkol and Leigh 2012). Some forms of Nephronophthisis are associated with significant ocular and other extra-renal manifestations (Hildebrandt, Benzing et al. 2011). Similar to polycystins, multiple NPHP proteins have been localized to the cilia, specifically, to the transition zone. Notably, patients with NPHP2, which is caused by mutations in *inversin* (inv) gene, have polycystic kidneys and *situs invertus*, highlighting the role of cilia in mediating left-right axis determination during development (Reiter and Leroux 2017). BBS is characterized by

cystic kidney but also has prominent extrarenal manifestations, including retinal abnormalities, obesity, diabetes mellitus, cognitive delay and polydactyly (Waters and Beales 2011, Scheidecker, Etard et al. 2014). Multiple BBS proteins localize to the basal body, and form a complex called the BBSome, which is essential for protein trafficking to the cilium and control of cilial gate (Nachury, Loktev et al. 2007).

1.3.3. Actin and its regulators

Coordinated cell movements are required for many biological processes including embryonic organogenesis, tissue repair and others. Actin cytoskeleton regulates a vital part of these processes by mediating the development of cellular structures (e.g. lamellipodia), cell shape, focal adhesion as well as cell interaction (Lee and Dominguez 2010). Actin is known to be the most abundant protein in eukaryotes including some plants and yeasts. Actin can be identified as a monomeric G- actin and filamentous F-actin (Holmes, Popp et al. 1990). The filamentous F-actin has polarity in its structure as all filaments are organized in the same direction. The pointed side is primarily at the ADP bound state, which is also known as the negative end. The barbed site is also known as positive end containing G-actin monomers; the barbed site can be extended easier than that the negative end and it is often the fast-growing end of actin filament. The mechanism of actin polymerization and depolymerization is a continuous cycle through which ADP is exchanged for ATP and then G-monomers are further added to the barbed end of the F-actin filaments (Wegner 1976). Once the F-actin is formed, its mechanical properties and stability can be modified by actin-binding proteins, such as profilins and actinins. Mechanistically, these proteins determine the conditions appropriate for the polymerization, crosslinking, capping and elongation of actin filaments. Additionally, capping proteins such as cofilins bind at the end of the filaments to

regulate its assembly and disassembly (Isenberg, Aebi et al. 1980). F-actin filaments, along with myosin II filaments, integrins and various actin-binding proteins, form focal adhesion complexes or adherens junctions, which attach cells through the cytoskeleton to the extracellular matrix (ECM) or neighbouring cells, respectively (Burridge and Chrzanowska-Wodnicka 1996)

1.3.3.1 Actin-myosin cytoskeleton organisation

The Rho GTPase family and its activators

The Rho GTPases family consists of a group of molecules with a pivotal role in regulating different aspects of actin cytoskeleton dynamics (Valencia, Chardin et al. 1991, Hall 2009). The most extensively studied molecules are: RhoA, which regulates the stress fibres and focal adhesion, Rac1, which controls filopodium development, and Cdc42, which regulates membrane raffling. All GTPases fluctuate between active GTP-bound form and inactive GDP-bound form (**Figure 1.10A**). There are three well-characterized Rho isoforms: RhoA, RhoB and RhoC. The three isoforms are ~ 85% similar to each other. RhoA is essential during cell migration for disassembly of cell adhesions, while RhoB obstructs the growth factor receptor trafficking (Wheeler and Ridley 2004). RhoC remodels the cytoskeleton via activation of formins mDIA1 and FMNL2 (Kitzing, Wang et al. 2010).

The regulators of Rho protein are grouped into three subcategories:

a. *Guanine nucleotide exchange factors (GEFs)* function by organising the release of GDP -bound (inactive) conformation and facilitating GTP-bound (active) conformation, which ultimately results in stabilization of Rho molecules in active state promoting the downstream signalling (Van Aelst and D'Souza-Schorey 1997).

b. *GTPase-activating proteins (GAPs)* hydrolyse GTP to GDP, hence regulating inactivation of Rho GTPases, reversing GEF function and effectively suppressing the signalling pathway (Lamarche and Hall 1994).

c. *Guanine nucleotide dissociation inhibitors (GDIs)* are regulatory proteins present in the cytosol. GDIs form complexes with inactive, GDP-bound, GTPases. GDIs restrict the exchange of GTPases between the cytosol and plasma membrane and also prevent localization of the GTPases at the cell membrane, therefore, prohibiting GEF-mediated activation of Rho GTPases (Robbe, Otto-Bruc et al. 2003).

A

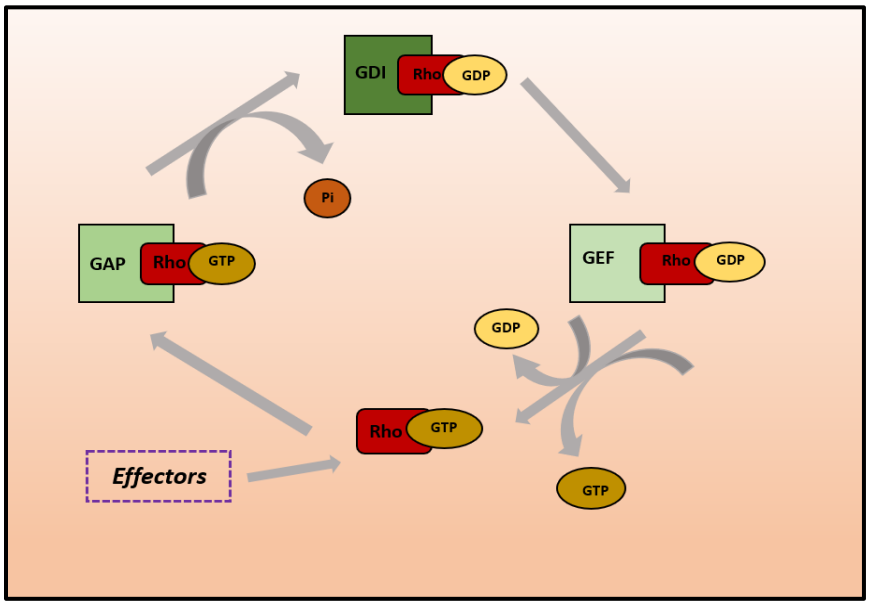

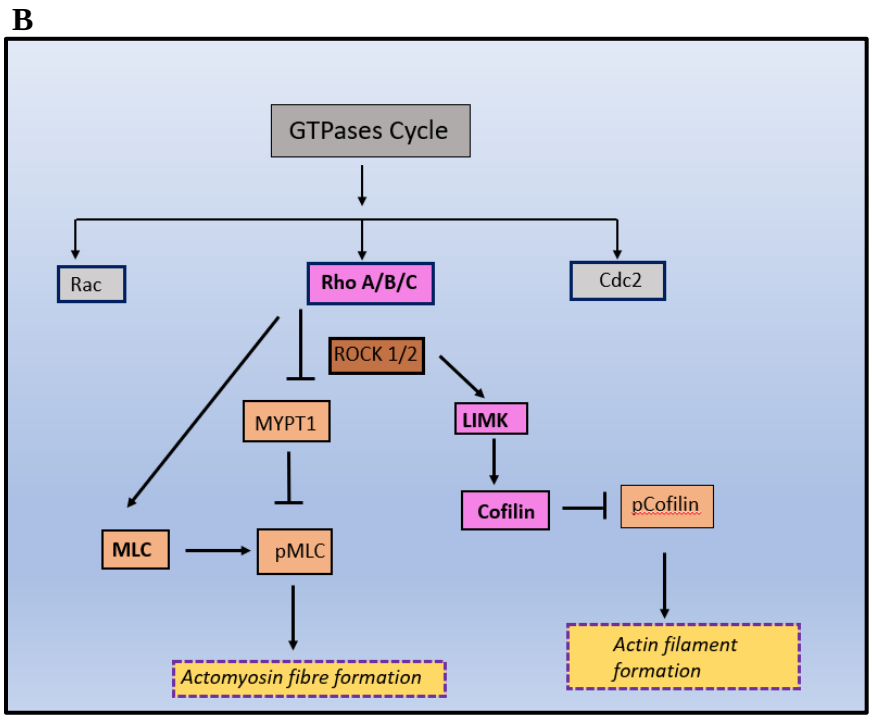

Figure 1.10. RhoA GTPase family members, their regulation and function

(A) The major three branches of the Rho-family of small GTPases are RhoA, Rac1 and Cdc42 that exist in active, GTP-bound form and inactive, GDP-bound form. The RhoA GTPase activity is tightly controlled by three major types of effectors: activation of Rho is initiated when GDP to GTP is exchanged by guanine-nucleotide exchange factors (GEFs). The inhibition of GTPases occurs by the action of GTPase activating proteins (GAPs), which accelerate GTP-hydrolysis to GDP-bound form. The GDP-loaded Rho members are concealed in the cytosol in an inactive form by guanine-nucleotide dissociation inhibitors (GDIs). (B) Active GTPases modulate actin cytoskeleton dynamics through activation of downstream kinases including ROCK1/2 and LIMK. ROCKs activate MYPT1 that phosphorylates (activates) MLC, which, in turn, activates actomyosin causing cell contractility. LIMK phosphorylates (inactivates) actin-severing protein cofilin, thereby removing actin polymerization "block" and enhancing actin polymerization. The proteins shown in pink-colored boxes have been implicated in ciliogenesis. GDP; guanosine

diphosphate; GTP, guanosine triphosphate; LIMK, LIM domain kinase; MLC, myosin light chain; MYPT1 Myosin phosphate target subunit 1, Pi, inorganic phosphate; ROCK, Rho-associated.

1.3.4 Actin in Ciliogenesis

Actin is critically involved in cilia formation and maintenance (Kohli, Hohne et al. 2017). Cilia form at G0/G1, when the mother centriole travels to and docks at the apical membrane in epithelia. The docking requires a clearance of cortical actin to permit nucleation of an axoneme. It has been revealed that actin cytoskeleton contributes to the elongation of axoneme, yet the mechanism of how actin influences the axoneme length and signalling remains elusive (Mirvis, Stearns et al. 2018). At the distal tip of the cilium, actin and Myosin6 mediate the scission of small membrane-covered vesicles, ectosomes, from a primary cilium tip, which is required for Shh signaling (Nager, Goldstein et al. 2017). This indicates that ecto-vesicle release may regulate cilia-specific signaling. Additionally, the ciliary membrane is enriched with actin-binding proteins that further accumulate when actin polymerization is disrupted (Kohli, Hohne et al. 2017), suggesting that a balance of actin polymerization is needed for proper cilia-specific functions. Very recently actin was detected within a cilium shaft, however, what is does there is completely unknown (Chaitin 1991, Mirvis, Stearns et al. 2018). Interestingly, it was demonstrated that mechanical stimuli such as cell shape, contractility and extracellular matrix rigidity are major determinants of ciliogenic activity; cell spatial confinement, low contractility or soft extracellular substrate facilitate ciliogenesis in quiescent cells (Pitaval, Tseng et al. 2010, Ishikawa and Marshall 2014), further suggesting a link between cytoskeleton and cilia functions .

Several studies have marked the involvement of the actin cytoskeleton in the regulation of ciliogenesis. An RNAi library screen for human genes that modulate ciliogenesis identified 36

positive and 13 negative ciliogenesis modulators, which include molecules involved in actin dynamics and vesicle trafficking. Several actin regulatory factors, including an actin-severing factor Gelsolin and an actin filament nucleator ARP2/3 complex were discovered as a positive and negative regulators of ciliogenesis, respectively (Kim, Lee et al. 2010). Moreover, an actin monomer-binding protein, MIM, was shown to promote ciliogenesis by antagonizing Cortactin, a nucleation promoting factor for ARP2/3 complex (Bershteyn, Atwood et al. 2010). An additional study also reported that a microRNA mir-129-3p promotes both ciliogenesis and cilium elongation by decreasing the expression of several actin regulatory factors that are required for branched actin network formation (Cao, Shen et al. 2012). It is noteworthy that aberrant actin polymerization by dysregulation of Rho GTPase was implicated in the pathogenesis of Bardet–Biedl syndrome (Nachury, Loktev et al. 2007). The increased amount of RhoA was observed in the Bbs4, Bbs6 and Bbs8 mouse mutant fibroblasts. RhoA plays an important role in the formation of an apical actin mesh important for the docking of cargo vesicles at the basal body and cilia elongation; hence, disruption in RhoA activation leads to defective docking and abnormal actin organization. This published evidence suggests a link between the actin organization and cilia elongation (Hernandez-Hernandez, Pravincumar et al. 2013). The organization and dynamics of the actin cytoskeleton are thought to modulate vesicle trafficking to the ciliary base and thus affect ciliary membrane biogenesis (Kim, Lee et al. 2010, Cao, Shen et al. 2012, Kim, Jo et al. 2015). Actin may also de-stabilize molecules that control cilia resorption (Smith, Lake et al. 2020). Overall, the body of accumulated experimental evidence suggests that excessive actin polymerization at the base of the cilium negatively affects cilia formation and that centrosomal actin cytoskeleton must be tightly regulated to enable successful cilia formation. However, the regulatory factors that control centrosomal actin polymerization remain largely unexplored.

1.3.5 p190A RhoGAP and its role in ciliogenesis

Members of Rho family of small GTPases function as critical regulators of actin cytoskeleton organization. These proteins mediate a variety of cellular processes, including migration, adhesion and shape change. The RhoGAP protein p190A encoded by *Arhgap35* gene (also known as, *Grfl1)* is a potent regulator of Rho GTPases. It is composed of a N-terminal GTPase domain necessary for its activity, a series of conserved FF domains, and a C-terminal RhoGAP domain (Li, Zhang et al. 1997, Levay, Settleman et al. 2009). p190A RhoGAP activity has been observed *in vitro* against the prototypical Rho GTPases, namely Rac1, Cdc42 and RhoA, with the strongest activity specifically toward RhoA (Ridley, Self et al. 1993, Burbelo, Miyamoto et al. 1995). Gene inactivation studies in the mouse identified an important role for p190A in neural tube closure, eye morphogenesis and mammary gland branching morphogenesis, differentiation and cell adhesion (Nemeth, Futosi et al. 2010).

In 2016, Maxime Bouchard's lab from McGill University identified a mutant strain after ENU mutagenesis characterized by occasional *exencephaly* (cranial NTD) and fully penetrant hypoplastic and glomerulocystic kidney phenotype (Stewart, Gaitan et al. 2016). Using a combination of classical single nucleotide polymorphism mapping and exome sequencing approaches, they identified a point mutation in *Arhgap 35* gene and mapped this mutation to the RhoA binding domain of the p190A protein. Unexpectedly, the researchers found that the reduction in p190A GAP activity perturbed cilia elongation in both kidney proximal tubule cells and mouse embryonic fibroblasts, and this was associated with dysregulated Rho GTPase signaling. Interestingly, while Rac1 inhibition only partially rescued ciliogenesis in the absence of p190A activity, inhibition of ROCK completely re-established both cilia number and length in the mutant cells (Stewart, Gaitan et al. 2016). Together, these results raised the intriguing possibility

that p190A played a role in controlling centrosomal actin by regulating activity of RhoA (and possibly Rac1) to allow the localized actin cytoskeleton rearrangement required for cilia elongation (Stewart, Gaitan et al. 2016). Stewart and colleagues confirmed that p190A deficiency resulted in ectopic actin polymerization at the basal body, leading to a compromised cilia elongation. Stewart et al study substantiated the first genetic demonstration that the negative regulation of Rho GTPases at the basal body is required for primary cilium elongation (Stewart, Gaitan et al. 2016). However, how p190A or other actin regulators are recruited to the basal body is completely unknown.

Rational of thesis

In humans, congenital anomalies of the kidney and urinary tract (CAKUT) are among the most common malformations observed at birth. Analysis of the genetic basis of CAKUT will improve our understanding of the pathogenic mechanisms of disease and may present a therapeutic and potential prognostic value to patients.

The planar cell polarity pathway is a highly conserved signalling pathway that regulates the development of many organs such as the neural tube, heart, limbs, and kidney. The PCP pathway was first discovered in *Drosophila*, where it is known to control the asymmetric distribution of cytoskeleton seen as e.g., the uniform patterning of small actin hair on wing cells. Phenotypic screens in flies identified several groups of PCP genes including the "PCP effector" genes. Multiple homologs of the *Drosophila* PCP genes have been identified in vertebrates. My thesis project focuses on the functions of the PCP effector gene *Fuzzy* in mammals. From the previous studies in our lab and by others, it has been established that Fuzzy participates in the process of ciliogenesis in vertebrates. Fuzzy appears to control the trafficking of certain molecules needed for the assembly of the primary cilium. The dysfunction of primary cilia leads to severe disturbances in the development of many organs and is involved in cystic transformation in the kidney in mice and humans. Homozygous *Fuzzy*$^{-/-}$ mice die in mid-gestation, but kidneys are formed, and we can study the early stages of kidney development.

Loss of *Fuzzy* affects mouse kidney development. At E16.5, *Fuzzy*$^{-/-}$ kidneys are smaller and characterized by the presence of tubular and glomerular cystic structures. The recent unpublished observations in our lab show that Fuzzy might act via Rho GAP p190A to contain actin polymerization at the base of the primary cilium. p190A is a GTPase activating protein (GAP) that acts as an inhibitor of RhoA GTPase and controls actin polymerization at the base of the cilium

required for proper cilia elongation. It has already been reported that loss of p190A gene *Arhgap35* causes renal hypoplasia and glomerulocystic kidneys which phenotypically appear to be identical to the E16.5 *Fuzzy*$^{-/-}$ kidneys. In this thesis, we test for the molecular, cellular and genetic interactions between Fuzzy and p190A. We demonstrate that there is a biochemical interaction between p190A and Fuzzy. We also show that p190A is lost at the base of cilium in *Fuzzy*$^{-/-}$ mutant cells, indicating that Fuzzy controls p190A localization at the basal body. We further extended our investigation to test for a genetic link between *Fuzzy* and *p190A*. We generated double heterozygous mice and further crossed double *Fuzzy*$^{+/-}$*;p190A*$^{+/-}$ mice to reduce the gene dosages acquiring 9 different genotypes. Thorough genotype-phenotype analysis revealed an increase in the frequency of NTD, eye and kidney defects that correlated with a decrease in the *Fuzzy* and *p190A* dosages. Collectively, our data indicate that Fuzzy may contain actin polymerization at the base of the cilium. Mechanistically, kidney defects, particularly hypoplasia and renal cysts in *Fuzzy* mutants may be related to the defective RhoA activity at the cilium. Based on our observations, we conclude that Fuzzy and p190A likely participate in the same pathway to control RhoA GTPase activity at the base of the cilium regulating ciliogenesis.

Chapter 2 Materials and Methods

2.1 Ethics statement

All animal experiments were approved by the McGill Animal Care Committee and conducted according to the Canadian Council of Animal Care ethical guidelines for animal experiments.

2.2 Mouse breeding

2.2.1 Fuzzy Mouse breeding

We generated *Fuzzy* transgenic mice at the McGill Transgenic Facility from a gene-trap ES cell line AN0439 as was previously described (Seo, Zilber et al. 2011). The gene-trap βGeo cassette is inserted in the third intron of *Fuzzy* gene, thus, disrupting the wildtype allele. Therefore, we consider this insertion of a loss-of-function (null) mutation. Homozygous *Fuzzy* $^{-/-}$ embryos were acquired by crossing heterozygous *Fuzzy*$^{+/-}$ mice (brother-sister mating), which were identified by genotyping. The plug on the morning after mating was considered embryonic (E) day 0.5. The pregnant females were sacrificed at E14.5 since homozygous *Fuzzy* mice in our colony rarely survive after E14.5.

2.2.2 p190 Mouse breeding

The heterozygous *p190A*$^{+/-}$ mice used in this project were originally generated in Dr Maxime Bouchard's lab (McGill University). The mutant p190A Rho GAP (*Arhgap35*) mouse bears a missense mutation as a result of an ENU mutagenesis approach. To generate germline mutation, N-ethyl N-nitrosourea (ENU, 90mg/kg) was administered 3 times/week by intraperitoneal injections to 8-week C57Bl/6J males. G0 males were originally crossed to wildtype C3H/HeNRl females (Charles River Laboratories) to establish G1 lines for screening; two independent *Arhgap35*^{D34} lines were identified by phenotypic screening and by new generation

sequencing. (Stewart, Gaitan et al. 2016). Subsequently, all mice were transferred to the C57/Bl6 background.

2.2.3 Double Heterozygous Mice (Fuzzy$^{+/-}$;p190A$^{+/-}$)

Fuzzy$^{+/-}$ mice were crossed with *p190A*$^{+/-}$ mice to acquire double heterozygous *Fuzzy*$^{+/-}$*;p190A*$^{+/-}$ mice, that were viable, fertile, and lacked any discernable phenotype. Double HETs were first genotyped to identify the mice with *Fuzzy*$^{+/-}$ mutant allele (as described below). PCP reactions with *p190A* primers were then performed only on *Fuzzy*$^{+/-}$ DNA samples (as described below). The *p190A* PCR fragments were assessed for quality on an agarose gel and then sent for Sanger's sequencing service (Genome Quebec) to identify the *p190A*$^{+/-}$ missense mutation.

The embryos with various gene dosages for *Fuzzy* and *p190A* genes were generated by timed pregnancies by crossing Double Heterozygous *Fuzzy*$^{+/-}$*;p190A*$^{+/-}$ male and female mice. The pregnant mice were sacrificed at E14.5 since majority of *Fuzzy*$^{+/-}$ embryos do not survive past this embryonic stage. The embryos were recovered and preserved by paraffin embedding. The piece of tissue was snipped from each E14.5 embryo for genotyping before processing.

2.3 Mouse genotyping

2.3.1 Fuzzy mice genotyping

All genotyping procedures were performed with DNA samples isolated from the mouse tail biopsies in adult mice by Fast-new genotyping kit (ZmTech Scientifique, Montreal) as described by the manufacturer. In experiments with embryos, DNA samples were isolated from limb biopsies with the same method as adult mice.

Genotyping was performed with the following primers:

The wild-type allele (500bp):

mFuzzy-Exon3-Forward primer: 5′-CACCTCTGAGCTGAGGCTGG-3′.

mFuzzy-Exon4- Reverse primer: 5′-CTCAATTCTTTCTTCAGTCTTTC-3′.

The gene-trapped allele (680 bp):

bGEO-1F primer: 5′-TTATCGATGAGCGTGGTGGTTATGC-3′.

bGEO-2R primer: 5′-GCGCGTACATCGGGCAAA TAATATC-3′.

Preparation of PCR mixture: 2μL of 10XPCR buffer, 0.6μL of 50mM Mgcl2, 0.5μL of 10mM dNTP mix, 0.5μL of 10mM forward primer, 0.5μL of 10mM reverse primer, 0.2μL of Taq polymerase, 13.7μL of PCR water. All the PCR reagents are from Invitrogen (USA). PCR conditions: 1. Heat activation (94°C for 5 min); 2. Denaturation (94°C for 30 sec); 3. Annealing (60°C for 45 sec); 4. Extension (72°C for 1 min); 5. Repeat step 2-4 for 34 cycles; 6. Final elongation (72°C for 5 min). Fluo-DNA ladder (ZmTech, Canada) was used and the PCP fragments were detected on 1% agarose gel by staining with 6x Fluo-DNA Loading Buffer (ZmTech, Canada).

2.3.2 p190 mice genotyping

The p190A mutation is a point mutation (Stewart, Gaitan et al. 2016). For genotyping of a missense p190A gene mutation, we used Sanger sequencing at the Genome Quebec Innovation Centre (Montreal, Canada). The following primers were used to generate 874bp fragment that encompasses the mutation:

Primer1-F: 5'-TGATTGTGGATGTGGTAGGCG-3'

Primer2-R: 3'-GCTTCTCACGGCAACATGGAAC-5'

The PCP fragment was first visualized on the 1% agarose gel to confirm that only a single fragment was present. Then the aliquots of the PCP fragments were sent for genotyping according to the Genome Quebec center instructions.

2.4 Tissue fixation for paraffin embedding

On the first day of paraffin embedding, all embryos were washed in cold PBS to remove traces of blood and then fixed overnight at 4°C in the cold room in 4% paraformaldehyde (PFA)/PBS. We used commercially available 16% PFA solution that was diluted in PBS to 4% right before usage. Leftovers were frozen as 10ml aliquots and stored at -20°C. On the second day, embryos were washed four to five times for 10 minutes each time in cold PBS and then dehydrated in the mix of Ethanol/PBS: three times in 25% EtOH/PBS, pH 7.4, 10 minutes each at room temperature (RT), two times in 50% EtOH/PBS at RT, 10 minutes each, transferred into 75% EtOH/PBS, quickly washed and transferred again to a fresh portion of 75% EtOH. All ethanol dilutions were prepared ahead of time as they could be stored at RT. 75% EtOH in PBS may precipitate, therefore after the precipitate sedimented, the clear fraction was transferred to the fresh bottle and stored at RT. Although tissues can be stored at 4°C for a long time after this step, we had all tissues embedded in paraffin blocks soon after fixation at the McGill University Health Center Research Institute Histology service.

2.5 Tissue sectioning

We pre-cooled the paraffin blocks at 4°C for 30-60 mins. 4μm sections were cut in the sagittal plane on a rotary microtome (Leica RM2235). The kidneys were identified by a visual inspection of paraffin sections during sectioning process using 5x magnification light microscopy, and all kidney sections were collected. To flatten the wrinkles, the sections were put into 5% Triton/H2O water bath at 42°C for 2 mins. The microscope slides (ThermoFisher Scientific, Pittsburgh, USA) were used to pick up the sections. The sections were then dried in an incubator at 37°C overnight. Sections are stored at room temperature until use.

2.6 Immunofluorescence on paraffin sections

The paraffin-embedded tissue sections were warmed up in a dry incubator at 55°C for 45-50 mins and then de-paraffinized by immersing into xylene 3 times for 5 mins each and an additional time in the fresh xylene for 5 mins. To hydrate the tissues, the slides were immersed in different concentrations of ethanol as follows: 100% EtOH –2 times for 3 min; 95% EtOH – 3 mins; 70% EtOH/0.25% NH4CL for 15 mins; 50% EtOH for 5 mins; 30% EtOH for 3 mins. Antigen retrieval was performed in boiled Antigen Unmasking solution (H-3300, Vector, California, USA) for 20 mins at power 4 in the microwave (Toshiba, Japan). Then slides were cooled down in the unmasking solution for 30 mins at RT and then washed in PBS for 10 mins. The tissues were permeabilized by incubating them with 1% Triton X-100/PBS for 1 hour at RT. They were then blocked with 3 % BSA (Bovine Serum Albumin (Bishop, Canada), 10% NGS (Normal goat serum)/NDS (Normal Donkey serum) (Jackson, USA) 0.2% TritonX-100/PBS for 1 hr at RT. The slides were then incubated at 4°C overnight with the primary antibody diluted in the mixture of 3% BSA, 3% NGS/NDA, 0.01% Triton-X-100/PBS. The following antibodies were used: rabbit anti-Calbindin D-28K (Calbiochem, Germany, 1:300), mouse anti-E-Cadherin (BD Transduction Laboratories TM, USA, (1:30), rabbit anti-Six2 (Proteintech, USA, 1:80). The fluorescently tagged agglutinins were used: LTA (Lotus tetragonolobus) (ProteinTech USA, 1:200) and DBA (Dolichos biflorus agglutinin) (ProteinTech USA, 1:200). The next day, slides were washed 4 times in PBS for 5 mins each. The slides were then incubated with secondary antibody for 1hr at RT in dark. The secondary antibodies were Alexa Flour 546 donkey anti-mouse/rabbit IgG (H+L) (Jackson, USA) and Alexa Flour 488 donkey anti-mouse (Jackson, USA). Slides are washed 4 times in PBS for 5 mins each and then incubated for 7 min in DAPI (4', 6-Diamidino-2-Phenylindole, Dihydrochloride, Invitrogen, USA; 1:500) in 0.1% Tween-20/PBS at

RT. Finally, the slides were mounted with coverslips (Fisher Scientific, USA) with a drop of ProLongTM Gold Antifade Mounting medium (Invitrogen Molecular probe, USA), and kept overnight in dark at RT.

2.7 Hematoxylin and Eosin staining

Wildtype and *Fuzzy*$^{-/-}$ paraffin-embedded embryonic sections were deparaffinized and hydrated as described above. After that, slides were stained in Mayer's Hematoxylin Solution (MHS16, Sigma) for 1-4 min (or more) at RT. If required, the hematoxylin solution was filtered before usage. The slides were then rinsed in warm running tap water until the water ran clear. Slides were placed in distilled water for 30 sec and then rinsed quickly in 95% EtOH. The slides were placed in Eosin Y alcoholic solution (HT110116, Sigma): glacial acetic acid, 1:200 for 1-2 sec, rinsed in warm running water until the water ran clear, and rinsed in distilled water for 30 sec. The slides were immersed in 95% EtOH 2 times for 2 mins each and in Xylene substitute 2 times for 3 mins each. Then, the slides were mounted with Shandon xylene substitute mounting medium (Therma Fisher, USA).

2.8 Imaging

All fluorescent images of LTA, DBA, calbindin, and DAPI-stained tissued were acquired on Zeiss Axio Observer 100.Z1 microscope (Zeiss, Germany) via a Zeiss AxioCam MRm monochrome camera. Magnification 5X, 10X and 40X were used for both controls and mutant tissues. For Hematoxylin and Eosin-stained slides and embryos of different gene dosages at E14.5, images were acquired using Zeiss AXIO Imager D2 capturing with Zeiss Axio CAMera ICc5. The Zen lite software (Zeiss, Germany) was used.

2.9 Analysis of renal tubule and glomerular morphology

To analyze morphology of the tubule and glomerular structures, we used E16.5 embryos (kindly provided by Dr Karen Liu, King College, London, UK). In Dr Liu's lab, the animals are on mixed Bl6/CD-1 background and can survive until E16.5 *in utero*. E16.5 paraffin 4µc kidney sections of control and *Fuzzy*$^{-/-}$ embryos were stained with LTA (specific marker for proximal tubule) and DBA (specific marker for collecting duct/ureteric bud). Quantitative analysis was performed on the transverse tubules by measuring the length and width of each tubule cross-section. The diameter of the tubule cross-section was interpreted as the longest measure (length); the width was considered as a perpendicular to the length. The tubule cross-sections with the ratio of the length to width between 0.9-1.1 were considered as "perfect" circular structures and were used for analysis. The number of cell nuclei stained with DAPI was counted for each tubule. 73 and 150 tubules were analyzed from *Fuzzy*$^{-/-}$ and control mice, respectively, for LTA staining. 102 and 138 tubules were analyzed from *Fuzzy* mutants and control mice for DBA, respectively. The statistical analysis was carried out between control and *Fuzzy*$^{-/-}$ embryos. Area of the curve was plotted to compare the differences between control and *Fuzzy*$^{-/-}$ embryo kidneys. The area of Bowman's capsule and area of tuft were measured by using the contour application in the Zen lite software (Zeiss, Germany). The average area was calculated for 135 and 110 glomeruli from wildtype and *Fuzzy* mutants.

2.10 Study of Ureteric Bud branching morphogenesis

All E14.5 kidney sections from the embryos of various genotypes were stained with antibody against Calbindin (D-28k) to visualize the ureteric bud and collecting duct structures; the images were acquired at 5X magnification. First, we identified "maximal" sagittal kidney sections: the collecting ducts of these sections could be traced from the center to the cortical layer. The

number of the UB tips per each maximal section was counted; two maximal sections per kidneys were analyzed.

2.11 Urine collection and analysis

For urine collection, independent metabolic cages were used. The metabolic apparatus was a normal mouse cage with no bedding and a small plastic grid placed at the bottom of the cage. Cages were autoclaved, dried, and mice were placed in the cage until urine was generated (~2 hours). Urine not contaminated by the fecal waste was collected in an Eppendorf tube and stored at -20°C or -80°C for long term storage. Urine Albumin-Creatinine ratio (UACR) was determined using the Mouse Albumin ELISA Assay kit (Bethyl labs, Texas, USA). 100µl of diluted Affinity purified Goat anti- Mouse Albumin Coating Antibody A90-134A (1ml at 1 mg/ml) (Bethyl Laboratories) was aliquoted to each well and urine samples were added and incubated overnight at 4°C. The next day, the plate was washed five times with wash buffer (50mM Tris, 0.14 M NaCl, 0.05% Tween-20, pH8.0). 200µl of blocking solution (50mM Tris, 0.14 M NaCl, 1% BSA, pH 8.0) was added and incubated at RT for 30 mins. 100µl of diluted HRP conjugated Goat anti – Mouse albumin Detection Antibody A90-134P (Bethyl laboratories) was added to each well, and the plate was incubated for 1 hr at RT. The plate was washed five times, and then 100µl of TMB Substrate Solution (Thermo Fisher Scientific) was added to each well. The plate was developed in the dark at room temperature for 15 mins. The reaction was stopped by adding 100µl od stop solution (2 M H_2SO_4) (ThermoFisher Scientific) to each well. The absorbance was measured on a plate reader at Optical Density 450nm.

2.12 Statistical Analysis and Graphing

In all experiments, mean values, standard deviation and error bars were calculated in Microsoft Excel 2019 for Windows. To calculate the kidney size and the number of ureteric bud

tips in the embryos with different gene dosages, Image J software version 4.0 was used (National Institute of Health, USA). Kidney sizes were calculated in μm^2. GraphPad Prism 9.0 software was used to create a graphical presentation of the results. The data were analyzed using an unpaired unequal variance t-test for most of the experiments. The p-value <0.05 was considered significant.

2.13 Basal Body Immunostaining and colocalization

Mouse embryonic fibroblasts were established as previously described (Seo, Zilber et al. 2011). MEFs$^{+/+}$ and *Fuzzy*$^{-/-}$ MEFs were plated into 12-well plates (Sarstedt, USA) containing collagen-coated cover slips and cultured in DMEM medium supplemented with 10% FBS (Wisent). The cells were transfected with Fugene (Promega, USA) in 1:2 DNA:Fugene solution as recommended by the manufacturer using 0.5-0.75μg of p190A-GFP (a kind gift from Maxime Bouchard, McGill University). The cells were incubated for 24 hours post-transfection in 500μl DMEM per well, 20% FBS at 37°C in 5% CO2 incubator. Each well was washed once with DMEM, and cells were incubated in 1ml of DMEM without serum for 24hr to induce ciliogenesis. The cells were fixed for 15 min with 4% PFA/PBS, washed with PBS 4 times for 3 min, permeabilized with 0.5% TritonX/PBS for 10 min. The cells were washed with 0.1% TritonX/PBS (ThermoFisher Scientific, USA) for 30 min and then in PBS 3 times and incubated with Fab Donkey anti-mouse (Jackson's Lab) 1:500 in PBS. After that, the cells were washed in 0.1% TritonX/PBS 3 times for 3 min and incubated with anti-gamma tubulin antibody (Sigma, 1:4000) in 5% NDS, 0.1%TritonX/PBS for 2hr at RT. The antibody was wash off with 0.1%TritonX/PBS 3 times for 3 min and incubated with Cy3 Fab Donkey anti-mouse (Jackson's lab, 1:800) and DAPI (Sigma,1:1000) in 5% NDS, 0.1% TritonX/PBS for 1hr at RT. The cells were mounted in

Fluoromount-G (USA). The images were acquired using confocal laser scanning microscope LSM880 (Zeiss, Germany).

2.14 Co-Immunoprecipitation assay

HEK293T cells were grown in 100mm Petry dishes in DMEM/10% FBS until 70-80% confluency for 24hr. The cells were then transfected with 2µg Fuzzy-HA (Seo, Zilber et al. 2011) and/or 1.5µg p190A-GFP cDNA (a kind gift from Maxime Bouchard) using Lipofectamin 2000 (ThermoFisher Scientific, Canada) at ratio 1:2 of DNA and Lipofectamine as recommended by the manufacturer. To achieve equal amounts of DNA in each dish, pcDNA3.1 plasmid was used, where appropriate. The cell lysates were prepared 24 hours later using lysis buffer (50mM HEPES, pH 7.5; 150mM NaCl, 10% Glycerol, 0.5% TritonX, 1.5mM MgCl, 1mM EGTA, 25mM NaF, 2mM Na3VO4, 10 mM Ppi, 1x PIC and 1mM PMSF); all inhibitors were from Sigma. The cells were scraped off in the lysis buffer into vials and lyzed by vigorous intermittent vertexing for 20 min. The cell lysates were precleared by centrifugation at 14,000rpm for 15 min. The protein concertation in each tube was measured using Bradford method. Minimum 50µl of each protein lysate was saved as "input" fraction.

Agarose beads were pre-cleared by extensive washing in the lysate buffer and then incubated with 1µg anti-HA monoclonal antibody (Covance, New Jersey, USA) for 45 min at 4°C in the lysate buffer on a rotating wheel. The protein lysates containing 0.75-1mg of total protein in 200µl were then added to the beads/antibody mix and incubated overnight at 4°C on the rotating wheel. The beads/HA antibody/proteins were quickly washed twice in the cold washing buffer 1 (50mM HEPES, pH 7.5, 200mM NaCl, 10% Glycerol, 0.5% TritonX/H2O, 1.5mM MgCl, 1mM EGTA and the same protease inhibitors as in the lysis buffer). Then the beads/HA antibody/proteins were quickly washed in washing buffer 2 (the same as Washing buffer 1 but

500mM NaCl). The beads were collected by centrifugation at 2000 rpm and 2x sample buffer, containing 5% mercaptoethanol, was added to each vial. The samples were heated for 10 min at 95-98°C and used for Western blotting or stored at -80°C.

2.15 Western immunoblotting assay

All samples were resolved on 7% acrylamide gel using routine techniques. Each co-IP variant and 20µg of each "input" fraction were resolved in parallel. The proteins from the gels were transferred onto Biotrace NT nitrocellulose membranes. The membranes were blocked in the blocking buffer (5% Bovine serum albumin, tris-buffered saline, pH8.0 supplemented with 1% Tween (TBST) for 1hr at RT. The co-IP and one of the input membranes were incubated with anti-p190A antibody (rabbit polyclonal, Cell Signaling; 1:1000) in the blocking buffer, O/N at 4°C in the rotating wheel , while the other input membrane was incubated with anti-HA antibody under the same conditions. All membranes were washed 4x10 min each in the TBST buffer and incubated with either HRP-mouse antibody (Jackson, USA 1:20000) to detect anti-HA antibody or with HRP-rabbit (Jackson,USA, 1:20000) to detect anti-190A antibody in the blocking buffer for 1hr at RT. The membranes were then washed in the washing buffer, and proteins detected using ThermoFisher.

Chapter 3: Results

3.1 Loss of Fuzzy causes dilatation in proximal tubules at E16.5

To uncover the role of the PCP gene *Fuzzy* in kidney morphogenesis, we generated *Fuzzy* transgenic mice from a gene-trap ES cell line AN0439. The βGeo gene-trap cassette is inserted in the third intron of *Fuzzy* gene, disrupting the wildtype allele, and generating a "null" allele. In our earlier studies, we discovered that at E14.5, *Fuzzy*$^{-/-}$ mice exhibit kidney hypoplasia (Wang *et al*, manuscript in preparation). *Fuzzy* homozygous embryos also exhibit neural tube defects (exencephaly), anophthalmia/microphthalmia (no eyes) and polydactyly, all of which can be easily detected by visual inspection. In the current study, we examined embryonic kidneys from the wildtype and *Fuzzy*$^{-/-}$ mutant mice at E16.5, the stage when a sufficient number of nephrons has already been formed, and the glomeruli and renal tubules are undergoing active maturation and elongation, respectively (**Figure 3.1 & 3.2 A-B**). Importantly, at ~E15.5 onward, the kidney starts to produce first urine, potentially providing a polarizing directional signal (urine flow) to the developing tubules. We discovered that E16.5 *Fuzzy*$^{-/-}$ kidneys are smaller and have tubular and glomerular dilatation (**Figure 3.2B**). During embryonic stage of kidney development, tubular dilatation may be caused by defective convergent extension (CE) that could be seen as an expansion of tubule cross-sectional area and an increase in the number of cells in the tubule cross-section (discussed in the Introduction in detail) (Karner, Chirumamilla et al. 2009). Importantly, CE in the developing renal tubules is controlled by PCP signaling (Derish, Lee et al. 2020). To ascertain whether loss of *Fuzzy* gene affects CE, we investigated proximal tubules and collecting duct tubules individually. Proximal tubules (PT) were visualized by staining with a well-characterized PT marker LTA (Lotus tetragonolobus) (Barresi, Tuccari et al. 1988). We measured the cross-sectional area, the tubule diameter along the longest axis (length) and the perpendicular

axis (width) and the cell number in the cross-sections (**Figure 3.2 C**). Only the tubules with length-to-width ratio between 0.9-1.1 were considered as "perfect' and used for analysis (Derish, Lee et al. 2020). We observed a dilatation in proximal tubules with increase of cross-sectional area by 76% and significant increase in the cell number in the *Fuzzy*$^{-/-}$ mouse kidneys comparing to control proximal tubules. Total number of tubular structures analyzed were wildtype, WT=150 (4 embryos) and *Fuzzy*$^{-/-}$ =73 (4 embryos). Thus, our results suggest that loss of *Fuzzy* leads to a significant dilatation of proximal tubules as early as E16.5 (**Figure 3.2 D-F**).

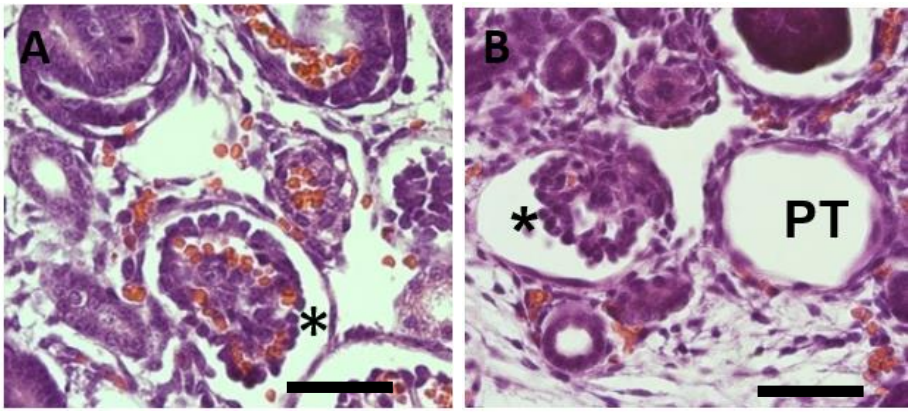

Figure 3.1: Morphology of *Fuzzy*$^{-/-}$ kidneys at E16.5

(A) Wildtype section and (B) *Fuzzy*$^{-/-}$ Hematoxylin and Eosin-stained sections (63X) are presented. Glomerular cysts (asterisks), proximal tubules (PT).

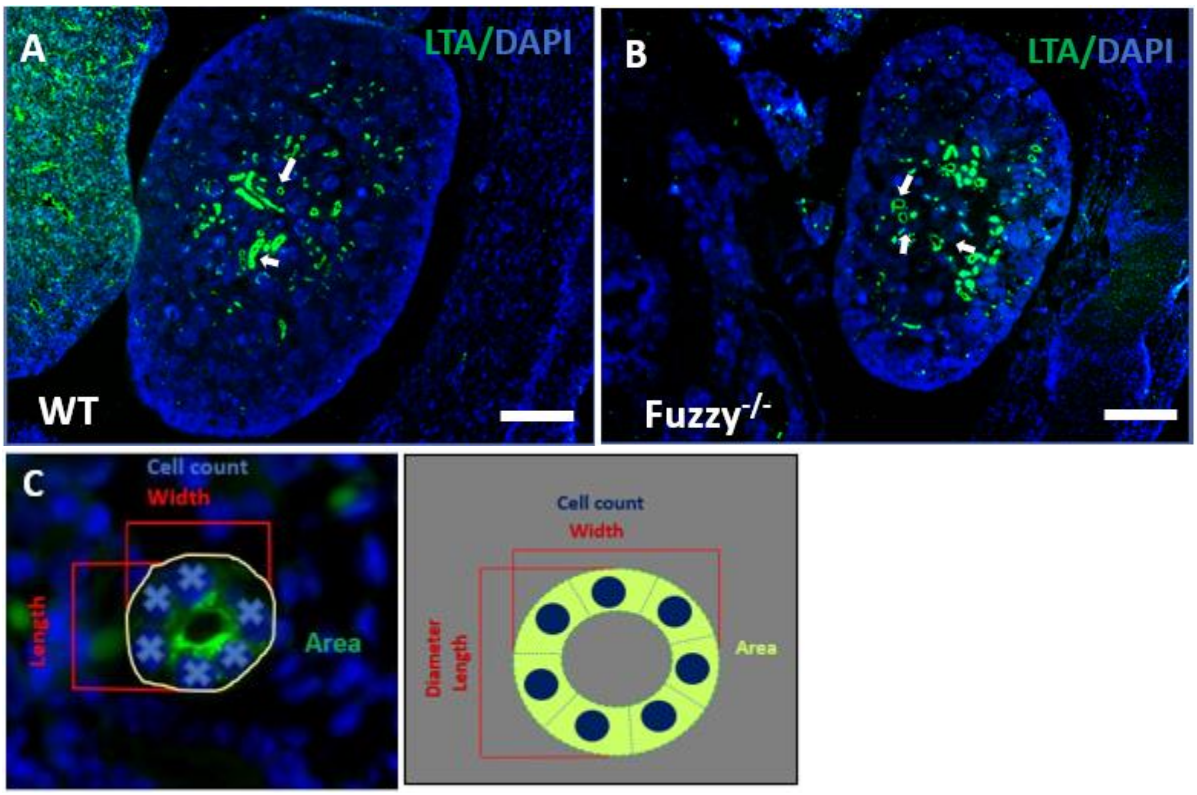
A
LTA/DAPI
WT
B
LTA/DAPI
Fuzzy-/-
C
Cell count
Width
Length
Area
Cell count
Width
Diameter
Length
Area
D
Average area of proximal tubule (µm²)
3000
2000
1000
0
***
WT
Fuzzy -/-
Genotype
E
% of events
80
60
40
20
0
Fuzzy-/-
WT
0
1000
2000
3000
Average area of PT (µm²)
F
PT Cell number per cross-sections
15
10
5
0
**
WT
Fuzzy-/-

Figure 3.2: Analysis of proximal tubule morphology in E16.5 wildtype and *Fuzzy*$^{-/-}$ embryos

(A-B) Immunofluorescence staining of E16.5 control and *Fuzzy*$^{-/-}$ kidney sections with LTA (marker for proximal tubules, green) and DAPI (marker for nuclei, blue), scale bar is 100 μm. (C) Immunostaining (right) and schematic representation (left) of measurements of area (area), length and width (red) and cell count (blue) in a tubule cross-section. (D) Measurement of average tubule area in the circular proximal tubule cross-section. (E) Percentage of events within a given range of cross-sectional area in proximal tubule. (F) Average cell count in the control and *Fuzzy*$^{-/-}$ proximal tubules. Only the tubule cross-sections with the ratio of the length-to-width between 0.9-1.1 were analyzed. Wildtype (WT) (n= 150), *Fuzzy-/-* (n=73) were analyzed; 4 embryos per genotype were analyzed. Standard error of mean is shown in all graphs; $p<0.05$ (*), $p<0.001$ (**), $p<0.0001$ (***).

3.2 Analysis of collecting duct morphology in Fuzzy$^{-/-}$ and wildtype kidneys at E16.5

To analyze the morphology of collecting duct tubules, we stained E16.5 wildtype and *Fuzzy*$^{-/-}$ embryonic sections with DBA (Dolichos biflorus agglutinin), a specific marker for collecting duct (CD) and ureteric bud (Holthofer, Schulte et al. 1987) (**Figure 3.3 A**). We conducted a quantitative analysis of the tubule size by measuring the length and the width of each tubule cross-section, the cross-sectional area and the number of the cells. As in the experiments with proximal tubules, only the tubule cross-sections with the ratio of the length-to-width between 0.9-1.1 were considered for analysis. We observed larger cross-sectional area in the *Fuzzy*$^{-/-}$ in the collecting duct with 74% increase in the mutant collecting ducts comparing to wildtype tissues. The number of cells in tubule cross-sections was also elevated in *Fuzzy*$^{-/-}$ tubules vs in the control structures. Total number of tubular structure analyzed were WT= 138 (4 embryos) and *Fuzzy*$^{-/-}$ = 102 (4 embryo per genotype were analyzed) (**Figure 3.3 B-C**).

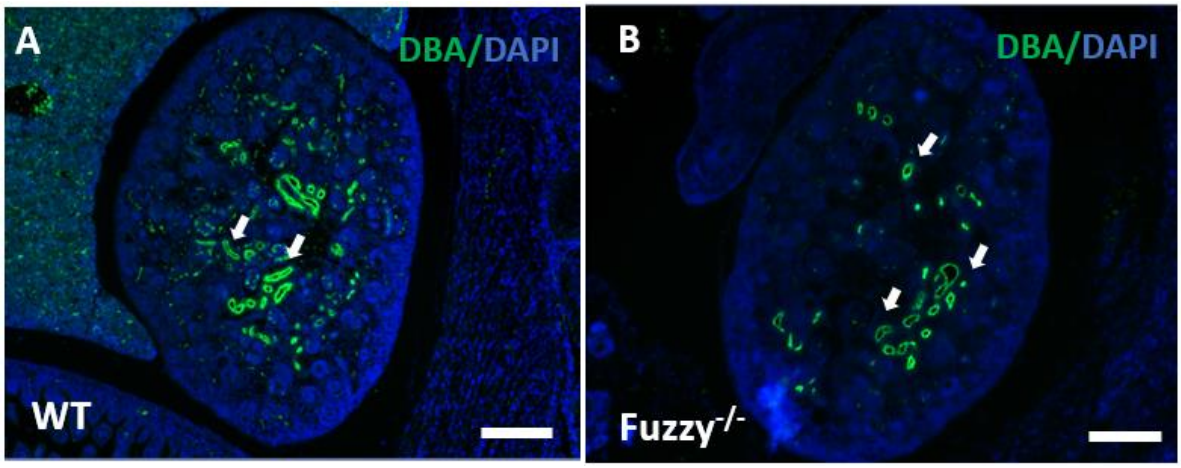
A
DBA/DAPI
WT
B
DBA/DAPI
Fuzzy-/-

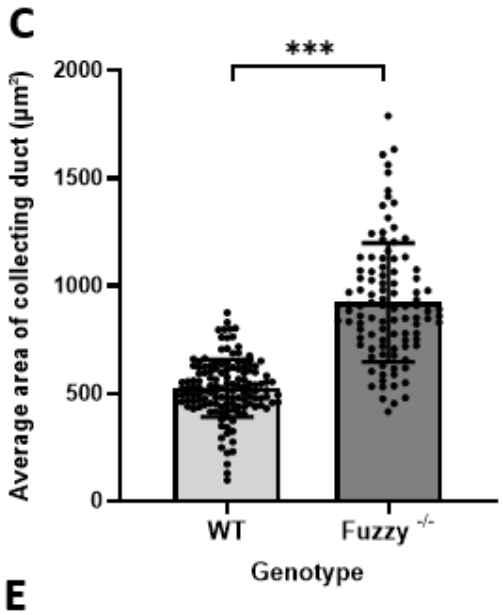
C
***
Average area of collecting duct (µm²)
2000
1500
1000
500
0
WT
Fuzzy -/-
Genotype

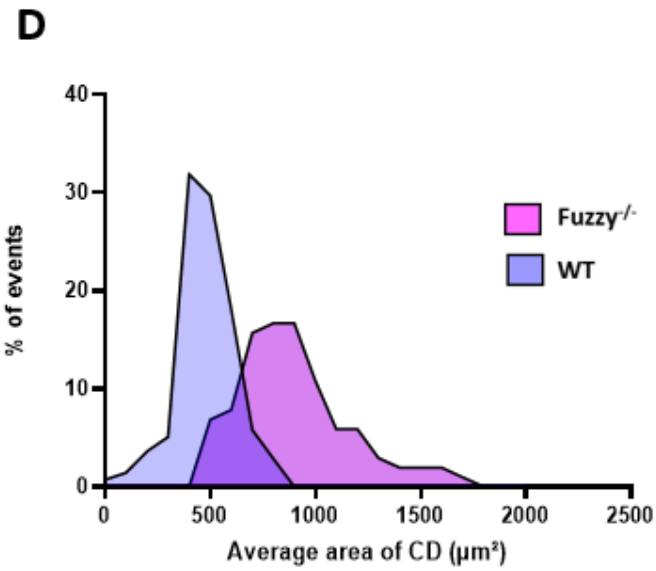
D
% of events
40
30
20
10
0
0
500
1000
1500
2000
2500
Average area of CD (µm²)
Fuzzy-/-
WT

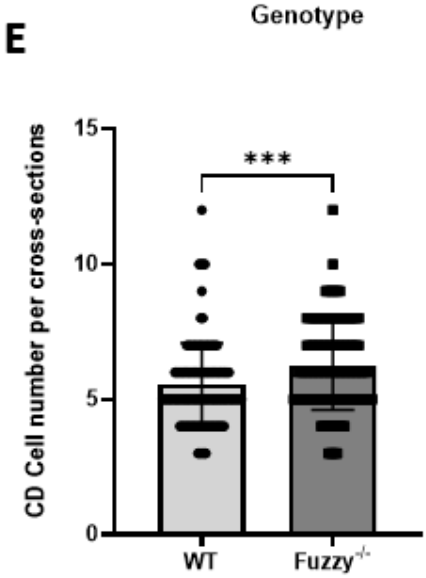
E
***
CD Cell number per cross-sections
15
10
5
0
WT
Fuzzy-/-

Figure 3.3: Analysis of collecting tubule morphology inE16.5 wildtype and *Fuzzy*$^{-/-}$ embryos

(A-B) Immunofluorescence staining of E16.5 wildtype and *Fuzzy*$^{-/-}$ kidney sections with DBA (marker for collecting duct, green) and DAPI (marker for nuclei, blue); scale bar is 100 μm. (C) Analysis of collecting ducts area in the wildtype and *Fuzzy*$^{-/-}$ kidneys. (D) Percentage of events within a given range of cross-sectional area in the collecting duct tubules. (E) Analysis of cell count in the transverse collecting duct tubule sections. Total structures analyzed: WT (n=138) and *Fuzzy*$^{-/-}$ (n=102); 4 embryos per genotype were analyzed. Mean ± standard error of mean is shown in all graphs; $p<0.05$ (*), $p<0.001$ (**), $p<0.0001$ (***).

3.3 Loss of Fuzzy results in expansion of Bowman's capsule

The renal glomerulus functions as the filtering unit of the kidney, containing a bundle of capillaries (Pollak, Quaggin et al. 2014). These capillaries are enclosed within the Bowman's capsule, a cup-like structure that protects the glomerular vascular bed, collects the glomerular filtrate, and passes it to the proximal tubule. Mesangial cells act to support capillaries and, together with podocytes, form glomerular tuft, that is also contained within the Bowman's capsule. To analyze the glomerular morphology, we first identified glomeruli by their characteristic cup-like structure and then carried out histological measurements of the Bowmans' capsule size and the size of the glomerular tuft. We observed glomerular cysts (significant expansion of the Bowman's capsule) exclusively in the juxta-medullary glomeruli at the border of cortical and medullary regions in the *Fuzzy*$^{-/-}$ kidneys but not in the glomeruli located in the cortical area (**Figure 3.4 A-B**): on average, the size of the Bowman's capsule of all *Fuzzy*$^{-/-}$ glomeruli was 38% larger comparing to the same structures in the wildtype E16.5 kidneys (**Figure 3.4 C-D**). Measurement of the tuft area revealed no increase in the *Fuzzy*$^{-/-}$ glomeruli vs control tissues in all glomeruli including the ones with the cystic Bowman's capsule (**Figure 3.4 E-F**). Our results indicate that the cysts likely arise in more mature glomeruli after production of the glomeruli filtrate. Total number of glomeruli analyzed WT=135 (4 embryos) and *Fuzzy*$^{-/-}$ = 110 (4 embryos).

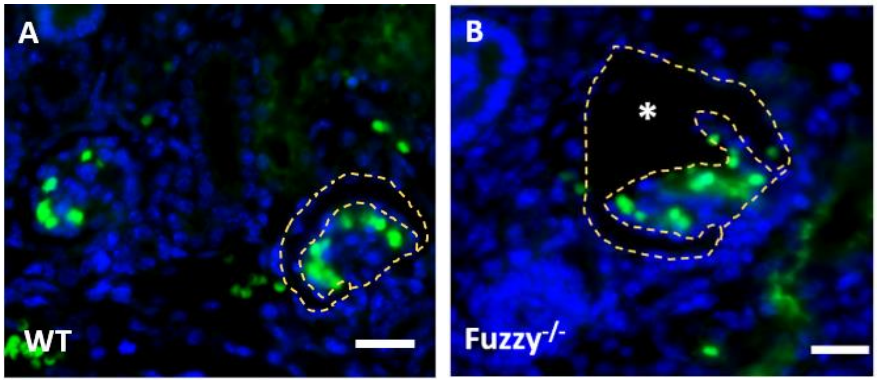
A
WT
B
Fuzzy-/-
*

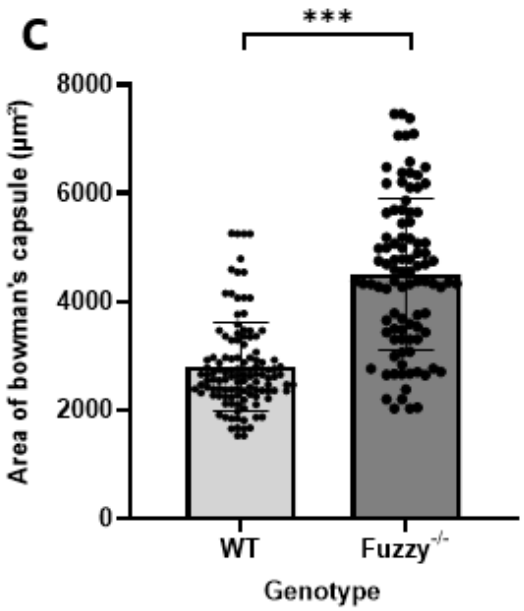
C
***
Area of bowman's capsule (µm²)
8000
6000
4000
2000
0
WT
Fuzzy-/-
Genotype

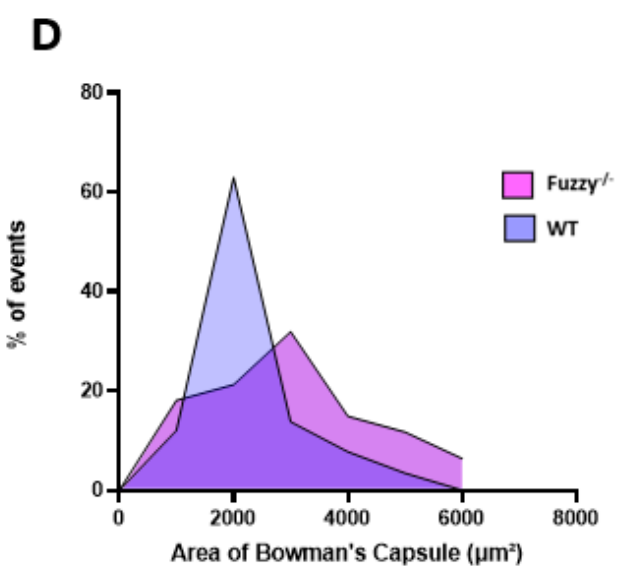
D
% of events
80
60
40
20
0
Fuzzy-/-
WT
0
2000
4000
6000
8000
Area of Bowman's Capsule (µm²)

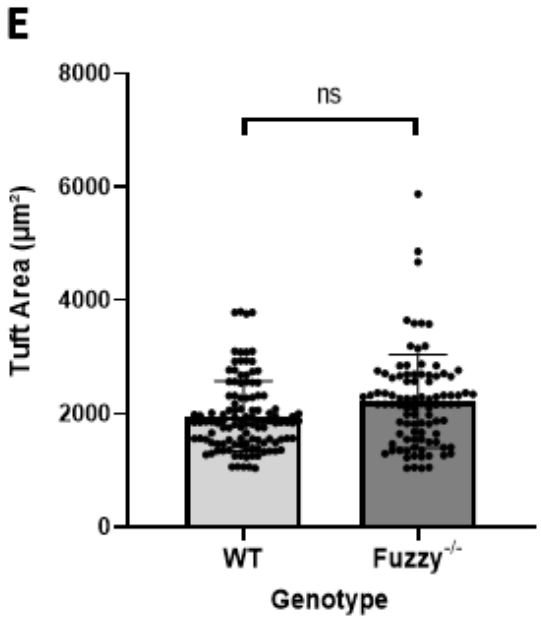
E
Tuft Area (µm²)
8000
6000
4000
2000
0
ns
WT
Fuzzy-/-
Genotype

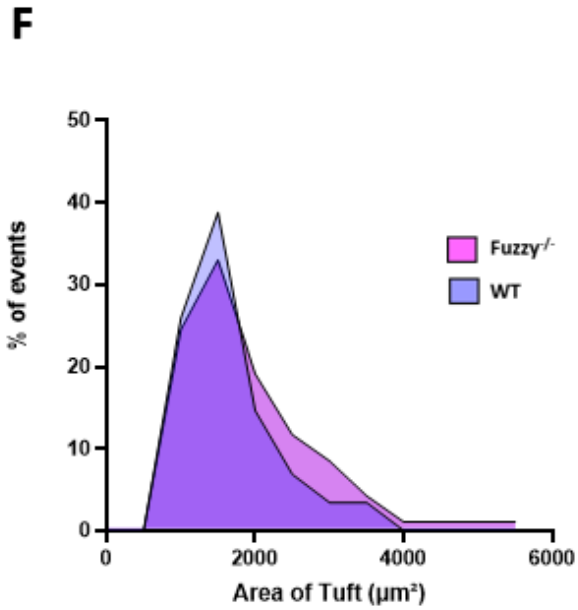
F
% of events
50
40
30
20
10
0
Fuzzy-/-
WT
0
2000
4000
6000
Area of Tuft (µm²)

Figure 3.4: Morphological analysis of glomeruli in wildtype and *Fuzzy*$^{-/-}$ E16.5 kidneys.

(A-B) Mature glomeruli at E16.5 in wildtype and *Fuzzy*$^{-/-}$ kidney sections (depicted by yellow dashed lines); scale bar is 50 μm. (C) Measurement of the Bowman's capsule size. (D) Percentage of events within a given range of area. (E) Measurement of tuft area. (F) Percentage of events within a given range of area. Mean and standard error of mean is presented in all graphs. WT (n=138), Fuzzy$^{-/-}$ (n=110) were analyzed. 4 embryos per genotype were analysed. $p<0.05$ (*), $p<0.001$ (**), $p<0.0001$ (***).

3.4 Analysis of the nephron progenitors in Fuzzy$^{-/-}$ and wildtype E16.5 kidneys

The signals secreted by the cells of the UB tip induce the metanephric mesenchyme around the UB tip to become committed nephron progenitors that form cap mesenchyme and undergo mesenchyme-to-epithelial transition to eventually give rise to all nephron segments (Brodbeck, Besenbeck et al. 2004). The nephron progenitors express Six2 transcription factor that is mainly required to maintain nephron progenitor population (Self, Lagutin et al. 2006). Our earlier finding of renal hypoplasia at E14.5 had been attributed mainly to the defective branching morphogenesis of the UB; the progenitor pool was not significantly affected at this early stage (not shown, Wang *et al*, manuscript in preparation). However, we questioned whether the hypoplastic kidney phenotype seen in E16.5 *Fuzzy*$^{-/-}$ mice might have been caused, at least in part, by abnormalities of nephron progenitor cells at later developmental stage. To detect cap mesenchyme cells, each kidney section was immunostained with two antibodies: anti-E-cadherin to detect ureteric buds and anti-Six2 to identified nephron progenitor cells. The number of the cells surrounding each UB tip was counted (**Figure 3.5 A-B**). The obtained results suggest no significant differences between the average size of the progenitor pool in the E16.5 wildtype and *Fuzzy*$^{-/-}$ kidneys. 146 wildtype (4 embryos) and 101 cap mesenchyme structures (4 *Fuzzy*$^{-/-}$ embryos) were analyzed (**Figure 3.5 C**).

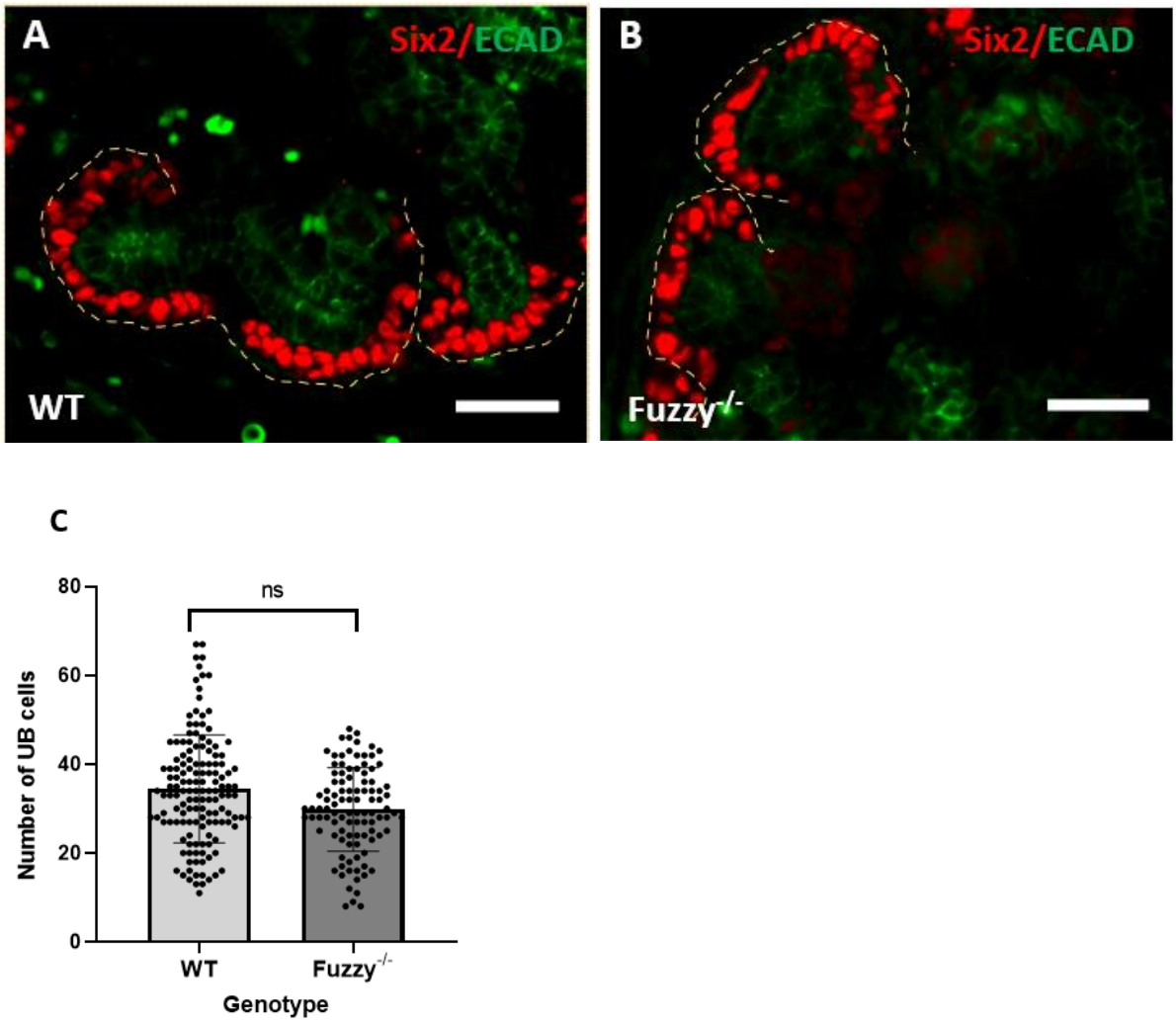

Figure 3.5: Progenitor cell pool size in the wildtype and *Fuzzy*$^{-/-}$ kidneys at E16.5

(A-B) E16.5 wildtype and *Fuzzy*$^{-/-}$ kidney sections were stained with anti-Six2 antibody (specific marker of nephron progenitor cells (red) and E-cadherin (marker of epithelial structures, green); white dashed lines depict the cap mesenchyme domains. Scale bar is 50 μm. (C) Quantification of Six2+ cells per UB tips. Wildtype (n= 146) and Fuzzy$^{-/-}$ (n=110) were analyzed; 4 embryos were analysed per genotype.

3.5 Interactions between PCP protein Fuzzy and Rho GTPases p190A

Loss of *Fuzzy* leads to the disruption of multiple developmental processes: e.g. in *Drosophila* it acts together with other PCP effector proteins, Inturned and Fritz, to contain actin polymerization during trichome formation (Strutt 2009). In vertebrates, however, Fuzzy and other PCP effectors appear to control ciliogenesis (Heydeck, Zeng et al. 2009). Previous studies from our lab and other groups showed that Fuzzy is required in cilia formation by recruiting certain proteins to the base of the cilium (Zilber, Babayeva et al. 2013). By reviewing literature, we noticed that mutations in p190A (encoded by the *ArhGAP35* gene) result in glomerular cystic kidneys phenotypically identical to the kidney features we found in the *Fuzzy*$^{-/-}$ kidneys at E16.5 (**Figure 3.6 A-D**). p190A functions as the main RhoA GAP in mammalian cells and controls actin polymerization at the base of the cilium; mutations in *ArhGAP35* gene lead to increased actin polymerization at the basal body and shortened cilia in the kidney epithelial cells (Stewart, Gaitan et al. 2016). Based on the published literature specifying the roles of Fuzzy and p190A in ciliogenesis, role of Fuzzy in actin regulation in *Drosophila*, overall emerging involvement of actin cytoskeleton in ciliogenesis, and striking similarities of kidney phenotypes in both *p190A* and *Fuzzy* mutant mice, we hypothesized that Fuzzy may participate in the recruitment of Rho GTPases p190A to the base of the cilia.

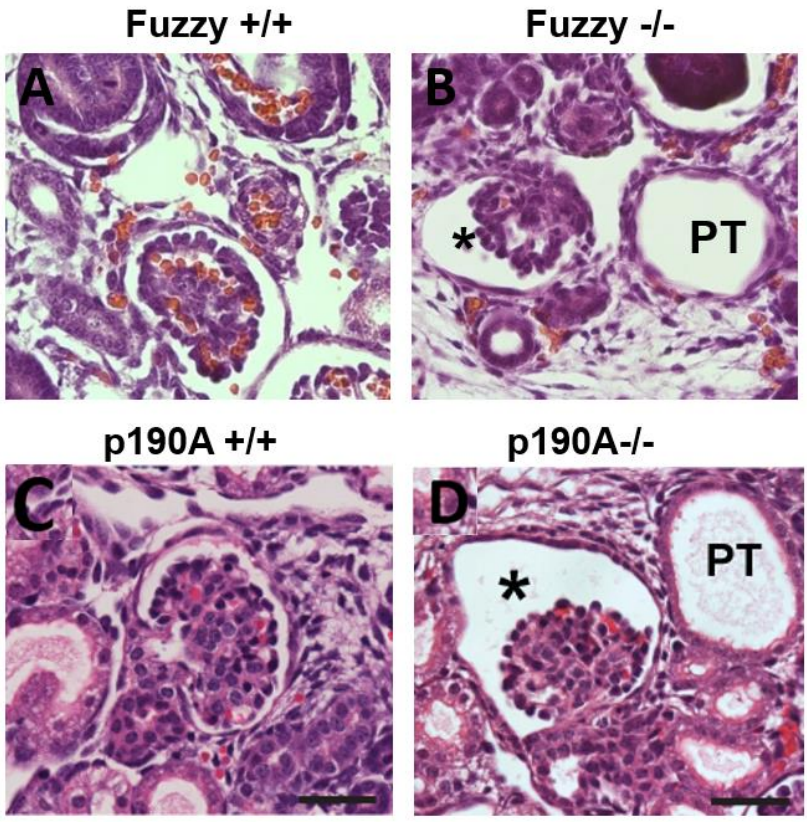

Figure 3.6: Phenotypic similarities between Fuzzy$^{-/-}$ and p190A$^{-/-}$

Hematoxylin and Eosin-stained sections show larger glomerular cysts (asterisks), accompanied by occasional proximal tubule (PT) dilation in both (B) *Fuzzy* deficient animals and (D) *p190A* deficient animals. Control kidneys (A, C) lack cystic structures. Note that the morphology of both *Fuzzy*$^{-/-}$ and *p190A*$^{-/-}$ is phenotypically identical. Scale bars 20μm.

Figure C-D Reprinted and modified from (Stewart, Gaitan et al. 2016).

To confirm – or refute - our novel hypothesis, we first explored whether Fuzzy and p190A proteins may interact biochemically. We transiently expressed both Fuzzy fused to HA epitope (Fuzzy-HA) and p190A fused to GFP (p190A-GFP) proteins in the HEK293 cells, prepared cell lyzates and immunoprecipitated protein mix with anti-HA antibody. The immunoprecipitated proteins were analyzed by Western immunoblotting with anti-p190A to detect p190A protein and with anti-HA antibody to detect Fuzzy-HA. As shown in (**Figure 3.7)**, p190A protein could be detected in the mix with Fuzzy-HA only after Fuzzy was immunoprecipitated with anti-HA antibody (3^{rd} lane) but not when p190A (1^{st} lane) or Fuzzy-HA (2^{nd} lane) was omitted in the cells or when specific anti-HA antibody was missing (4^{th} lane). The expression of all proteins in the HEK293 cells is shown in the "input" panels. Therefore, our results indicate that Fuzzy and p190A interact biochemically.

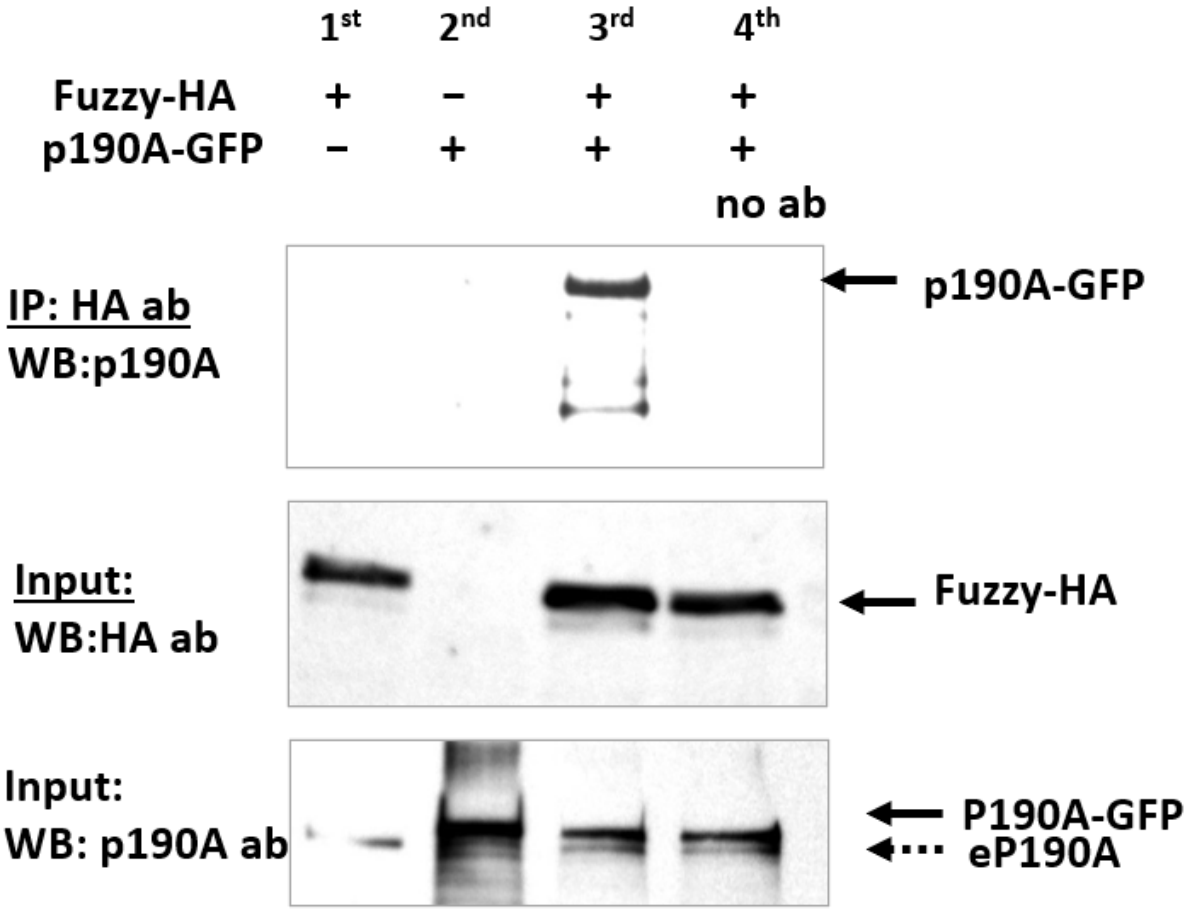

Figure 3.7: Co-immunoprecipitation assay

Fuzzy-HA and p190A-GFP proteins were expressed in the HEK293 cells, and cell lysates were then immunoprecipitated with HA antibody. Western blotting with anti-p190A to detect p190A protein and anti-HA antibody to detect Fuzzy -HA. The top panel is the Western blotting following co-IP; the middle and bottom panels are inputs; ep190A is endogenous p190A protein detected with anti-p190A antibody.

3.6 Localization of p190A at the basal body in Fuzzy$^{-/-}$ cells

We previously established immortalized mouse embryonic fibroblast (MEF) from E12.5 wildtype and *Fuzzy*$^{-/-}$ embryos (Seo, Zilber et al. 2011). The mutant cells grow well, but lack cilia; recruitment of Rab8, a small GTPase protein critical for trafficking and fusion of cargo vesicles to the basal body, is defective (Zilber, Babayeva et al. 2013). To evaluate whether Fuzzy is required for the recruitment of p190A to the basal body, we transfected both wildtype MEFs$^{+/+}$ and *Fuzzy*$^{-/-}$ MEFs with p190A-GFP expression construct, induced ciliogenesis by serum withdrawal and fixed the cells in 24 hours after ciliogenesis was initiated. The basal bodies were identified by immunostaining with anti-γ-tubulin antibody, and the presence of GFP signal at the base of the cilium was visualized by confocal microscopy (**Figure 3.8 A**). Almost 85% of the MEFs$^{+/+}$ retained GFP fluorescence signal at the basal body while only ~ 15% of the *Fuzzy*$^{-/-}$ MEFs exhibited GFP signal (**Figure 3.8 B**). Thus, our new data suggest that Fuzzy likely regulates recruitment of p190A to the basal body.

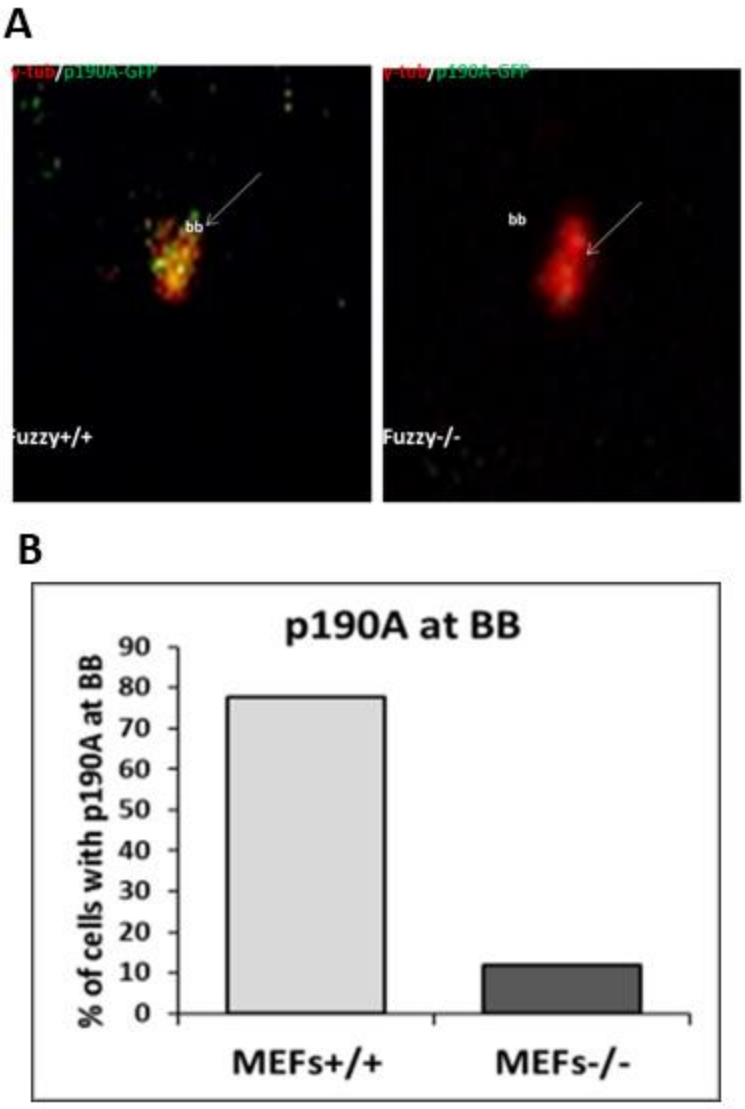

Figure 3.8: Analysis of p190A localization at the basal body

(A) Wildtype & *Fuzzy*$^{-/-}$ mouse embryonic fibroblasts were transfected with p190A-GFP protein expression construct. The basal body (BB, arrow) was visualized with anti-γ-tubulin antibody (red, specific marker of centrosome and basal body). Presence of GFP at the basal body is seen as yellow color; absence of GFP at the basal body is seen as red color. (B) Statistical analysis of percentage of the cells with p190-GFP at the basal body.

3.7 Genetic interaction between Fuzzy and p190A

Based on our observations above showing biochemical interactions between Fuzzy and p190A and a loss of p190A at the basal body of *Fuzzy*$^{-/-}$ cells, we hypothesised that the two genes may be acting in the same pathway and interact genetically. To explore whether the genetic link exists and to better understand a functional mechanism between Fuzzy and p190A, we generated double heterozygous (HETS) mice *Fuzzy*$^{+/-}$*;p190A*$^{+/-}$, which were acquired by crossing *Fuzzy*$^{+/-}$ and *p190A*$^{+/-}$ heterozygous mice. Based on our analysis of 295 progeny, majority of the double HETS mice appeared to have survived to adulthood, were viable and fertile, and we found no phenotype in these adult mice. However, we consistently observed the lower number of double heterozygous *Fuzzy*$^{+/-}$*;p190A*$^{+/-}$ mice than expected (**Table 3.1**): the theoretical expected genotypes is 25% *WT* : 25% *Fuzzy*$^{+/-}$: 25% *p190A*$^{+/-}$: 25% *Fuzzy*$^{+/-}$*;p190A*$^{+/-}$, whereas the obtained percentages for each genotype were 30% *WT* : 30% *Fuzzy*$^{+/-}$: 22.5% *p190A*$^{+/-}$: 17.5% *Fuzzy*$^{+/-}$*;p190A*$^{+/-}$. The statistical analysis revealed that the loss of double heterozygous mice was statistically significant (p=0069), suggesting a potential, likely embryonic, loss of Double HET animals.

Table 3.1: Genotype distribution in adult *Fuzzy*$^{+/-}$ X *p190*$^{+/-}$ crosses

Genotype	**Percentage number of mice/Total number of mice***
WT	30% (86/295)
Fuzzy HETS	30% (86/295)
P190 HETS	22% (65/295)
Double HETS	17.9% (53/295)
Ratio of Male and Female in Double HETS	**29:24**
P value (chi test)	**0.0069**

*All animals were genotyped at the time of weaning at 3 weeks of age. No pup death was detected prior to weaning. All adult animals appeared healthy and fertile.

We analysed kidney function in the adult wildtype and double heterozygous males at 6 months of age by collecting urine output and measuring protein in the urine (**Figure 3.9**). We detected no functional abnormalities (no urinary protein above normal excretion) in the urine of the animals of either genotype.

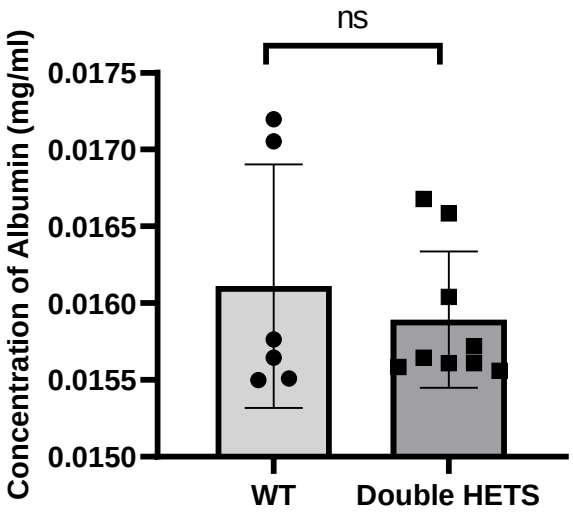

Figure 3.9: Urine analysis of adult wildtype vs double heterozygous mice

Urine was collected from 6 months old male mice (n=6 per genotype) and concentration of Albumin (mg/ml) was analyzed. *ns* – not significant

Since majority of the double heterozygous mice survived, we reasoned that we would need to remove additional alleles to reveal potential genetic interactions between *Fuzzy* and *p190A* genes. We generated mice with various dosages of *Fuzzy* and *p190A* genes by crossing *Fuzzy*$^{+/-}$*;p190A*$^{+/-}$ **X** *Fuzzy* $^{+/-}$*;p190A*$^{+/-}$. We acquired 27 litters which included 9 different genotypes (**Table 3.2**). Since majority of *Fuzzy*$^{-/-}$ embryos do not survive past E14.5 in our colony, we recovered embryos and analysed all the genotypes at E14.5. All embryos were first visually inspected and photographed, the genotypes were then identified by PCR of genomic DNA, and the embryos were processed and preserved by paraffin embedding. As expected, single *Fuzzy*$^{+/-}$ or *p190A*$^{+/-}$ HETS had no phenotype, however, 2.5 % (2/80) of Double HETS (*Fuzzy*$^{+/-}$*;p190A*$^{+/-}$) exhibited cranial NTD and 3.7% (3/80) had no visually detectable eyes, indicating severe perturbation of the embryonic development in these mice. The detected embryonic phenotype in double HETs -- albeit in a low percentage of the animals – is consistent with the observed loss of some double HETS in our adult colony.

Fuzzy$^{-/-}$ embryos had 100% penetrance for polydactyly (7 digits in all 4 limbs) and bilateral anophthalmia (no eyes), however, no NTD was detected. When one *p190A* allele was removed on *Fuzzy*$^{-/-}$ background (*Fuzzy*$^{-/-}$*;p190A*$^{+/-}$), cranial NTD was detected in 60% of the embryos, suggesting that further dosage reduction exacerbates NTD. Single *p190A*$^{-/-}$ embryos exhibited cranial NTD in 33.3% (4/12) embryos, and developmental delay was detected. Importantly, removal of one *Fuzzy* allele (*Fuzzy*$^{+/-}$*;p190A*$^{-/-}$ embryos) resulted in appearance of *spina bifida* (spinal NTD) in 20% (2/10) and anophthalmia in 20% (2/20) of the animals. Surprisingly, we detected no cranial NTDs in these mice, however, neither anophthalmia nor *spina bifida* was ever detected in the heterozygous *Fuzzy*$^{+/-}$ or homozygous *p190A*$^{-/-}$ mice, suggesting

that these new phenotypes had arisen as a result of genetic interactions between the two genes. Double homozygous *Fuzzy*$^{-/-}$*;p190A*$^{-/-}$ embryos had 100% penetrance (3/3) for cranial NTD, bilateral anophthalmia and polydactyly in all limbs and were smaller (developmental delay), showing a further exacerbation of congenital defects. Overall, our macro-phenotypic observations are consistent with the genetic interactions between *Fuzzy* and *p190A* genes (**Figure 3.10**).

Table 3.2. Macro-Phenotypic analysis of E14.5 embryos with various gene dosages.

Genotype			Phenotype				
Fuzzy	p190A	No. of embryos	NTD		Polydactyly	Eye	Developmental Delay
			Exencephaly	Spina bifida			
WT	WT	6	0.0 (0/6)	0.0 (0/6)	0.0 (0/6)	0.0 (0/6)	0.0 (0/6)
HETS	WT	43	0.0 (0/43)	0.0 (0/43)	0.0 (0/43)	0.0 (0/43)	0.0 (0/43)
WT	HETS	42	0.0 (0/42)	0.0 (0/42)	0.0 (0/42)	0.0 (0/42)	0.0 (0/42)
HETS	HETS	80	2.5% (2/80)	0.0 (0/80)	0.0 (0/80)	3.7% (3/80)	3.7% (3/80)
HOMO	WT	14	0.0 (0/14)	0.0 (0/14)	100% (14/14)	100% (14/14)	35.7% (5/14)
HOMO	HETS	15	60.0% (9/15)	0.0 (0/15)	100% (15/15)	100% (15/15)	40.0% (6/15)
WT	HOMO	12	33.3% (4/12)	0.0% (0/12)	0.0 (0/13)	0.0 (0/13)	8.3% (1/12)
HETS	HOMO	10	0.0 (0/10)	20.0% (2/10)	0.0 (0/10)	20.0% (2/10)	20.0% (2/10)
HOMO	HOMO	3	100% (3/3)	0.0 (0/3)	100% (3/3)	100% (3/3)	100%(3/3)
Total number of embryos		225					

*In *Fuzzy*$^{+/-}$*;p190A*$^{-/-}$ we found 2 embryos (2/10) exhibiting spina bifida, a phenotype that was never seen before in either *p190A*$^{-/-}$ *or Fuzzy*$^{-/-}$*;* kidneys were analyzed in 6 embryos, we found 4 embryos (4/6) had renal agenesis. In *Fuzzy*$^{-/-}$*;p190A*$^{-/-}$ 3 embryos were analyzed; (1/3) embryos had renal agenesis.

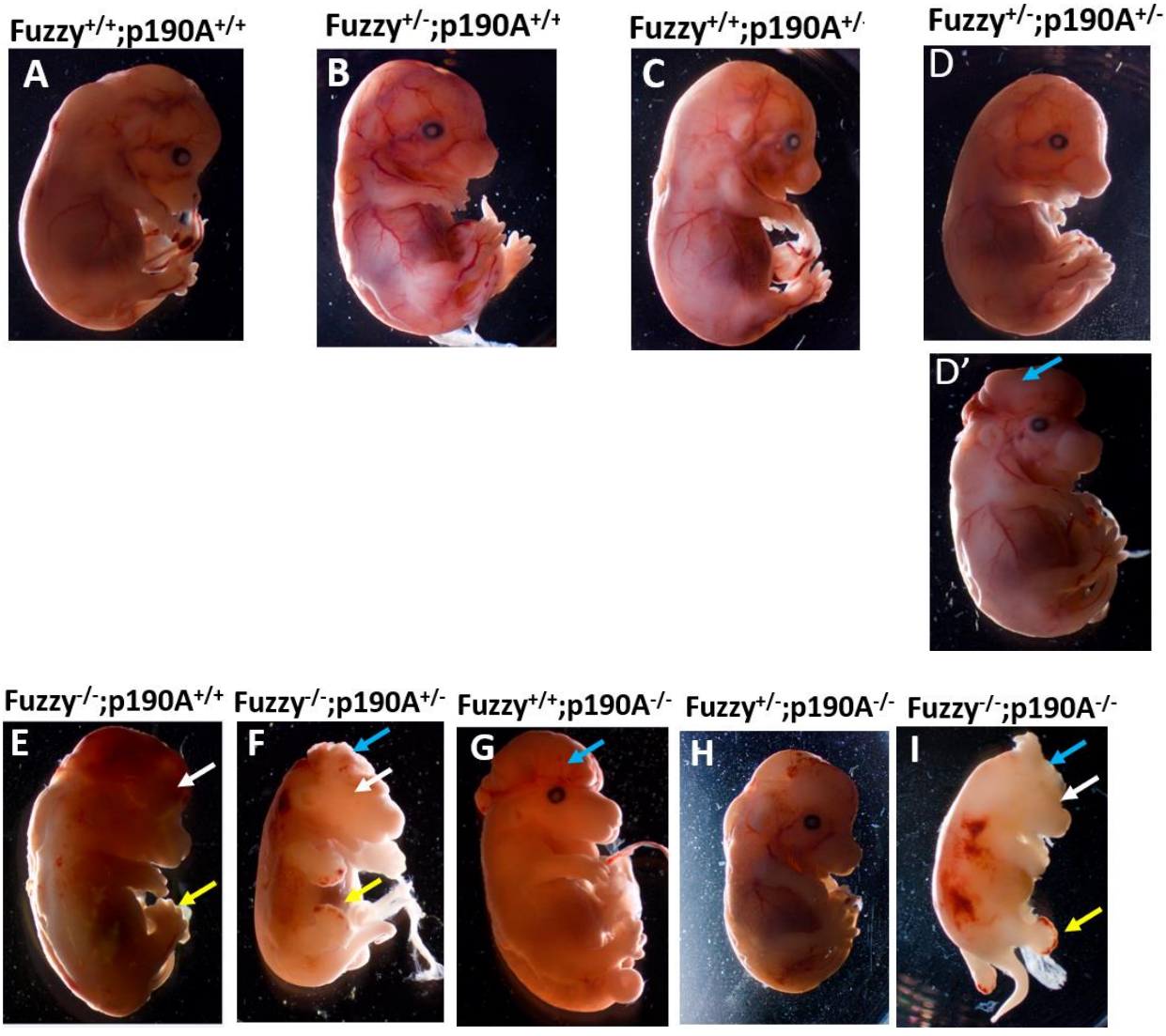
Fuzzy+/+;p190A+/+
A
Fuzzy+/-;p190A+/+
B
Fuzzy+/+;p190A+/-
C
Fuzzy+/-;p190A+/-
D
D'
Fuzzy-/-;p190A+/+
E
Fuzzy-/-;p190A+/-
F
Fuzzy+/+;p190A-/-
G
Fuzzy+/-;p190A-/-
H
Fuzzy-/-;p190A-/-
I

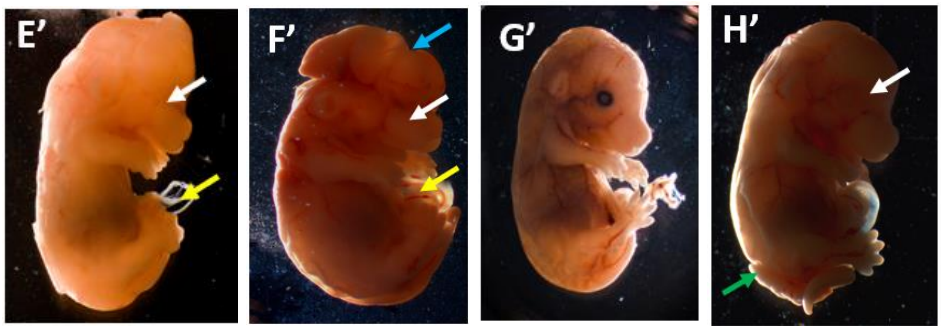

Figure 3.10: Phenotypic analysis of double *Fuzzy-p190* HET crosses at E14.5.

(A) Wildtype embryo *Fuzzy*$^{+/+}$;*p190A*$^{+/+}$. (B-C) Single Heterozygous *Fuzzy*$^{+/-}$;*p190A*$^{+/+}$ *and Fuzzy* $^{+/+}$;*p190A*$^{+/-}$ embryos. (D – D') Double Heterozygous *Fuzzy*$^{+/-}$;*p190A*$^{+/-}$ embryos: representative image is presented in D and the NTD/eye defect that occurs in 2.5% Double HETS is presented in D'. (E-E') Representative images of homozygous *Fuzzy*$^{-/-}$;*p190A*$^{+/+}$ embryos that exhibit polydactyly, no eyes with or without developmental delay. (F-F') *Fuzzy*$^{-/-}$;*p190*$^{+/-}$ embryos exhibit polydactyly and anophthalmia; further reducing one *p190A* allele on *Fuzzy*$^{-/-}$ background leads to increase in penetrance of NTD. (G-G') *p190A* single homozygous embryo (*Fuzzy*$^{+/+}$;*p190*$^{-/-}$) displays normal phenotype shown in G; a representative image of the embryo with NTD and developmental delay is shown in G'. (H-H') *Fuzzy*$^{+/-}$;*p190A*$^{-/-}$ animals display either normal morphology as in H or spina bifida shown in H'. (I) *Fuzzy*$^{-/-}$;*p190A*$^{-/-}$ embryos exhibit NTD, no eyes, polydactyly, and developmental delay. Blue Arrow: NTDs; Green arrow: Spina bifida; White arrows: Eye defects; Yellow arrow: Polydactyly.

3.8 Genetic interaction between Fuzzy and p190A during kidney development

To ascertain whether decreased *Fuzzy* and *p190A* gene dosages adversely and synergistically affect kidney development, we analyzed tractable kidney parameters: the size of the maximal cross-sections and the number of UB tips in the maximal sections. Each UB tip induces cells of the metanephric mesenchyme to become a nephron. Hence, the number of UB tips corresponds to the number of nephrons at each developmental stage. For each embryo, we analyzed two maximal sections that were chosen based on the pattern of UB branching: i.e., the branching collecting duct and UB tubules should be seen at the center of the kidney section and tracked from the center to the cortical layer (**Figure 3.11**). First, we used an Image J tool to measure the size of the maximal sections and calculated the average size for each genotype (**Figure 3.12 A-B**). We found no differences in the kidney size between wildtype, single $Fuzzy^{+/-}$ and $p190A^{+/-}$ or double $Fuzzy^{+/-};p190A^{+/-}$ embryos. The kidneys of the $Fuzzy^{-/-}$ and $p190A^{-/-}$ were significantly smaller than that of wildtype. Removal of one *p190A* allele on the $Fuzzy^{-/-}$ background further significantly decreased the kidney size. Loss of one *Fuzzy* allele on the $p190A^{-/-}$ background led to an unexpected phenotype – complete renal agenesis in 4/6 animals examined. To incorporate renal agenesis in the data set, we presented the size of the kidneys from the animal with agenesis as "0" and calculated the average size of the maximal sections for the entire set for the given genotype. We

observed a highly significant decreased in the kidney size in the E14.5 *Fuzzy*$^{+/-}$*;p190A*$^{-/-}$ embryos. Homozygous *Fuzzy*$^{-/-}$*;p190A*$^{-/-}$ embryos had only residual kidney tissues, and renal agenesis was found in 1/2 of the analyzed double E14.5 HOMO embryos.

To visualize UB tubules and the UB tips, staining with anti-calbindin antibody (specific marker for the UB lineage) was carried out, and the number of UB tips per maximal section for each embryonic kidney was manually counted (**Figure 3.12 C-D**). Our analysis revealed that the average UB tip numbers in single heterozygous and double heterozygous mice were statistically indistinguishable from the wildtype animals. However, we detected significantly lower number of UB tips in homozygous *Fuzzy*$^{-/-}$ and *p190A*$^{-/-}$ embryos vs control. Importantly, loss of one *p190A* allele on *Fuzzy*$^{-/-}$ background resulted in a significantly lower UB tip number. Likewise, loss of one *Fuzzy* allele on *p190A*$^{-/-}$ background led to fewer average UB tips, when we took into account 4/6 embryos with no kidneys. Comparison of double homozygous *Fuzzy*$^{-/-}$*;p190A*$^{-/-}$ animals to single homozygous animals or other genotypes revealed that number of UB tips was drastically and highly significantly reduced. Thus, our results indicate that either partial or complete loss of *Fuzzy* and *p190A* genes, synergistically precipitated renal hypoplasia affecting kidney development as observed in each single homozygote suggesting a robust genetic interaction between the two genes.

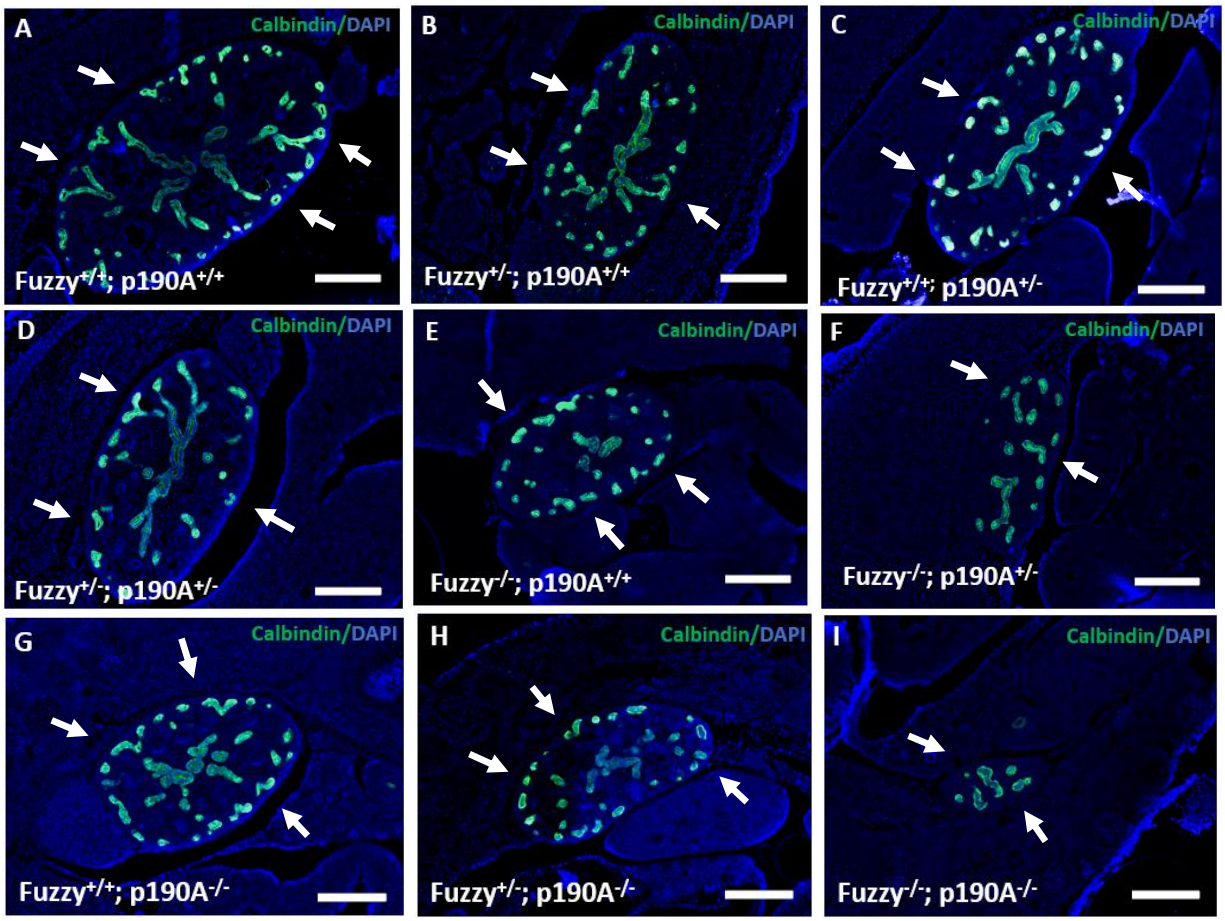

Figure 3.11: Analysis of kidney phenotype in E14.5 *Fuzzy* and *p190A* crosses

(A- I) Various kidney phenotypes in the brother-sister crosses of *Fuzzy*$^{+/-}$;*p190*$^{+/-}$ animals; representative images of maximal kidney cross-sections for each of 9 different genotypes are presented. (A) *Fuzzy*$^{+/+}$;*p190A*$^{+/+}$. (B) *Fuzzy*$^{+/-}$;*p190A*$^{+/+}$. (C) *Fuzzy*$^{+/+}$;*p190A*$^{+/-}$. (D) *Fuzzy*$^{+/-}$;*p190A*$^{+/-}$. (E) *Fuzzy*$^{-/-}$;*p190A*$^{+/+}$. (F) *Fuzzy*$^{-/-}$;*p190A*$^{+/-}$. (G) *Fuzzy*$^{+/+}$;*p190A*$^{-/-}$. (H) *Fuzzy*$^{+/-}$;*p190A*$^{-/-}$. *Scale bar is 200um.* Ureteric bud structures are identified by immunostaining with anti-calbindin antibody (green). UB tips are designated with arrows.

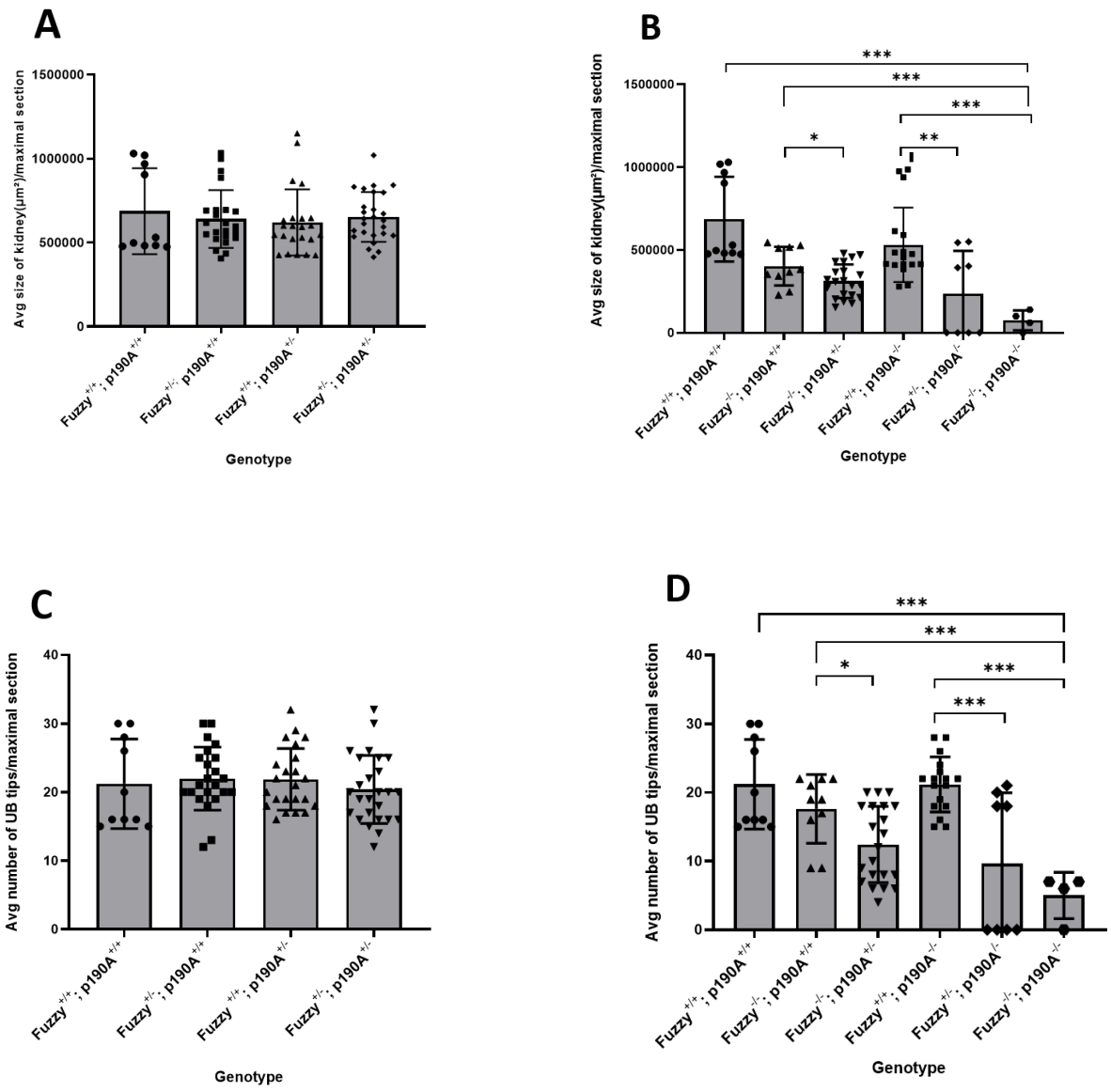

Figure 3.12: Statistical analysis of the kidney phenotype in various *Fuzzy* X *p190A* crosses.

(A) Statistical analysis of the average kidney sizes (μm2) in the wildtype *Fuzzy*$^{+/+}$;*p190A*$^{+/+}$, single *Fuzzy*$^{+/-}$;*p190A*$^{+/+}$ and *Fuzzy*$^{+/+}$;*p190A*$^{+/-}$ and double heterozygous *Fuzzy*$^{+/-}$;*p190A*$^{+/-}$. kidneys at E14.5. (B) Statistical analysis of the average kidney sizes (μm2) of *Fuzzy*$^{+/+}$;*p190A*$^{+/+}$ *vs* mutant phenotypes *Fuzzy*$^{-/-}$;*p190A*$^{+/+}$, *Fuzzy*$^{-/-}$;*p190A*$^{+/-}$, *Fuzzy*$^{+/+}$;*p190A*$^{-/-}$, *Fuzzy+/-;p190A-/-*. (C) Analysis of the number of UB tips in the kidneys of *Fuzzy*$^{+/+}$;*p190A*$^{+/+}$, *Fuzzy*$^{+/-}$;*p190A*$^{+/+}$, *Fuzzy*$^{+/+}$;*p190A*$^{+/-}$, *Fuzzy*$^{+/-}$;*p190A*$^{+/-}$ stained with anti-calbindin antibody. (D) Comparative

analysis of the number of the UB tips in *Fuzzy*$^{+/+}$*;p190A*$^{+/+}$, *Fuzzy*$^{-/-}$*;p190A*$^{+/+}$, *Fuzzy*$^{-/-}$*;p190A*$^{+/-}$, *Fuzzy*$^{+/+}$*;p190A*$^{-/-}$, and *Fuzzy*$^{+/-}$*;p190A*$^{-/-}$. Mean ± standard error of mean is shown in all graphs; $p<0.05$ (*), $p<0.001$ (**), $p<0.0001$ (***).

Chapter 4 The Discussion

My thesis focuses on the cellular, molecular, and genetic mechanisms involving the Planar Cell Polarity effector gene, *Fuzzy*. Loss of *Fuzzy* in mice leads to severe developmental defects: the *Fuzzy*$^{-/-}$ embryos carrying a gene-trap mutation exhibit neural tube defects (open cranial neural tube and looped tail; the latter is considered a mild NTD), skeletal defects (polydactyly), eye defects (anophthalmia), cardiac and other defects (Gray, Abitua et al. 2009). We also established a crucial role for *Fuzzy* gene in mammalian kidney development. Given the extensive expertise of Torban's lab in the morphogenetic processes during mammalian kidney development, we used the mouse kidney development as the main model to investigate how the loss of *Fuzzy* affects tissue morphogenesis and to explore our new hypothesis on the potential mechanistic and genetic links between Fuzzy and RhoA GAP p190A.

Previous studies in our lab identified renal hypoplasia in E14.5 *Fuzzy*$^{-/-}$ mouse embryos (described in Wang *et al*, manuscript in preparation). In the present study, we found cystic and dilated renal tubules and glomeruli in the E16.5 *Fuzzy*$^{-/-}$ kidneys (**Figure 3.2**). The tubule diameter and elongation are regulated by two main processes, which are mechanistically linked yet distinct from each other: convergent extension (CE), that occurs during the embryonical phase when cells around the tubules intercalate directionally, and oriented cell division (OCD), that takes place early postnatally (Karner, Chirumamilla et al. 2009). The diameter of renal tubules is strictly regulated (Karner, Chirumamilla et al. 2009): it becomes progressively narrower from E13.5 to E19.5, after which, the diameter appears to have reached its final size and is considered "fixed". The process of tubule narrowing leads to a reduction in the number of cells surrounding each tubular lumen, and this is accomplished via directional cells intercalations. At the same time, the tubule structure elongates in the direction perpendicular to the diameter along the tubular plane. The tissue

elongation in one direction with a concomitant narrowing in the perpendicular direction is regulated by a convergent extension (CE). In many tissues, including the vertebrate kidney, CE is controlled by the PCP components, and disruption of PCP signalling may lead to an abnormal tubule formation as was previously shown in the mouse with mutations in the core PCP genes, Vangl1 and Vangl2 (Kunimoto, Bayly et al. 2017, Derish, Lee et al. 2020). The cell divisions are random during embryonic development and become oriented only around the time of birth when the diameter of tubules has already been established (Karner, Chirumamilla et al. 2009). Thus, any tubular dilatation seen during mid-gestation is likely driven by deregulation in CE.

Fuzzy belongs to the PCP effectors, and some - but not all - features of *Fuzzy* mutant embryos (such as looped tail or cardiac abnormalities of the aorta) are similar to the defects detected in the *Vangl2* and *Vangl1* mutant mice (Torban, Patenaude et al. 2008). Thorough morphometric analysis of E16.5 *Fuzzy*$^{-/-}$ vs control kidneys revealed a profound tubular dilatation and cysts in both proximal and collecting duct tubules, reminiscent of the tubular dilatation observed in the E17.5 *Vangl2*$^{-/-}$ kidneys (Derish, Lee et al. 2020). Furthermore, the increased number of the tubule cells in the cross-sections of these nephron segments suggests that loss of *Fuzzy* gene indeed affects CE. Thus, loss of *Fuzzy* may lead to tubule dilatation by disturbing CE, a prototypic PCP-dependent morphogenetic process. Our data, therefore, are consistent with Fuzzy playing a role in PCP signalling, at least in some instances of tissue morphogenesis.

At E16.5, *Fuzzy*$^{-/-}$ kidneys are smaller than wildtype kidneys. Renal hypoplasia may arise by multiple pathogenetic mechanisms that include reduced branching morphogenesis of the ureteric bud, smaller pool of nephron progenitor cells or block of mesenchyme-to-epithelial transition and other mechanisms (Porteous, Torban et al. 2000, Dressler 2009). UB branching provides cues to the nephron formation, and defects in UB branching morphogenesis lead to fewer

nephrons and overall smaller size of kidneys. Consistent with this causation, findings in our lab made on E14.5 *Fuzzy*$^{-/-}$ tissues suggested that renal hypoplasia at this early stage was due to the defective branching morphogenesis of the UB. The progenitor cells were not significantly affected at this early stage (Wang, manuscript in preparation). Upon receiving signals from the UB tip cells, mesenchymal cells condense around the UB tip to become nephron progenitors (Kobayashi, Valerius et al. 2008). These cells start expressing several key transcriptional factors including Six2; the latter maintains self-renewal of the nephron progenitor population. Loss of Six2+ cells leads to renal hypoplasia (Kobayashi, Valerius et al. 2008). Our results show that the size of Six2+ progenitor pools in E16.5 *Fuzzy*$^{-/-}$ kidneys are similar to that in controls. This implies that the inductive signals from the UB cells are not defective in *Fuzzy*$^{-/-}$ tissues We also observed no loss of proximal tubules or glomeruli in E16.5 *Fuzzy*$^{-/-}$ kidney vs control kidneys, suggesting that the proliferation and differentiation of the progenitor epithelial cells into more mature nephron structures are largely unaffected.

We found glomerular cysts in the E16.5 *Fuzzy*$^{-/-}$ kidneys that present as a significant expansion of the Bowman's capsule: the average size of the Bowman's capsule in *Fuzzy* mutant embryos was 38% larger comparing to the glomeruli structure in the controls. However, the size of the tuft area, including the glomeruli with cystic Bowman's capsule, was unaffected. Interestingly, the cystic glomeruli were found exclusively in the juxta-medullary zone situated at the border between the cortical and medullary regions. The glomerulus develops at the proximal aspect of the S-shaped body in the cortical area. As the S-shaped body-derived tubular segments elongate, a maturing glomerulus is displaced away from the cortical area into a deeper organ's layer closer to the medullary zone. In mice, the glomeruli become sufficiently mature to produce glomerular filtrate at ~ E15.5. Thus, our results suggest that cysts in E16.5 *Fuzzy*$^{-/-}$ kidneys develop

in more mature glomeruli likely after the production of the glomerular filtrate has started. It is possible that abnormal development of tubular nephron segments downstream from the glomerulus causes abnormal draining of the glomerular filtrate from the Bowman's capsule, increasing pressure within the capsule leading to the capsule's volume expansion.

Alternatively, to the Fuzzy's function as a PCP component, a known role of Fuzzy in ciliogenesis in vertebrate cells has let us question if the cystic transformation along with nephron segments in the *Fuzzy*$^{-/-}$ kidneys might mechanistically be related to cilia abnormalities. Indeed, glomerulocystic kidney disease has been found in young infants with ADPKD before the renal parenchyma is distorted by large cysts or in the probands with Meckel-Gruber syndrome (prototypical ciliopathy) (Bissler, Siroky et al. 2010). The involvement of Fuzzy and of the other PPE proteins (Inturned and WDPCP) in ciliogenesis has been well-established (Toriyama, Lee et al. 2016). Fuzzy and the other PPE proteins were recently re-named as CPLANE (Ciliogenesis and Planar Polarity Effector proteins (Toriyama, Lee et al. 2016) to reflect their predominantly ciliogenic functions in vertebrate cells. Mutations in *Fuzzy* and other CPLANE genes lead to shorter cilia on the cells in many tissues (Park, Haigo et al. 2006, Gray, Abitua et al. 2009, Cui, Chatterjee et al. 2013). Moreover, mutations in the CPLANE genes cause several human ciliopathies such as embryonically lethal Short-Rib and Polydactyly Syndrome (SRPS), Bardet-Biedl Syndrome (BBS), Orofacial-Digital Syndrome (OFD) and Nephronophthisis NPHP) (Gray, Abitua et al. 2009, Toriyama, Lee et al. 2016). NTDs in humans were also associated with missense mutation in the *FUZZY* gene (Seo, Zilber et al. 2011). In the latter study, Torban's group demonstrated that the FUZZY proteins with the NTD-associated missense mutations were unable to efficiently rescue ciliogenesis in the unciliated *Fuzzy*$^{-/-}$ mouse embryonic fibroblasts, mechanistically linking cilia defects to human NTDs (Seo, Zilber et al. 2011).

Interestingly, by reviewing the literature we found that mutations in *p190A* (*ArhGAP35)* gene cause glomerulocystic kidney phenotype strikingly similar to the phenotype seen in E16.5 *Fuzzy*$^{-/-}$ kidney (**Figure 3.6**) (Stewart, Gaitan et al. 2016). p190A is the major RhoA GAP in mammalian cells and was recently shown to contain actin polymerization at the basal body, thereby regulating the formation and length of the primary cilia (Stewart, Gaitan et al. 2016). The role of polymerized actin in ciliogenesis is just beginning to emerge, yet a strong evidence to date suggests that excessive actin polymerization at the base of the primary cilium negatively affects ciliogenesis (Smith, Lake et al. 2020). Intriguingly, in *Drosophila*, PCP effectors Fuzzy, Inturned and Fritz act to contain actin polymerization during trichome formation (Adler and Wallingford 2017), however, in vertebrates, their role in actin arrangement is largely unknown. Instead, these proteins appear to be essential for cilia formation by organizing vesicle trafficking and recruitment of various proteins to the basal body (Zilber, Babayeva et al. 2013, Toriyama, Lee et al. 2016).

Intrigued by the known role of the PPE proteins in actin regulation in *Drosophila* and by the similarities in the *p190A*$^{-/-}$ and *Fuzzy*$^{-/-}$ kidney phenotypes, we hypothesized that Fuzzy might act via p190A RhoGAP to contain actin polymerization at the base of the primary cilium. We tested for and detected biochemical interactions between Fuzzy and p190A proteins (**Figure 3.7**). We also showed that p190A was lost at the basal body in *Fuzzy*$^{-/-}$ MEFs (**Figure 3.8**), consistent with Fuzzy controlling p190A localization at the basal body. Based on these preliminary data, we further tested for genetic interactions between *Fuzzy* and *p190A* genes. Most double heterozygous *Fuzzy*$^{+/-}$*;p190A*$^{+/-}$ mice survived; however, we detected a low but specific loss of double heterozygous mice in our adult colony. Indeed, recovering embryos of various genotypes at E14.5 revealed that ~2.5% of double heterozygous embryos displayed exencephaly, a congenital defect that is perinatally lethal, suggesting a severe disturbance of developmental events. Thus, we

surmised that some loss of double heterozygous *Fuzzy*$^{+/-}$;*p190A*$^{+/-}$ adult animals was likely caused by embryonic lethality. The 3.7% of *Fuzzy*$^{+/-}$;*p190*$^{+/-}$ embryos also exhibit eye defects, a phenotypic trait that is normally detected in *Fuzzy* homozygous embryos. We conclude that a genetic interaction between *Fuzzy* and *p190A* genes exists and can be observed infrequently in phenotypic double heterozygous animals.

We also observed that the frequency of NTD was heightened in *Fuzzy*$^{-/-}$;*p190*$^{+/-}$ animals (three allele are lost) as compared to the single *Fuzzy*$^{-/-}$ or *p190A*$^{-/-}$ animals. Additionally, 40% of *Fuzzy*$^{-/-}$;*p190*$^{+/-}$ exhibited developmental delay, indicating a significant loss of fitness in these embryos. The penetrance of cranial NTD phenotype in *p190A*$^{-/-}$ animals was 33.3.%. Surprisingly, we did not find *exencephaly* in the *Fuzzy*$^{+/-}$;*p190A*$^{-/-}$ animals (three alleles are lost). Instead, *Fuzzy*$^{+/-}$;*p190A*$^{-/-}$ embryos exhibited *spina bifida*, a phenotype never before seen in either *p190A*$^{-/-}$ or *Fuzzy*$^{-/-}$ embryos. Of note, missense mutations in *FUZZY* were found in patients with *spina bifida* (Seo, Zilber et al. 2011) confirming that morphogenesis of the spinal neural tube is sensitive to decreased Fuzzy function. The double homozygous *Fuzzy*$^{-/-}$;*p190*$^{-/-}$ animals had 100% phenotypic penetrance of NTD, polydactyly, anophthalmia and significant developmental delay. Thus, our results are consistent with genetic interactions between *Fuzzy* and *p190A* genes.

We detected the effects of *Fuzzy* and *p190A* dosage decrease on kidney development. The average number of ureteric buds in single heterozygous and double heterozygous mice was statistically indistinguishable from the wildtype kidneys. Both E14.5 *Fuzzy*$^{-/-}$ and *p190A*$^{-/-}$ kidneys were statistically smaller with fewer UB tips comparing to the wildtype or single and double heterozygous animals. Importantly, we found 4/6 *Fuzzy*$^{+/-}$;*p190*$^{-/-}$ (loss of three alleles) embryos completely lacking kidneys, the phenotype that was never detected in either single *p190A*$^{-/-}$ or *Fuzzy*$^{-/-}$ mice. 1/3 *Fuzzy*$^{-/-}$;*p190*$^{-/-}$ embryos also exhibited renal agenesis, while the kidneys in the

remaining two double homozygous embryos were rather rudimental with a drastic, highly significant, decrease in the kidney size and extent of UB branching.

How a decrease or a complete loss of *Fuzzy* and *p190A* leads to renal agenesis is unclear and requires further investigation. There are several mutant mouse models or gene mutations in humans that display small/no kidney phenotype. For example, mutations in Ret or GDNF may lead to both anephria and renal hypoplasia, depending on the specific mutations (Costantini 2010). Similarly, loss of PCP pathway ligand, Wnt5a, may cause both renal agenesis and renal hypoplasia (Perantoni 2017). It would be of interest to ascertain whether GDNF-Ret axis or Wnt5a signalling is perturbed in *Fuzzy*$^{-/-}$ or *Fuzzy*$^{+/-}$*;p190A*$^{-/-}$ kidneys.

In summary, in this thesis, I studied the requirement for *Fuzzy* in mouse development with a specific emphasis on the development of the kidney. Our results show that loss of *Fuzzy* leads to dilatation of proximal and distal nephron segments via defective CE, suggesting that Fuzzy participates in PCP signalling. It is equally possible that glomerular cysts arise as a result of abnormal ciliogenesis in *Fuzzy* mutant tissues since primary cilia are scarce and shorter in the mammalian kidney (unpublished observations). With regards to ciliogenesis, our results largely confirm the correctness of our novel hypothesis that Fuzzy and p190A act in the same signaling pathway to regulate actin polymerization at the base of the primary cilium: 1) We established biochemical interactions between Fuzzy and p190A proteins; 2) We found that in the absence of *Fuzzy* gene, p190A is lost at the basal body indicating that Fuzzy is required for p190A localization at the basal body; 3) We identified genetic interaction between *Fuzzy* and *p190A* genes, which is seen in increased frequency of NTD and eye defects and more severe renal hypoplasia as *Fuzzy* and *p190A* dosages decrease. We also found novel phenotypes such as *spina bifida* and renal agenesis in the compound *Fuzzy*$^{+/-}$ *;p190A*$^{-/-}$ embryos. Based on our results, the hypothetical role

of Fuzzy in ciliogenesis is depicted in **Figure 4.1.** Fuzzy (and likely other PPE proteins) recruit specific actin regulators, including p190A, to the basal body. At the basal body, p190A functions to fine-tune actin polymerization required for the successful formation of the primary cilium. When *Fuzzy* is mutated, p190A is lost from the base of the cilium. This would lead to excessive actin polymerization that interferes with ciliogenesis, resulting in short or no cilia.

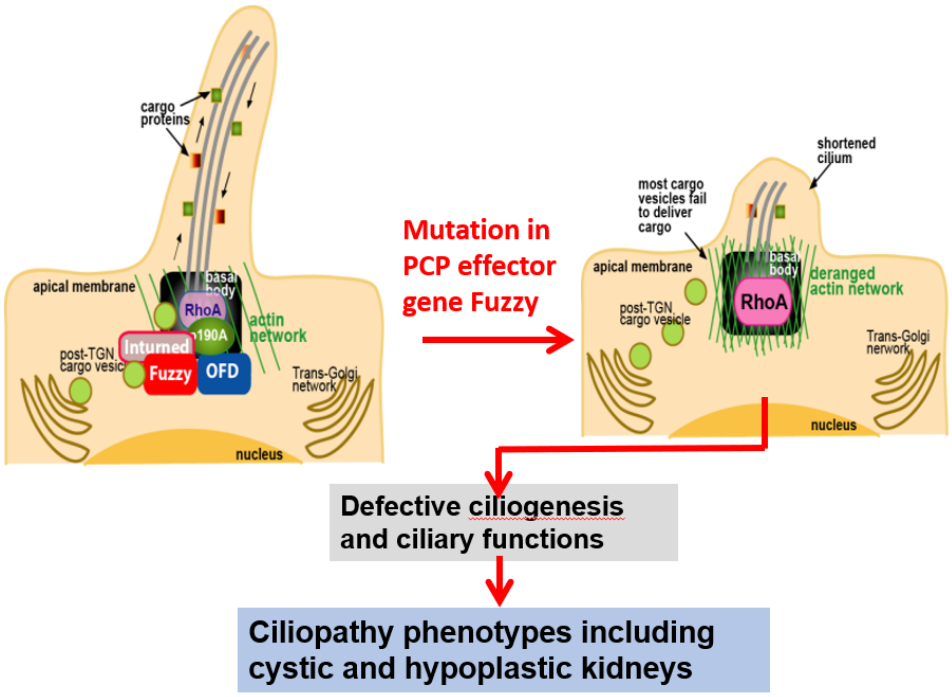

Figure 4.1 Role of PCP effector Fuzzy in regulating ciliogenesis

PCP effector Fuzzy recruits specific protein at basal body, such as p190A, p190A then functions to regulate the actin polymerization at basal body required for cilia formation. Loss of Fuzzy might lead to the aberration of p190A and increase in actin at the base of the cilia causing smaller or no cilia.

In the future, we will focus on analysing RhoA activity and actin polymerisation at the basal body in the wildtype and *Fuzzy*$^{-/-}$ mutant cells and whether cilia and the kidney hypoplasia may be rescued by manipulating actin polymerization using chemical inhibitors, siRNAs and genetic editing of specific components downstream from Fuzzy and p190A.

Chapter 5 References

Adler, P. N. (2002). "Planar signaling and morphogenesis in Drosophila." Dev Cell **2**(5): 525-535.
Adler, P. N. (2012). "The frizzled/stan pathway and planar cell polarity in the Drosophila wing." Curr Top Dev Biol **101**: 1-31.
Adler, P. N. and J. B. Wallingford (2017). "From Planar Cell Polarity to Ciliogenesis and Back: The Curious Tale of the PPE and CPLANE proteins." Trends Cell Biol **27**(5): 379-390.
Adler, P. N., C. Zhu and D. Stone (2004). "Inturned localizes to the proximal side of wing cells under the instruction of upstream planar polarity proteins." Curr Biol **14**(22): 2046-2051.
Aigouy, B., R. Farhadifar, D. B. Staple, A. Sagner, J. C. Roper, F. Julicher and S. Eaton (2010). "Cell flow reorients the axis of planar polarity in the wing epithelium of Drosophila." Cell **142**(5): 773-786.
Airik, R. and A. Kispert (2007). "Down the tube of obstructive nephropathies: the importance of tissue interactions during ureter development." Kidney Int **72**(12): 1459-1467.
Atsuta, Y., R. Tadokoro, D. Saito and Y. Takahashi (2013). "Transgenesis of the Wolffian duct visualizes dynamic behavior of cells undergoing tubulogenesis in vivo." Dev Growth Differ **55**(4): 579-590.
Attrill, H., K. Falls, J. L. Goodman, G. H. Millburn, G. Antonazzo, A. J. Rey, S. J. Marygold and C. FlyBase (2016). "FlyBase: establishing a Gene Group resource for Drosophila melanogaster." Nucleic Acids Res **44**(D1): D786-792.
Babayeva, S., Y. Zilber and E. Torban (2011). "Planar cell polarity pathway regulates actin rearrangement, cell shape, motility, and nephrin distribution in podocytes." Am J Physiol Renal Physiol **300**(2): F549-560.
Barr, M. M. and P. W. Sternberg (1999). "A polycystic kidney-disease gene homologue required for male mating behaviour in C. elegans." Nature **401**(6751): 386-389.
Barresi, G., G. Tuccari and F. Arena (1988). "Peanut and Lotus tetragonolobus binding sites in human kidney from congenital nephrotic syndrome of Finnish type." Histochemistry **89**(2): 117-120.
Basson, M. A., S. Akbulut, J. Watson-Johnson, R. Simon, T. J. Carroll, R. Shakya, I. Gross, G. R. Martin, T. Lufkin, A. P. McMahon, P. D. Wilson, F. D. Costantini, I. J. Mason and J. D. Licht (2005). "Sprouty1 is a critical regulator of GDNF/RET-mediated kidney induction." Dev Cell **8**(2): 229-239.
Basson, M. A., J. Watson-Johnson, R. Shakya, S. Akbulut, D. Hyink, F. D. Costantini, P. D. Wilson, I. J. Mason and J. D. Licht (2006). "Branching morphogenesis of the ureteric epithelium during kidney development is coordinated by the opposing functions of GDNF and Sprouty1." Dev Biol **299**(2): 466-477.
Bates, C. M. (2011). "Role of fibroblast growth factor receptor signaling in kidney development." Am J Physiol Renal Physiol **301**(2): F245-251.
Behal, R. H., M. S. Miller, H. Qin, B. F. Lucker, A. Jones and D. G. Cole (2012). "Subunit interactions and organization of the Chlamydomonas reinhardtii intraflagellar transport complex A proteins." J Biol Chem **287**(15): 11689-11703.
Bershteyn, M., S. X. Atwood, W. M. Woo, M. Li and A. E. Oro (2010). "MIM and cortactin antagonism regulates ciliogenesis and hedgehog signaling." Dev Cell **19**(2): 270-283.
Bissler, J. J., B. J. Siroky and H. Yin (2010). "Glomerulocystic kidney disease." Pediatr Nephrol **25**(10): 2049-2056; quiz 2056-2049.
Blacque, O. E., N. Scheidel and S. Kuhns (2018). "Rab GTPases in cilium formation and function." Small GTPases **9**(1-2): 76-94.
Blake, J. and N. D. Rosenblum (2014). "Renal branching morphogenesis: morphogenetic and signaling mechanisms." Semin Cell Dev Biol **36**: 2-12.
Bouchard, M., A. Souabni, M. Mandler, A. Neubuser and M. Busslinger (2002). "Nephric lineage specification by Pax2 and Pax8." Genes Dev **16**(22): 2958-2970.

Breunig, J. J., M. R. Sarkisian, J. I. Arellano, Y. M. Morozov, A. E. Ayoub, S. Sojitra, B. Wang, R. A. Flavell, P. Rakic and T. Town (2008). "Primary cilia regulate hippocampal neurogenesis by mediating sonic hedgehog signaling." Proc Natl Acad Sci U S A **105**(35): 13127-13132.
Brodbeck, S., B. Besenbeck and C. Englert (2004). "The transcription factor Six2 activates expression of the Gdnf gene as well as its own promoter." Mech Dev **121**(10): 1211-1222.
Brophy, P. D., L. Ostrom, K. M. Lang and G. R. Dressler (2001). "Regulation of ureteric bud outgrowth by Pax2-dependent activation of the glial derived neurotrophic factor gene." Development **128**(23): 4747-4756.
Burbelo, P. D., S. Miyamoto, A. Utani, S. Brill, K. M. Yamada, A. Hall and Y. Yamada (1995). "p190-B, a new member of the Rho GAP family, and Rho are induced to cluster after integrin cross-linking." J Biol Chem **270**(52): 30919-30926.
Burridge, K. and M. Chrzanowska-Wodnicka (1996). "Focal adhesions, contractility, and signaling." Annu Rev Cell Dev Biol **12**: 463-518.
Butler, M. T. and J. B. Wallingford (2017). "Planar cell polarity in development and disease." Nat Rev Mol Cell Biol **18**(6): 375-388.
Cao, J., Y. Shen, L. Zhu, Y. Xu, Y. Zhou, Z. Wu, Y. Li, X. Yan and X. Zhu (2012). "miR-129-3p controls cilia assembly by regulating CP110 and actin dynamics." Nat Cell Biol **14**(7): 697-706.
Carroll, T. J., J. S. Park, S. Hayashi, A. Majumdar and A. P. McMahon (2005). "Wnt9b plays a central role in the regulation of mesenchymal to epithelial transitions underlying organogenesis of the mammalian urogenital system." Dev Cell **9**(2): 283-292.
Carvajal-Gonzalez, J. M. and M. Mlodzik (2014). "Mechanisms of planar cell polarity establishment in Drosophila." F1000Prime Rep **6**: 98.
Chaitin, M. H. (1991). "Actin filaments in the photoreceptor cilium of the rds mutant mouse." Exp Eye Res **53**(1): 107-113.
Chi, L., S. Zhang, Y. Lin, R. Prunskaite-Hyyrylainen, R. Vuolteenaho, P. Itaranta and S. Vainio (2004). "Sprouty proteins regulate ureteric branching by coordinating reciprocal epithelial Wnt11, mesenchymal Gdnf and stromal Fgf7 signalling during kidney development." Development **131**(14): 3345-3356.
Chi, X., O. Michos, R. Shakya, P. Riccio, H. Enomoto, J. D. Licht, N. Asai, M. Takahashi, N. Ohgami, M. Kato, C. Mendelsohn and F. Costantini (2009). "Ret-dependent cell rearrangements in the Wolffian duct epithelium initiate ureteric bud morphogenesis." Dev Cell **17**(2): 199-209.
Chia, I., D. Grote, M. Marcotte, E. Batourina, C. Mendelsohn and M. Bouchard (2011). "Nephric duct insertion is a crucial step in urinary tract maturation that is regulated by a Gata3-Raldh2-Ret molecular network in mice." Development **138**(10): 2089-2097.
Chuykin, I., O. Ossipova and S. Y. Sokol (2018). "Par3 interacts with Prickle3 to generate apical PCP complexes in the vertebrate neural plate." Elife **7**.
Clevers, H. (2006). "Wnt/beta-catenin signaling in development and disease." Cell **127**(3): 469-480.
Collier, S., H. Y. Chan, T. Toda, C. McKimmie, G. Johnson, P. N. Adler, C. O'Kane and M. Ashburner (2000). "The Drosophila embargoed gene is required for larval progression and encodes the functional homolog of schizosaccharomyces Crm1." Genetics **155**(4): 1799-1807.
Collier, S., H. Lee, R. Burgess and P. Adler (2005). "The WD40 repeat protein fritz links cytoskeletal planar polarity to frizzled subcellular localization in the Drosophila epidermis." Genetics **169**(4): 2035-2045.
Corkins, M. E., V. Krneta-Stankic, M. Kloc, P. D. McCrea, A. B. Gladden and R. K. Miller (2019). "Divergent roles of the Wnt/PCP Formin Daam1 in renal ciliogenesis." PLoS One **14**(8): e0221698.
Costantini, F. (2006). "Renal branching morphogenesis: concepts, questions, and recent advances." Differentiation **74**(7): 402-421.
Costantini, F. (2010). "GDNF/Ret signaling and renal branching morphogenesis: From mesenchymal signals to epithelial cell behaviors." Organogenesis **6**(4): 252-262.

Costantini, F. and R. Kopan (2010). "Patterning a complex organ: branching morphogenesis and nephron segmentation in kidney development." Dev Cell **18**(5): 698-712.
Cui, C., B. Chatterjee, T. P. Lozito, Z. Zhang, R. J. Francis, H. Yagi, L. M. Swanhart, S. Sanker, D. Francis, Q. Yu, J. T. San Agustin, C. Puligilla, T. Chatterjee, T. Tansey, X. Liu, M. W. Kelley, E. T. Spiliotis, A. V. Kwiatkowski, R. Tuan, G. J. Pazour, N. A. Hukriede and C. W. Lo (2013). "Wdpcp, a PCP protein required for ciliogenesis, regulates directional cell migration and cell polarity by direct modulation of the actin cytoskeleton." PLoS Biol **11**(11): e1001720.
Davis, E. E. and N. Katsanis (2012). "The ciliopathies: a transitional model into systems biology of human genetic disease." Curr Opin Genet Dev **22**(3): 290-303.
De Franceschi, N., K. Wild, A. Schlacht, J. B. Dacks, I. Sinning and F. Filippini (2014). "Longin and GAF domains: structural evolution and adaptation to the subcellular trafficking machinery." Traffic **15**(1): 104-121.
Dell, K. M. (2015). "The role of cilia in the pathogenesis of cystic kidney disease." Curr Opin Pediatr **27**(2): 212-218.
Delling, M., P. G. DeCaen, J. F. Doerner, S. Febvay and D. E. Clapham (2013). "Primary cilia are specialized calcium signalling organelles." Nature **504**(7479): 311-314.
Derish, I., J. K. H. Lee, M. Wong-King-Cheong, S. Babayeva, J. Caplan, V. Leung, C. Shahinian, M. Gravel, M. R. Deans, P. Gros and E. Torban (2020). "Differential role of planar cell polarity gene Vangl2 in embryonic and adult mammalian kidneys." PLoS One **15**(3): e0230586.
Devenport, D. (2014). "The cell biology of planar cell polarity." J Cell Biol **207**(2): 171-179.
Djiane, A., S. Yogev and M. Mlodzik (2005). "The apical determinants aPKC and dPatj regulate Frizzled-dependent planar cell polarity in the Drosophila eye." Cell **121**(4): 621-631.
Dressler, G. R. (1995). "The genetic control of renal development." Curr Opin Nephrol Hypertens **4**(3): 253-257.
Dressler, G. R. (2006). "The cellular basis of kidney development." Annu Rev Cell Dev Biol **22**: 509-529.
Dressler, G. R. (2009). "Advances in early kidney specification, development and patterning." Development **136**(23): 3863-3874.
Dressler, G. R. (2011). "Patterning and early cell lineage decisions in the developing kidney: the role of Pax genes." Pediatr Nephrol **26**(9): 1387-1394.
Drews, C., S. Senkel and G. U. Ryffel (2011). "The nephrogenic potential of the transcription factors osr1, osr2, hnf1b, lhx1 and pax8 assessed in Xenopus animal caps." BMC Dev Biol **11**: 5.
Duncan, J. S., M. L. Stoller, A. F. Francl, F. Tissir, D. Devenport and M. R. Deans (2017). "Celsr1 coordinates the planar polarity of vestibular hair cells during inner ear development." Dev Biol **423**(2): 126-137.
Eley, L., L. M. Yates and J. A. Goodship (2005). "Cilia and disease." Curr Opin Genet Dev **15**(3): 308-314.
Etheridge, S. L., S. Ray, S. Li, N. S. Hamblet, N. Lijam, M. Tsang, J. Greer, N. Kardos, J. Wang, D. J. Sussman, P. Chen and A. Wynshaw-Boris (2008). "Murine dishevelled 3 functions in redundant pathways with dishevelled 1 and 2 in normal cardiac outflow tract, cochlea, and neural tube development." PLoS Genet **4**(11): e1000259.
Fan, M. J., W. Gruning, G. Walz and S. Y. Sokol (1998). "Wnt signaling and transcriptional control of Siamois in Xenopus embryos." Proc Natl Acad Sci U S A **95**(10): 5626-5631.
Fanto, M., U. Weber, D. I. Strutt and M. Mlodzik (2000). "Nuclear signaling by Rac and Rho GTPases is required in the establishment of epithelial planar polarity in the Drosophila eye." Curr Biol **10**(16): 979-988.
Ferkol, T. W. and M. W. Leigh (2012). "Ciliopathies: the central role of cilia in a spectrum of pediatric disorders." J Pediatr **160**(3): 366-371.

Gao, B., H. Song, K. Bishop, G. Elliot, L. Garrett, M. A. English, P. Andre, J. Robinson, R. Sood, Y. Minami, A. N. Economides and Y. Yang (2011). "Wnt signaling gradients establish planar cell polarity by inducing Vangl2 phosphorylation through Ror2." Dev Cell **20**(2): 163-176.
Garcia-Bellido, A. and J. R. Merriam (1971). "Genetic analysis of cell heredity in imaginal discs of Drosophila melanogaster." Proc Natl Acad Sci U S A **68**(9): 2222-2226.
Gerondopoulos, A., H. Strutt, N. L. Stevenson, T. Sobajima, T. P. Levine, D. J. Stephens, D. Strutt and F. A. Barr (2019). "Planar Cell Polarity Effector Proteins Inturned and Fuzzy Form a Rab23 GEF Complex." Curr Biol **29**(19): 3323-3330 e3328.
Gray, R. S., P. B. Abitua, B. J. Wlodarczyk, H. L. Szabo-Rogers, O. Blanchard, I. Lee, G. S. Weiss, K. J. Liu, E. M. Marcotte, J. B. Wallingford and R. H. Finnell (2009). "The planar cell polarity effector Fuz is essential for targeted membrane trafficking, ciliogenesis and mouse embryonic development." Nat Cell Biol **11**(10): 1225-1232.
Green, J., R. Nusse and R. van Amerongen (2014). "The role of Ryk and Ror receptor tyrosine kinases in Wnt signal transduction." Cold Spring Harb Perspect Biol **6**(2).
Grieshammer, U., C. Cebrian, R. Ilagan, E. Meyers, D. Herzlinger and G. R. Martin (2005). "FGF8 is required for cell survival at distinct stages of nephrogenesis and for regulation of gene expression in nascent nephrons." Development **132**(17): 3847-3857.
Grote, D., S. K. Boualia, A. Souabni, C. Merkel, X. Chi, F. Costantini, T. Carroll and M. Bouchard (2008). "Gata3 acts downstream of beta-catenin signaling to prevent ectopic metanephric kidney induction." PLoS Genet **4**(12): e1000316.
Hains, D., S. Sims-Lucas, K. Kish, M. Saha, K. McHugh and C. M. Bates (2008). "Role of fibroblast growth factor receptor 2 in kidney mesenchyme." Pediatr Res **64**(6): 592-598.
Hall, A. (2009). "The cytoskeleton and cancer." Cancer Metastasis Rev **28**(1-2): 5-14.
Halt, K. and S. Vainio (2014). "Coordination of kidney organogenesis by Wnt signaling." Pediatr Nephrol **29**(4): 737-744.
Hayes, M., M. Naito, A. Daulat, S. Angers and B. Ciruna (2013). "Ptk7 promotes non-canonical Wnt/PCP-mediated morphogenesis and inhibits Wnt/beta-catenin-dependent cell fate decisions during vertebrate development." Development **140**(8): 1807-1818.
Heisenberg, C. P., M. Tada, G. J. Rauch, L. Saude, M. L. Concha, R. Geisler, D. L. Stemple, J. C. Smith and S. W. Wilson (2000). "Silberblick/Wnt11 mediates convergent extension movements during zebrafish gastrulation." Nature **405**(6782): 76-81.
Heliot, C., A. Desgrange, I. Buisson, R. Prunskaite-Hyyrylainen, J. Shan, S. Vainio, M. Umbhauer and S. Cereghini (2013). "HNF1B controls proximal-intermediate nephron segment identity in vertebrates by regulating Notch signalling components and Irx1/2." Development **140**(4): 873-885.
Hernandez-Hernandez, V., P. Pravincumar, A. Diaz-Font, H. May-Simera, D. Jenkins, M. Knight and P. L. Beales (2013). "Bardet-Biedl syndrome proteins control the cilia length through regulation of actin polymerization." Hum Mol Genet **22**(19): 3858-3868.
Herzlinger, D. and R. Hurtado (2014). "Patterning the renal vascular bed." Semin Cell Dev Biol **36**: 50-56.
Heydeck, W. and A. Liu (2011). "PCP effector proteins inturned and fuzzy play nonredundant roles in the patterning but not convergent extension of mammalian neural tube." Dev Dyn **240**(8): 1938-1948.
Heydeck, W., H. Zeng and A. Liu (2009). "Planar cell polarity effector gene Fuzzy regulates cilia formation and Hedgehog signal transduction in mouse." Dev Dyn **238**(12): 3035-3042.
Hildebrandt, F., T. Benzing and N. Katsanis (2011). "Ciliopathies." N Engl J Med **364**(16): 1533-1543.
Hildebrandt, F. and W. Zhou (2007). "Nephronophthisis-associated ciliopathies." J Am Soc Nephrol **18**(6): 1855-1871.
Holmes, K. C., D. Popp, W. Gebhard and W. Kabsch (1990). "Atomic model of the actin filament." Nature **347**(6288): 44-49.

Holthofer, H., B. A. Schulte and S. S. Spicer (1987). "Expression of binding sites for Dolichos biflorus agglutinin at the apical aspect of collecting duct cells in rat kidney." Cell Tissue Res **249**(3): 481-485.
Huang, H. C. and P. S. Klein (2004). "The Frizzled family: receptors for multiple signal transduction pathways." Genome Biol **5**(7): 234.
Isenberg, G., U. Aebi and T. D. Pollard (1980). "An actin-binding protein from Acanthamoeba regulates actin filament polymerization and interactions." Nature **288**(5790): 455-459.
Ishikawa, H. and W. F. Marshall (2014). "Mechanobiology of Ciliogenesis." Bioscience **64**(12): 1084-1091.
Jacob, M., B. Christ, H. J. Jacob and R. E. Poelmann (1991). "The role of fibronectin and laminin in development and migration of the avian Wolffian duct with reference to somitogenesis." Anat Embryol (Berl) **183**(4): 385-395.
Jeanpierre, C., G. Mace, M. Parisot, V. Moriniere, A. Pawtowsky, M. Benabou, J. Martinovic, J. Amiel, T. Attie-Bitach, A. L. Delezoide, P. Loget, P. Blanchet, D. Gaillard, M. Gonzales, W. Carpentier, P. Nitschke, F. Tores, L. Heidet, C. Antignac, R. Salomon and F. Societe Francaise de (2011). "RET and GDNF mutations are rare in fetuses with renal agenesis or other severe kidney development defects." J Med Genet **48**(7): 497-504.
Jiang, Z., J. Y. Seo, H. Ha, E. A. Lee, Y. S. Kim, D. C. Han, S. T. Uh, C. S. Park and H. B. Lee (2003). "Reactive oxygen species mediate TGF-beta1-induced plasminogen activator inhibitor-1 upregulation in mesangial cells." Biochem Biophys Res Commun **309**(4): 961-966.
Karner, C. M., R. Chirumamilla, S. Aoki, P. Igarashi, J. B. Wallingford and T. J. Carroll (2009). "Wnt9b signaling regulates planar cell polarity and kidney tubule morphogenesis." Nat Genet **41**(7): 793-799.
Karner, C. M., A. Das, Z. Ma, M. Self, C. Chen, L. Lum, G. Oliver and T. J. Carroll (2011). "Canonical Wnt9b signaling balances progenitor cell expansion and differentiation during kidney development." Development **138**(7): 1247-1257.
Ke, Y. N. and W. X. Yang (2014). "Primary cilium: an elaborate structure that blocks cell division?" Gene **547**(2): 175-185.
Kibar, Z., K. J. Vogan, N. Groulx, M. J. Justice, D. A. Underhill and P. Gros (2001). "Ltap, a mammalian homolog of Drosophila Strabismus/Van Gogh, is altered in the mouse neural tube mutant Loop-tail." Nat Genet **28**(3): 251-255.
Kiefer, S. M., L. Robbins, K. M. Stumpff, C. Lin, L. Ma and M. Rauchman (2010). "Sall1-dependent signals affect Wnt signaling and ureter tip fate to initiate kidney development." Development **137**(18): 3099-3106.
Kim, J., H. Jo, H. Hong, M. H. Kim, J. M. Kim, J. K. Lee, W. D. Heo and J. Kim (2015). "Actin remodelling factors control ciliogenesis by regulating YAP/TAZ activity and vesicle trafficking." Nat Commun **6**: 6781.
Kim, J., J. E. Lee, S. Heynen-Genel, E. Suyama, K. Ono, K. Lee, T. Ideker, P. Aza-Blanc and J. G. Gleeson (2010). "Functional genomic screen for modulators of ciliogenesis and cilium length." Nature **464**(7291): 1048-1051.
Kim, S. and B. D. Dynlacht (2013). "Assembling a primary cilium." Curr Opin Cell Biol **25**(4): 506-511.
Kispert, A., S. Vainio, L. Shen, D. H. Rowitch and A. P. McMahon (1996). "Proteoglycans are required for maintenance of Wnt-11 expression in the ureter tips." Development **122**(11): 3627-3637.
Kitzing, T. M., Y. Wang, O. Pertz, J. W. Copeland and R. Grosse (2010). "Formin-like 2 drives amoeboid invasive cell motility downstream of RhoC." Oncogene **29**(16): 2441-2448.
Kobayashi, A., K. M. Kwan, T. J. Carroll, A. P. McMahon, C. L. Mendelsohn and R. R. Behringer (2005). "Distinct and sequential tissue-specific activities of the LIM-class homeobox gene Lim1 for tubular morphogenesis during kidney development." Development **132**(12): 2809-2823.
Kobayashi, A., M. T. Valerius, J. W. Mugford, T. J. Carroll, M. Self, G. Oliver and A. P. McMahon (2008). "Six2 defines and regulates a multipotent self-renewing nephron progenitor population throughout mammalian kidney development." Cell Stem Cell **3**(2): 169-181.

Kobayashi, H., K. Kawakami, M. Asashima and R. Nishinakamura (2007). "Six1 and Six4 are essential for Gdnf expression in the metanephric mesenchyme and ureteric bud formation, while Six1 deficiency alone causes mesonephric-tubule defects." Mech Dev **124**(4): 290-303.
Kohli, P., M. Hohne, C. Jungst, S. Bertsch, L. K. Ebert, A. C. Schauss, T. Benzing, M. M. Rinschen and B. Schermer (2017). "The ciliary membrane-associated proteome reveals actin-binding proteins as key components of cilia." EMBO Rep **18**(9): 1521-1535.
Komatsu, Y. and Y. Mishina (2013). "Establishment of left-right asymmetry in vertebrate development: the node in mouse embryos." Cell Mol Life Sci **70**(24): 4659-4666.
Krause, M., A. Rak-Raszewska, I. Pietila, S. E. Quaggin and S. Vainio (2015). "Signaling during Kidney Development." Cells **4**(2): 112-132.
Kume, T., K. Deng and B. L. Hogan (2000). "Murine forkhead/winged helix genes Foxc1 (Mf1) and Foxc2 (Mfh1) are required for the early organogenesis of the kidney and urinary tract." Development **127**(7): 1387-1395.
Kunimoto, K., R. D. Bayly, E. K. Vladar, T. Vonderfecht, A. R. Gallagher and J. D. Axelrod (2017). "Disruption of Core Planar Cell Polarity Signaling Regulates Renal Tubule Morphogenesis but Is Not Cystogenic." Curr Biol **27**(20): 3120-3131 e3124.
Kurtzeborn, K., H. N. Kwon and S. Kuure (2019). "MAPK/ERK Signaling in Regulation of Renal Differentiation." Int J Mol Sci **20**(7).
Kuure, S., C. Cebrian, Q. Machingo, B. C. Lu, X. Chi, D. Hyink, V. D'Agati, C. Gurniak, W. Witke and F. Costantini (2010). "Actin depolymerizing factors cofilin1 and destrin are required for ureteric bud branching morphogenesis." PLoS Genet **6**(10): e1001176.
Lamarche, N. and A. Hall (1994). "GAPs for rho-related GTPases." Trends Genet **10**(12): 436-440.
Lancaster, M. A., J. Schroth and J. G. Gleeson (2011). "Subcellular spatial regulation of canonical Wnt signalling at the primary cilium." Nat Cell Biol **13**(6): 700-707.
Landin Malt, A., Z. Dailey, J. Holbrook-Rasmussen, Y. Zheng, A. Hogan, Q. Du and X. Lu (2019). "Par3 is essential for the establishment of planar cell polarity of inner ear hair cells." Proceedings of the National Academy of Sciences **116**(11): 4999-5008.
Lawrence, P. A. and J. Casal (2013). "The mechanisms of planar cell polarity, growth and the Hippo pathway: some known unknowns." Dev Biol **377**(1): 1-8.
Lee, S. H. and R. Dominguez (2010). "Regulation of actin cytoskeleton dynamics in cells." Mol Cells **29**(4): 311-325.
Levay, M., J. Settleman and E. Ligeti (2009). "Regulation of the substrate preference of p190RhoGAP by protein kinase C-mediated phosphorylation of a phospholipid binding site." Biochemistry **48**(36): 8615-8623.
Li, R., B. Zhang and Y. Zheng (1997). "Structural determinants required for the interaction between Rho GTPase and the GTPase-activating domain of p190." J Biol Chem **272**(52): 32830-32835.
Lienkamp, S. S., K. Liu, C. M. Karner, T. J. Carroll, O. Ronneberger, J. B. Wallingford and G. Walz (2012). "Vertebrate kidney tubules elongate using a planar cell polarity-dependent, rosette-based mechanism of convergent extension." Nat Genet **44**(12): 1382-1387.
Lin, F., T. Hiesberger, K. Cordes, A. M. Sinclair, L. S. Goldstein, S. Somlo and P. Igarashi (2003). "Kidney-specific inactivation of the KIF3A subunit of kinesin-II inhibits renal ciliogenesis and produces polycystic kidney disease." Proc Natl Acad Sci U S A **100**(9): 5286-5291.
Lindgren, D., J. Sjolund and H. Axelson (2018). "Tracing Renal Cell Carcinomas back to the Nephron." Trends Cancer **4**(7): 472-484.
Linton, J. M., G. R. Martin and L. F. Reichardt (2007). "The ECM protein nephronectin promotes kidney development via integrin alpha8beta1-mediated stimulation of Gdnf expression." Development **134**(13): 2501-2509.

Little, M., K. Georgas, D. Pennisi and L. Wilkinson (2010). "Kidney development: two tales of tubulogenesis." Curr Top Dev Biol **90**: 193-229.
Liu, Z., S. Chen, S. Boyle, Y. Zhu, A. Zhang, D. R. Piwnica-Worms, M. X. Ilagan and R. Kopan (2013). "The extracellular domain of Notch2 increases its cell-surface abundance and ligand responsiveness during kidney development." Dev Cell **25**(6): 585-598.
Lu, Q., D. A. Schafer and P. N. Adler (2015). "The Drosophila planar polarity gene multiple wing hairs directly regulates the actin cytoskeleton." Development **142**(14): 2478-2486.
Lu, Q., J. Yan and P. N. Adler (2010). "The Drosophila planar polarity proteins inturned and multiple wing hairs interact physically and function together." Genetics **185**(2): 549-558.
Lu, X., A. G. Borchers, C. Jolicoeur, H. Rayburn, J. C. Baker and M. Tessier-Lavigne (2004). "PTK7/CCK-4 is a novel regulator of planar cell polarity in vertebrates." Nature **430**(6995): 93-98.
Majumdar, A., S. Vainio, A. Kispert, J. McMahon and A. P. McMahon (2003). "Wnt11 and Ret/Gdnf pathways cooperate in regulating ureteric branching during metanephric kidney development." Development **130**(14): 3175-3185.
Mao, Y., P. Francis-West and K. D. Irvine (2015). "Fat4/Dchs1 signaling between stromal and cap mesenchyme cells influences nephrogenesis and ureteric bud branching." Development **142**(15): 2574-2585.
Mao, Y., J. Mulvaney, S. Zakaria, T. Yu, K. M. Morgan, S. Allen, M. A. Basson, P. Francis-West and K. D. Irvine (2011). "Characterization of a Dchs1 mutant mouse reveals requirements for Dchs1-Fat4 signaling during mammalian development." Development **138**(5): 947-957.
Matakatsu, H. and S. S. Blair (2012). "Separating planar cell polarity and Hippo pathway activities of the protocadherins Fat and Dachsous." Development **139**(8): 1498-1508.
Matis, M. and J. D. Axelrod (2013). "Regulation of PCP by the Fat signaling pathway." Genes Dev **27**(20): 2207-2220.
Mayr, T., U. Deutsch, M. Kuhl, H. C. Drexler, F. Lottspeich, R. Deutzmann, D. Wedlich and W. Risau (1997). "Fritz: a secreted frizzled-related protein that inhibits Wnt activity." Mech Dev **63**(1): 109-125.
Meyer, T. N., C. Schwesinger, R. V. Sampogna, D. A. Vaughn, R. O. Stuart, D. L. Steer, K. T. Bush and S. K. Nigam (2006). "Rho kinase acts at separate steps in ureteric bud and metanephric mesenchyme morphogenesis during kidney development." Differentiation **74**(9-10): 638-647.
Mezzacappa, C., Y. Komiya and R. Habas (2012). "Activation and function of small GTPases Rho, Rac, and Cdc42 during gastrulation." Methods Mol Biol **839**: 119-131.
Michael, L. and J. A. Davies (2004). "Pattern and regulation of cell proliferation during murine ureteric bud development." J Anat **204**(4): 241-255.
Michos, O., C. Cebrian, D. Hyink, U. Grieshammer, L. Williams, V. D'Agati, J. D. Licht, G. R. Martin and F. Costantini (2010). "Kidney development in the absence of Gdnf and Spry1 requires Fgf10." PLoS Genet **6**(1): e1000809.
Mirvis, M., T. Stearns and W. James Nelson (2018). "Cilium structure, assembly, and disassembly regulated by the cytoskeleton." Biochem J **475**(14): 2329-2353.
Mitchell, B., J. L. Stubbs, F. Huisman, P. Taborek, C. Yu and C. Kintner (2009). "The PCP pathway instructs the planar orientation of ciliated cells in the Xenopus larval skin." Curr Biol **19**(11): 924-929.
Miyazaki, Y., K. Oshima, A. Fogo and I. Ichikawa (2003). "Evidence that bone morphogenetic protein 4 has multiple biological functions during kidney and urinary tract development." Kidney Int **63**(3): 835-844.
Moore, M. W., R. D. Klein, I. Farinas, H. Sauer, M. Armanini, H. Phillips, L. F. Reichardt, A. M. Ryan, K. Carver-Moore and A. Rosenthal (1996). "Renal and neuronal abnormalities in mice lacking GDNF." Nature **382**(6586): 76-79.

Morris, A. R., J. Drawbridge and M. S. Steinberg (2003). "Axolotl pronephric duct migration requires an epidermally derived, laminin 1-containing extracellular matrix and the integrin receptor alpha6beta1." Development **130**(23): 5601-5608.
Mugford, J. W., J. Yu, A. Kobayashi and A. P. McMahon (2009). "High-resolution gene expression analysis of the developing mouse kidney defines novel cellular compartments within the nephron progenitor population." Dev Biol **333**(2): 312-323.
Murdoch, J. N., C. Damrau, A. Paudyal, D. Bogani, S. Wells, N. D. Greene, P. Stanier and A. J. Copp (2014). "Genetic interactions between planar cell polarity genes cause diverse neural tube defects in mice." Dis Model Mech **7**(10): 1153-1163.
Murdoch, J. N., D. J. Henderson, K. Doudney, C. Gaston-Massuet, H. M. Phillips, C. Paternotte, R. Arkell, P. Stanier and A. J. Copp (2003). "Disruption of scribble (Scrb1) causes severe neural tube defects in the circletail mouse." Hum Mol Genet **12**(2): 87-98.
Nachury, M. V. (2018). "The molecular machines that traffic signaling receptors into and out of cilia." Current Opinion in Cell Biology **51**: 124-131.
Nachury, M. V., A. V. Loktev, Q. Zhang, C. J. Westlake, J. Peranen, A. Merdes, D. C. Slusarski, R. H. Scheller, J. F. Bazan, V. C. Sheffield and P. K. Jackson (2007). "A core complex of BBS proteins cooperates with the GTPase Rab8 to promote ciliary membrane biogenesis." Cell **129**(6): 1201-1213.
Nager, A. R., J. S. Goldstein, V. Herranz-Perez, D. Portran, F. Ye, J. M. Garcia-Verdugo and M. V. Nachury (2017). "An Actin Network Dispatches Ciliary GPCRs into Extracellular Vesicles to Modulate Signaling." Cell **168**(1-2): 252-263 e214.
Nakai, S., Y. Sugitani, H. Sato, S. Ito, Y. Miura, M. Ogawa, M. Nishi, K. Jishage, O. Minowa and T. Noda (2003). "Crucial roles of Brn1 in distal tubule formation and function in mouse kidney." Development **130**(19): 4751-4759.
Nauli, S. M., F. J. Alenghat, Y. Luo, E. Williams, P. Vassilev, X. Li, A. E. Elia, W. Lu, E. M. Brown, S. J. Quinn, D. E. Ingber and J. Zhou (2003). "Polycystins 1 and 2 mediate mechanosensation in the primary cilium of kidney cells." Nat Genet **33**(2): 129-137.
Nemeth, T., K. Futosi, C. Hably, M. R. Brouns, S. M. Jakob, M. Kovacs, Z. Kertesz, B. Walzog, J. Settleman and A. Mocsai (2010). "Neutrophil functions and autoimmune arthritis in the absence of p190RhoGAP: generation and analysis of a novel null mutation in mice." J Immunol **185**(5): 3064-3075.
O'Brien, L. L. and A. P. McMahon (2014). "Induction and patterning of the metanephric nephron." Semin Cell Dev Biol **36**: 31-38.
Ohata, S., J. Nakatani, V. Herranz-Perez, J. Cheng, H. Belinson, T. Inubushi, W. D. Snider, J. M. Garcia-Verdugo, A. Wynshaw-Boris and A. Alvarez-Buylla (2014). "Loss of Dishevelleds disrupts planar polarity in ependymal motile cilia and results in hydrocephalus." Neuron **83**(3): 558-571.
Ohazama, A., C. J. Haycraft, M. Seppala, J. Blackburn, S. Ghafoor, M. Cobourne, D. C. Martinelli, C. M. Fan, R. Peterkova, H. Lesot, B. K. Yoder and P. T. Sharpe (2009). "Primary cilia regulate Shh activity in the control of molar tooth number." Development **136**(6): 897-903.
Omori, Y., C. Zhao, A. Saras, S. Mukhopadhyay, W. Kim, T. Furukawa, P. Sengupta, A. Veraksa and J. Malicki (2008). "Elipsa is an early determinant of ciliogenesis that links the IFT particle to membrane-associated small GTPase Rab8." Nat Cell Biol **10**(4): 437-444.
Ooi, Y. S., K. M. Stiles, C. Y. Liu, G. M. Taylor and M. Kielian (2013). "Genome-Wide RNAi Screen Identifies Novel Host Proteins Required for Alphavirus Entry." PLoS Pathog **9**(12): e1003835.
Ostendorf, T., P. Boor, C. R. van Roeyen and J. Floege (2014). "Platelet-derived growth factors (PDGFs) in glomerular and tubulointerstitial fibrosis." Kidney Int Suppl (2011) **4**(1): 65-69.
Packard, A., K. Georgas, O. Michos, P. Riccio, C. Cebrian, A. N. Combes, A. Ju, A. Ferrer-Vaquer, A. K. Hadjantonakis, H. Zong, M. H. Little and F. Costantini (2013). "Luminal mitosis drives epithelial cell dispersal within the branching ureteric bud." Dev Cell **27**(3): 319-330.

Palmer, R. E., A. Kotsianti, B. Cadman, T. Boyd, W. Gerald and D. A. Haber (2001). "WT1 regulates the expression of the major glomerular podocyte membrane protein Podocalyxin." Curr Biol **11**(22): 1805-1809.
Park, T. J., S. L. Haigo and J. B. Wallingford (2006). "Ciliogenesis defects in embryos lacking inturned or fuzzy function are associated with failure of planar cell polarity and Hedgehog signaling." Nat Genet **38**(3): 303-311.
Park, T. J., B. J. Mitchell, P. B. Abitua, C. Kintner and J. B. Wallingford (2008). "Dishevelled controls apical docking and planar polarization of basal bodies in ciliated epithelial cells." Nat Genet **40**(7): 871-879.
Park, W. J., J. Liu, E. J. Sharp and P. N. Adler (1996). "The Drosophila tissue polarity gene inturned acts cell autonomously and encodes a novel protein." Development **122**(3): 961-969.
Pataki, C., T. Matusek, E. Kurucz, I. Ando, A. Jenny and J. Mihaly (2010). "Drosophila Rab23 is involved in the regulation of the number and planar polarization of the adult cuticular hairs." Genetics **184**(4): 1051-1065.
Patel, V., R. Chowdhury and P. Igarashi (2009). "Advances in the pathogenesis and treatment of polycystic kidney disease." Curr Opin Nephrol Hypertens **18**(2): 99-106.
Peng, Y., C. Han and J. D. Axelrod (2012). "Planar polarized protrusions break the symmetry of EGFR signaling during Drosophila bract cell fate induction." Dev Cell **23**(3): 507-518.
Perantoni, K. Y. a. A. O. (2017). "Hydronephrosis in the Wnt5a-ablated kidney is caused by an abnormal ureter-bladder connection." HHS Public Access.
Pichel, J. G., L. Shen, H. Z. Sheng, A. C. Granholm, J. Drago, A. Grinberg, E. J. Lee, S. P. Huang, M. Saarma, B. J. Hoffer, H. Sariola and H. Westphal (1996). "Defects in enteric innervation and kidney development in mice lacking GDNF." Nature **382**(6586): 73-76.
Pitaval, A., Q. Tseng, M. Bornens and M. Thery (2010). "Cell shape and contractility regulate ciliogenesis in cell cycle-arrested cells." J Cell Biol **191**(2): 303-312.
Pohl, M., R. O. Stuart, H. Sakurai and S. K. Nigam (2000). "Branching morphogenesis during kidney development." Annu Rev Physiol **62**: 595-620.
Pollak, M. R., S. E. Quaggin, M. P. Hoenig and L. D. Dworkin (2014). "The glomerulus: the sphere of influence." Clin J Am Soc Nephrol **9**(8): 1461-1469.
Porteous, S., E. Torban, N. P. Cho, H. Cunliffe, L. Chua, L. McNoe, T. Ward, C. Souza, P. Gus, R. Giugliani, T. Sato, K. Yun, J. Favor, M. Sicotte, P. Goodyer and M. Eccles (2000). "Primary renal hypoplasia in humans and mice with PAX2 mutations: evidence of increased apoptosis in fetal kidneys of Pax2(1Neu) +/- mutant mice." Hum Mol Genet **9**(1): 1-11.
Potter, S. S., H. A. Hartman, K. M. Kwan, R. R. Behringer and L. T. Patterson (2007). "Laser capture-microarray analysis of Lim1 mutant kidney development." Genesis **45**(7): 432-439.
Praetorius, H. A. and K. R. Spring (2001). "Bending the MDCK cell primary cilium increases intracellular calcium." J Membr Biol **184**(1): 71-79.
Praetorius, H. A. and K. R. Spring (2003). "Removal of the MDCK cell primary cilium abolishes flow sensing." J Membr Biol **191**(1): 69-76.
Qian, D., C. Jones, A. Rzadzinska, S. Mark, X. Zhang, K. P. Steel, X. Dai and P. Chen (2007). "Wnt5a functions in planar cell polarity regulation in mice." Dev Biol **306**(1): 121-133.
Quarmby, L. (2014). "Cilia assembly: a role for F-actin in IFT recruitment." Curr Biol **24**(17): R796-798.
Reiter, J. F. and M. R. Leroux (2017). "Genes and molecular pathways underpinning ciliopathies." Nat Rev Mol Cell Biol **18**(9): 533-547.
Riccio, P., C. Cebrian, H. Zong, S. Hippenmeyer and F. Costantini (2016). "Ret and Etv4 Promote Directed Movements of Progenitor Cells during Renal Branching Morphogenesis." PLoS Biol **14**(2): e1002382.
Ridley, A. J., A. J. Self, F. Kasmi, H. F. Paterson, A. Hall, C. J. Marshall and C. Ellis (1993). "rho family GTPase activating proteins p190, bcr and rhoGAP show distinct specificities in vitro and in vivo." EMBO J **12**(13): 5151-5160.

Robbe, K., A. Otto-Bruc, P. Chardin and B. Antonny (2003). "Dissociation of GDP dissociation inhibitor and membrane translocation are required for efficient activation of Rac by the Dbl homology-pleckstrin homology region of Tiam." J Biol Chem **278**(7): 4756-4762.
Rocque, B. L., S. Babayeva, J. Li, V. Leung, L. Nezvitsky, A. V. Cybulsky, P. Gros and E. Torban (2015). "Deficiency of the planar cell polarity protein Vangl2 in podocytes affects glomerular morphogenesis and increases susceptibility to injury." J Am Soc Nephrol **26**(3): 576-586.
Rodriguez, I. (2004). "The dachsous gene, a member of the cadherin family, is required for Wg-dependent pattern formation in the Drosophila wing disc." Development **131**(13): 3195-3206.
Saburi, S., I. Hester, E. Fischer, M. Pontoglio, V. Eremina, M. Gessler, S. E. Quaggin, R. Harrison, R. Mount and H. McNeill (2008). "Loss of Fat4 disrupts PCP signaling and oriented cell division and leads to cystic kidney disease." Nat Genet **40**(8): 1010-1015.
Sajithlal, G., D. Zou, D. Silvius and P. X. Xu (2005). "Eya 1 acts as a critical regulator for specifying the metanephric mesenchyme." Dev Biol **284**(2): 323-336.
Sanchez, M. P., I. Silos-Santiago, J. Frisen, B. He, S. A. Lira and M. Barbacid (1996). "Renal agenesis and the absence of enteric neurons in mice lacking GDNF." Nature **382**(6586): 70-73.
Sang, L., J. J. Miller, K. C. Corbit, R. H. Giles, M. J. Brauer, E. A. Otto, L. M. Baye, X. Wen, S. J. Scales, M. Kwong, E. G. Huntzicker, M. K. Sfakianos, W. Sandoval, J. F. Bazan, P. Kulkarni, F. R. Garcia-Gonzalo, A. D. Seol, J. F. O'Toole, S. Held, H. M. Reutter, W. S. Lane, M. A. Rafiq, A. Noor, M. Ansar, A. R. Devi, V. C. Sheffield, D. C. Slusarski, J. B. Vincent, D. A. Doherty, F. Hildebrandt, J. F. Reiter and P. K. Jackson (2011). "Mapping the NPHP-JBTS-MKS protein network reveals ciliopathy disease genes and pathways." Cell **145**(4): 513-528.
Scheidecker, S., C. Etard, N. W. Pierce, V. Geoffroy, E. Schaefer, J. Muller, K. Chennen, E. Flori, V. Pelletier, O. Poch, V. Marion, C. Stoetzel, U. Strahle, M. V. Nachury and H. Dollfus (2014). "Exome sequencing of Bardet-Biedl syndrome patient identifies a null mutation in the BBSome subunit BBIP1 (BBS18)." J Med Genet **51**(2): 132-136.
Scheidel, N. and O. E. Blacque (2018). "Intraflagellar Transport Complex A Genes Differentially Regulate Cilium Formation and Transition Zone Gating." Curr Biol **28**(20): 3279-3287 e3272.
Schell, C., N. Wanner and T. B. Huber (2014). "Glomerular development--shaping the multi-cellular filtration unit." Semin Cell Dev Biol **36**: 39-49.
Schneider, L., M. Cammer, J. Lehman, S. K. Nielsen, C. F. Guerra, I. R. Veland, C. Stock, E. K. Hoffmann, B. K. Yoder, A. Schwab, P. Satir and S. T. Christensen (2010). "Directional cell migration and chemotaxis in wound healing response to PDGF-AA are coordinated by the primary cilium in fibroblasts." Cell Physiol Biochem **25**(2-3): 279-292.
Schuchardt, A., V. D'Agati, L. Larsson-Blomberg, F. Costantini and V. Pachnis (1994). "Defects in the kidney and enteric nervous system of mice lacking the tyrosine kinase receptor Ret." Nature **367**(6461): 380-383.
Sedzinski, J., E. Hannezo, F. Tu, M. Biro and J. B. Wallingford (2017). "RhoA regulates actin network dynamics during apical surface emergence in multiciliated epithelial cells." J Cell Sci **130**(2): 420-428.
Self, M., O. V. Lagutin, B. Bowling, J. Hendrix, Y. Cai, G. R. Dressler and G. Oliver (2006). "Six2 is required for suppression of nephrogenesis and progenitor renewal in the developing kidney." EMBO J **25**(21): 5214-5228.
Seo, J. H., Y. Zilber, S. Babayeva, J. Liu, P. Kyriakopoulos, P. De Marco, E. Merello, V. Capra, P. Gros and E. Torban (2011). "Mutations in the planar cell polarity gene, Fuzzy, are associated with neural tube defects in humans." Hum Mol Genet **20**(22): 4324-4333.
Sepich, D. S., M. Usmani, S. Pawlicki and L. Solnica-Krezel (2011). "Wnt/PCP signaling controls intracellular position of MTOCs during gastrulation convergence and extension movements." Development **138**(3): 543-552.

Shakya, R., T. Watanabe and F. Costantini (2005). "The role of GDNF/Ret signaling in ureteric bud cell fate and branching morphogenesis." Dev Cell **8**(1): 65-74.
Sim, E. U., A. Smith, E. Szilagi, F. Rae, P. Ioannou, M. H. Lindsay and M. H. Little (2002). "Wnt-4 regulation by the Wilms' tumour suppressor gene, WT1." Oncogene **21**(19): 2948-2960.
Simons, M., J. Gloy, A. Ganner, A. Bullerkotte, M. Bashkurov, C. Kronig, B. Schermer, T. Benzing, O. A. Cabello, A. Jenny, M. Mlodzik, B. Polok, W. Driever, T. Obara and G. Walz (2005). "Inversin, the gene product mutated in nephronophthisis type II, functions as a molecular switch between Wnt signaling pathways." Nat Genet **37**(5): 537-543.
Smalley, M. J., N. Signoret, D. Robertson, A. Tilley, A. Hann, K. Ewan, Y. Ding, H. Paterson and T. C. Dale (2005). "Dishevelled (Dvl-2) activates canonical Wnt signalling in the absence of cytoplasmic puncta." J Cell Sci **118**(Pt 22): 5279-5289.
Smallwood, P. M., J. Williams, Q. Xu, D. J. Leahy and J. Nathans (2007). "Mutational analysis of Norrin-Frizzled4 recognition." J Biol Chem **282**(6): 4057-4068.
Smith, C. E. L., A. V. R. Lake and C. A. Johnson (2020). "Primary Cilia, Ciliogenesis and the Actin Cytoskeleton: A Little Less Resorption, A Little More Actin Please." Front Cell Dev Biol **8**: 622822.
Song, H., J. Hu, W. Chen, G. Elliott, P. Andre, B. Gao and Y. Yang (2010). "Planar cell polarity breaks bilateral symmetry by controlling ciliary positioning." Nature **466**(7304): 378-382.
Soofi, A., I. Levitan and G. R. Dressler (2012). "Two novel EGFP insertion alleles reveal unique aspects of Pax2 function in embryonic and adult kidneys." Dev Biol **365**(1): 241-250.
Spassky, N. and A. Aguilar (2008). "[Shh regulates neurogenesis through primary cilia]." Med Sci (Paris) **24**(10): 790-791.
Stewart, K., Y. Gaitan, M. E. Shafer, L. Aoudjit, D. Hu, R. Sharma, M. Tremblay, H. Ishii, M. Marcotte, D. Stanga, Y. C. Tang, S. K. Boualia, A. H. Nguyen, T. Takano, N. Lamarche-Vane, S. Vidal and M. Bouchard (2016). "A Point Mutation in p190A RhoGAP Affects Ciliogenesis and Leads to Glomerulocystic Kidney Defects." PLoS Genet **12**(2): e1005785.
Strutt, D. (2008). "The planar polarity pathway." Curr Biol **18**(19): R898-902.
Strutt, D. (2009). "Gradients and the specification of planar polarity in the insect cuticle." Cold Spring Harb Perspect Biol **1**(5): a000489.
Strutt, D. I., U. Weber and M. Mlodzik (1997). "The role of RhoA in tissue polarity and Frizzled signalling." Nature **387**(6630): 292-295.
Strutt, H. and D. Strutt (2008). "Differential stability of flamingo protein complexes underlies the establishment of planar polarity." Curr Biol **18**(20): 1555-1564.
Takabatake, Y., T. Sugiyama, H. Kohara, T. Matsusaka, H. Kurihara, P. A. Koni, Y. Nagasawa, T. Hamano, I. Matsui, N. Kawada, E. Imai, T. Nagasawa, H. Rakugi and Y. Isaka (2009). "The CXCL12 (SDF-1)/CXCR4 axis is essential for the development of renal vasculature." J Am Soc Nephrol **20**(8): 1714-1723.
Taschner, M., S. Bhogaraju and E. Lorentzen (2012). "Architecture and function of IFT complex proteins in ciliogenesis." Differentiation **83**(2): S12-22.
Tomita, M., M. Asada, N. Asada, J. Nakamura, A. Oguchi, A. Y. Higashi, S. Endo, E. Robertson, T. Kimura, T. Kita, A. N. Economides, J. Kreidberg and M. Yanagita (2013). "Bmp7 maintains undifferentiated kidney progenitor population and determines nephron numbers at birth." PLoS One **8**(8): e73554.
Torban, B. R. a. E. (2015). "Planar Cell Polarity Pathway in Kidney Development and Function." Hindawi **2015**.
Torban, E., C. Kor and P. Gros (2004). "Van Gogh-like2 (Strabismus) and its role in planar cell polarity and convergent extension in vertebrates." Trends Genet **20**(11): 570-577.
Torban, E., A. M. Patenaude, S. Leclerc, S. Rakowiecki, S. Gauthier, G. Andelfinger, D. J. Epstein and P. Gros (2008). "Genetic interaction between members of the Vangl family causes neural tube defects in mice." Proc Natl Acad Sci U S A **105**(9): 3449-3454.

Toriyama, M., C. Lee, S. P. Taylor, I. Duran, D. H. Cohn, A. L. Bruel, J. M. Tabler, K. Drew, M. R. Kelly, S. Kim, T. J. Park, D. A. Braun, G. Pierquin, A. Biver, K. Wagner, A. Malfroot, I. Panigrahi, B. Franco, H. A. Al-Lami, Y. Yeung, Y. J. Choi, G. University of Washington Center for Mendelian, Y. Duffourd, L. Faivre, J. B. Riviere, J. Chen, K. J. Liu, E. M. Marcotte, F. Hildebrandt, C. Thauvin-Robinet, D. Krakow, P. K. Jackson and J. B. Wallingford (2016). "The ciliopathy-associated CPLANE proteins direct basal body recruitment of intraflagellar transport machinery." Nat Genet **48**(6): 648-656.
Tufro, A., J. Teichman, C. Woda and G. Villegas (2008). "Semaphorin3a inhibits ureteric bud branching morphogenesis." Mech Dev **125**(5-6): 558-568.
Usui, T., Y. Shima, Y. Shimada, S. Hirano, R. W. Burgess, T. L. Schwarz, M. Takeichi and T. Uemura (1999). "Flamingo, a seven-pass transmembrane cadherin, regulates planar cell polarity under the control of Frizzled." Cell **98**(5): 585-595.
Valencia, A., P. Chardin, A. Wittinghofer and C. Sander (1991). "The ras protein family: evolutionary tree and role of conserved amino acids." Biochemistry **30**(19): 4637-4648.
Van Aelst, L. and C. D'Souza-Schorey (1997). "Rho GTPases and signaling networks." Genes Dev **11**(18): 2295-2322.
Wallingford, J. B. (2006). "Planar cell polarity, ciliogenesis and neural tube defects." Hum Mol Genet **15 Spec No 2**: R227-234.
Wallingford, J. B., T. Goto, R. Keller and R. M. Harland (2002). "Cloning and expression of Xenopus Prickle, an orthologue of a Drosophila planar cell polarity gene." Mech Dev **116**(1-2): 183-186.
Wallingford, J. B., B. A. Rowning, K. M. Vogeli, U. Rothbacher, S. E. Fraser and R. M. Harland (2000). "Dishevelled controls cell polarity during Xenopus gastrulation." Nature **405**(6782): 81-85.
Wang, J., N. S. Hamblet, S. Mark, M. E. Dickinson, B. C. Brinkman, N. Segil, S. E. Fraser, P. Chen, J. B. Wallingford and A. Wynshaw-Boris (2006). "Dishevelled genes mediate a conserved mammalian PCP pathway to regulate convergent extension during neurulation." Development **133**(9): 1767-1778.
Wang, J., S. Mark, X. Zhang, D. Qian, S. J. Yoo, K. Radde-Gallwitz, Y. Zhang, X. Lin, A. Collazo, A. Wynshaw-Boris and P. Chen (2005). "Regulation of polarized extension and planar cell polarity in the cochlea by the vertebrate PCP pathway." Nat Genet **37**(9): 980-985.
Wang, Y. and J. Nathans (2007). "Tissue/planar cell polarity in vertebrates: new insights and new questions." Development **134**(4): 647-658.
Wang, Y., J. Yan, H. Lee, Q. Lu and P. N. Adler (2014). "The proteins encoded by the Drosophila Planar Polarity Effector genes inturned, fuzzy and fritz interact physically and can re-pattern the accumulation of "upstream" Planar Cell Polarity proteins." Dev Biol **394**(1): 156-169.
Waters, A. M. and P. L. Beales (2011). "Ciliopathies: an expanding disease spectrum." Pediatr Nephrol **26**(7): 1039-1056.
Wegner, A. (1976). "Head to tail polymerization of actin." J Mol Biol **108**(1): 139-150.
Wellik, D. M., P. J. Hawkes and M. R. Capecchi (2002). "Hox11 paralogous genes are essential for metanephric kidney induction." Genes Dev **16**(11): 1423-1432.
Wheatley, D. N. (1995). "Primary cilia in normal and pathological tissues." Pathobiology **63**(4): 222-238.
Wheeler, A. P. and A. J. Ridley (2004). "Why three Rho proteins? RhoA, RhoB, RhoC, and cell motility." Exp Cell Res **301**(1): 43-49.
Wickman, L., F. Afshinnia, S. Q. Wang, Y. Yang, F. Wang, M. Chowdhury, D. Graham, J. Hawkins, R. Nishizono, M. Tanzer, J. Wiggins, G. A. Escobar, B. Rovin, P. Song, D. Gipson, D. Kershaw and R. C. Wiggins (2013). "Urine podocyte mRNAs, proteinuria, and progression in human glomerular diseases." J Am Soc Nephrol **24**(12): 2081-2095.
Wu, J. and M. Mlodzik (2009). "A quest for the mechanism regulating global planar cell polarity of tissues." Trends Cell Biol **19**(7): 295-305.

Yamanaka, H., T. Moriguchi, N. Masuyama, M. Kusakabe, H. Hanafusa, R. Takada, S. Takada and E. Nishida (2002). "JNK functions in the non-canonical Wnt pathway to regulate convergent extension movements in vertebrates." EMBO Rep **3**(1): 69-75.
Yan, J., D. Huen, T. Morely, G. Johnson, D. Gubb, J. Roote and P. N. Adler (2008). "The multiple-wing-hairs gene encodes a novel GBD-FH3 domain-containing protein that functions both prior to and after wing hair initiation." Genetics **180**(1): 219-228.
Yasunaga, T., S. Hoff, C. Schell, M. Helmstadter, O. Kretz, S. Kuechlin, T. A. Yakulov, C. Engel, B. Muller, R. Bensch, O. Ronneberger, T. B. Huber, S. S. Lienkamp and G. Walz (2015). "The polarity protein Inturned links NPHP4 to Daam1 to control the subapical actin network in multiciliated cells." J Cell Biol **211**(5): 963-973.
Yates, L. L., J. Papakrivopoulou, D. A. Long, P. Goggolidou, J. O. Connolly, A. S. Woolf and C. H. Dean (2010). "The planar cell polarity gene Vangl2 is required for mammalian kidney-branching morphogenesis and glomerular maturation." Hum Mol Genet **19**(23): 4663-4676.
Yoder, B. K. (2007). "Role of primary cilia in the pathogenesis of polycystic kidney disease." J Am Soc Nephrol **18**(5): 1381-1388.
Yoshimura, S., J. Egerer, E. Fuchs, A. K. Haas and F. A. Barr (2007). "Functional dissection of Rab GTPases involved in primary cilium formation." J Cell Biol **178**(3): 363-369.
Yu, J., T. J. Carroll and A. P. McMahon (2002). "Sonic hedgehog regulates proliferation and differentiation of mesenchymal cells in the mouse metanephric kidney." Development **129**(22): 5301-5312.
Yu, J., T. J. Carroll, J. Rajagopal, A. Kobayashi, Q. Ren and A. P. McMahon (2009). "A Wnt7b-dependent pathway regulates the orientation of epithelial cell division and establishes the cortico-medullary axis of the mammalian kidney." Development **136**(1): 161-171.
Zallen, J. A. and J. T. Blankenship (2008). "Multicellular dynamics during epithelial elongation." Semin Cell Dev Biol **19**(3): 263-270.
Zeng, H., A. N. Hoover and A. Liu (2010). "PCP effector gene Inturned is an important regulator of cilia formation and embryonic development in mammals." Dev Biol **339**(2): 418-428.
Zhang, J., M. Wu, S. Wang, J. V. Shah, P. D. Wilson and J. Zhou (2010). "Polycystic kidney disease protein fibrocystin localizes to the mitotic spindle and regulates spindle bipolarity." Hum Mol Genet **19**(17): 3306-3319.
Zilber, Y., S. Babayeva, J. H. Seo, J. J. Liu, S. Mootin and E. Torban (2013). "The PCP effector Fuzzy controls cilial assembly and signaling by recruiting Rab8 and Dishevelled to the primary cilium." Mol Biol Cell **24**(5): 555-565.